MODELING OF WIRELESS CHANNEL

A thesis

submitted towards the partial fulfilment of the requirement for the award of the degree of

DOCTOR OF PHILOSOPHY

in

Department of Electronics and Communication Engineering

by

VINOD KUMAR
(2K14/PHD/EC/05)

DEPARTMENT OF ELECTRONICS & COMMUNICATION ENGINEERING

DELHI TECHNOLOGICAL UNIVERSITY
(FORMERLY DELHI COLLEGE OF ENGINEERING)
DELHI-110042 INDIA
FEBRUARY 2021

DELHI TECHNOLOGICAL UNIVERSITY

Established by Govt. Of Delhi vide Act 6 of 2009

(Formerly Delhi College of Engineering)

SHAHBAD DAULATPUR, BAWANA ROAD, DELHI- 110042

CERTIFICATE

This is to certify that the thesis entitled "**Modeling of Wireless Channel**" submitted by Vinod Kumar (2K14/PHD/EC/05) for the award of the degree of Doctor of Philosophy to the Delhi Technological University is based on the original research work carried out by him under our supervision. He has fulfilled the requirements which to our knowledge have reached the requisite standard for the submission of this thesis. It is further certified that the work embodied in this thesis has neither partially nor fully submitted to any other university or institution for the award of any degree or diploma.

Prof. S. K. Soni
Joint-Supervisor
Professor
Department of ECE
MMMUT, Gorakhpur (UP)

Prof. N. S. Raghava
Supervisor
Professor & Head
Department of ECE
DTU, Delhi, INDIA

CANDIDATE'S DECLARATION

I hereby certify that the research work which is being presented in the thesis entitled, "**Modeling of Wireless Channel**" in fulfilment of requirements of the award of the degree of Doctor of Philosophy is an authentic record of my research work carried under the supervision of Prof. N. S. Raghava and Prof. Sanjay Kumar Soni.

The matter presented in this thesis has not been submitted elsewhere in part or fully to any other University or Institute for the award of any degree.

Vinod Kumar
2K14/PHD/EC/05
Department of Electronics and Communication Engineering
Delhi Technological University
Delhi – 110042, India

ACKNOWLEDGEMENTS

First of all, I would like to pay my thanks to Almighty God, faculties and parents who gave me life and power, without which the work would not have seen the light of the day. The paucity of words does not compromise for extending my thanks to all the persons who have directly or indirectly helped me in completing this thesis.

I feel the privilege to express my sincere thanks to my endearing supervisors Dr N. S. Raghava, Professor & Head, Department of Electronics and Communication Engineering, Delhi Technological University, Delhi and Dr Sanjay Kumar Soni, Professor, Department of Electronics and Communication Engineering, Madan Mohan Malaviya University of Technology, Gorakhpur, Uttar Pradesh; for the valuable suggestions, special guidance and providing the environment of independent thinking during the thesis. I always availed his priceless supervision, continuous motivation and ever unforgettable humanitarian considerations.

I am thankful to all the faculty members of the Department of Electronics and Communication Engineering for their time to time advice, support and help. My special thanks to the members of the DRC committee for their constructive suggestions.

I gratefully acknowledge the academic branch and administration of DTU for providing the environment and facilities to carry out my research work. I also express my thanks to the office staff of the Department of ECE for all kinds of support.

I would also like to express my thanks to Dr Bajrang Bansal, Dr Sandeep Kumar, Dr P. K. Verma, Dr Rahul Bansal, and Dr Ashish Kumar who always helped me and motivated me in numerous ways. I want to acknowledge Akhilesh Verma, Rehan, Dr Abhishek Kumar, and Ram Pratap for their constant support and encouragement. I express my thanks to all research scholars of the Department of ECE.

I am also grateful to Vice-Chancellor, Delhi Technological University for providing the research environment in the institute.

I express my deep sense of respect and gratitude to my parents and my brother Dr Ram Shankar Gupta. Finally, I would like to thanks my wife Dr Shilpa Kaushal for the constant source of motivation and moral support for me. Her scarifies and endless prayers helped me at every stage of my PhD work.

(*Vinod Kumar*)

TABLE OF CONTENTS

All the corrections suggested by the Examiner have been incorporated. (Page 4-8,56,68,86,100)

LIST OF FIGURES

LIST OF TABLES

LIST OF SYMBOLS

$x(t)$	Transmitted UWB pulse
$h(t)$	Channel response
$y(t)$	Output response
$*$	Sign of convolution
$\cdot$	Sign of multiplication
$Y(\omega)$	FD solution of output response
ω	Angular frequency
$y^{+}(t)$	Complex solution
$H[y(t)]$	Hilbert's transform
pv	Cauchy principal value integration
$\text{sgn}(\omega)$	Signum function
$Y(s)$	Laplace transform of $y(t)$
ϕ'	Incident angle
ϕ	Diffracted angle
φ	Wedge angle
(r_1, ϕ')	Points of transmission
(r_2, ϕ)	Points of reception
E_{Total}	Total Electric Field
E_i	Incident Field
E_r	Reflected Field
E_t	Transmitted Field
E_d	Diffracted Field
E_{GO}	Geometric Optics fields
D	Diffraction coefficients

L	Distance parameter
A	Amplitude spreading factor
n	Angle parameter
r_1	Distance from transmitter
r_2	Distance from the diffracted point to the receiver
$k = \omega/c$	Wavenumber
c	Speed of light,
s	Soft polarization
h	Hard polarization
$F(X)$	Transition function
$erfc(X)$	Complementary error function
R_0	Fresnel reflection coefficient for $0-$ face
R_n	Fresnel reflection coefficient for $n-$face
θ_n	Reflection angles
ε	Complex permittivity
σ	Conductivity in S/m
ε_0	Permittivity of free space
ε_r	Relative permittivity
$\Upsilon_{s,h}$	Modified reflection
$d_{s,h}(t)$	TD diffraction coefficient
$u(t)$	Heaviside step function
$r_{0,n,s,h}(t)$	TD Fresnel reflection coefficient
$\delta(t)$	Dirac delta function
$I_q(t)$	Modified Bessel function of order q
$-(+)$	Soft (hard) polarization
$\gamma_{s,h}(t)$	Modified TD reflection coefficient

LIST OF ABBREVIATIONS

UWB	Ultra-wideband
TD	Time-domain
SSI	Single side illumination
DSI	Double side illumination
GO	Geometrical Optics
GTD	Geometrical Theory of Diffraction
UTD	Uniform Theory of Diffraction
PO	Physical Optics
UAPO	Uniform Asymptotic Theory of Diffraction
PTD	Physical Theory of Diffraction
MTPO	Modified Theory of Physical Optics
FD	Frequency-domain
IoT	Internet of Things
5G	Fifth-generation
4G	Fourth-generation
6G	Sixth-generation
WPAN	Wireless personal area network
NLOS	Non-Line of sight
LOS	Line-of-sight
IFT	Inverse Fourier Transform
ILT	Inverse Laplace Transform
IFFT	Inverse Fast Fourier Transform
RSB	Reflection shadow boundary
ISB	Incident shadow boundary
FDTD	Finite difference time domain
TSB	Transmitted shadow boundary

ABSTRACT

With the speedy development of wireless mobile communication, the dimensions of a cell are changing into smaller, and also the design of the mobile system needs information about transmission over certain sites. An electromagnetic wave propagation model needs to detect a wireless system. In the last few decades, several statistical and deterministic channel models have been planned in small urban areas. Compared to a statistical channel model, a deterministic channel model can solve specific, real-life situations. Considering the design of the future communication system, the Ultra-wideband (UWB) system will be one of the most important application features in wireless communication, and its scenario is very complex and flexible. It is hard for general statistical channel models to differentiate these variations, making it difficult to obtain an accurate model. Currently, radio broadcasts are simulated to obtain the specific channel features of a specific situation in a determination channel model. The deterministic channel model has maintained its acceptance among scholars for a long time. In particular, uniform theory of diffraction (UTD) based approaches are still being considered even if the surrounding is complex. The subsequent subsections will acquaint the reader with the outline of contributions created during this thesis.

In this study, some new time-domain (TD) solutions are proposed for non-perfectly conducting wedges. A new TD solution for single diffraction is proposed where the incident pulse illuminates one or both sides of the dielectric wedge with unlike wedge angles. Thereafter, a TD solution for double diffraction is proposed that works to all possible illumination regions of wedges. The reflection angles and reflection coefficients are modified in different wedge regions. Thereafter, a TD solution is proposed for higher-order diffraction using a single diffraction coefficient. It looks at all possible variations between the dual wedges. This technique can be applied for more than two wedges that consider all the diffraction orders. Following this, the coefficients of Uniform Theory of

Diffraction (UTD) coefficients in TD are proposed to be considered for transmission and diffraction phenomena from the thin dielectric wedge.

Finally, novel coefficients are proposed for frequency- domain (FD) and TD. The frequency-domain Uniform Theory of Diffraction (FD-UTD) coefficient was shown to be accurate in all the regions with a thin lossy wedge. It allows the calculation of the transmitted ray by a dielectric wedge by inserting two more terms into the four-terms FD-UTD coefficient. This six-terms FD-UTD coefficient is confirmed by the available finite difference time domain (FDTD) technique. In the deep shadow region between the incident shadow boundary (ISB) and the transmitted shadow boundary (TSB), where only diffracted ray exists, the proposed FD solutions give a 14 percent improvement over the previous technique on average. Next, the doubly diffracted field by the slope diffraction coefficient behind the double wedge structure and a high lossy building is also presented. Also, the coefficient of the novel time-domain Uniform Theory of Diffraction (TD-UTD) was presented based on the inverse Laplace transform of the proposed FD solutions. Different input pulses and wedge materials have been used to test the full functionality of the proposed TD techniques. TD-UTD results are confirmed by inverse fast Fourier transform of frequency domain (IFFT-FD) results, and excellent agreements have been reported. An impulse response has also been introduced to explain the distortion of the pulse in various conditions. Finally, the TD-UTD procedure is shown to be more effective than the IFFT-FD method.

Chapter 1

Introduction

This chapter discusses the need for channel modeling for Ultra-wideband (UWB) applications, the high-frequency phenomenon of electromagnetic waves, the study positions, and the research objectives. Finally, the organization of the thesis is presented.

1.1 The Need of Wireless Channel Modeling

Mobile communication technology is undergoing new changes every decade. There is also a significant improvement in the performance of all generations of technology. This technological shift is largely due to the persistent practice of mobile phones, the advent of the Internet of Things (IoT), and the demand for high-quality video content. The watching time of users is also increasing; it is becoming the norm for users to watch full-length TV programmes and movies via streaming video. Also, these things are predicted to rise at high rates [1]. Fifth-generation technology (5G) will soon be installed globally with additional features compared to fourth-generation technology (4G) to meet the needs in this current environment. In general, 5G is also likely to allow for the Industrial Revolution (Industry 4.0) where everything will be digitally connected with the advanced mobile broadband of users. Also, a new level of mobile communication, a sixth-generation (6G) communication system is expected to be implemented before 2030 with full support for industrial automation and artificial intelligence [2-3].

One of the most challenging problems for 5G systems is to strengthen spectral competency and capacity by 10 and 1,000 times to support dynamic conditions. One of the most advanced wireless technology is the Ultra-Wideband (UWB) (3.1-10.6 GHz) communication for 5G picocell and femtocells solution. It can operate with an unlicensed band in the same way as existing radio communications without interruption [4]. UWB provides short-range digital

transmission using very low power. This technology is favoured by personal wireless network (WPAN) systems which means a wireless computer connected to a digital projector in a conference room, the transfer of digital images from a digital camera to a computer without the need for a cable, etc. The bandwidth of UWB is more than 20 percent of the centre frequency equal to 7.5 GHz. UWB communication is non-Line of sight (NLOS) communication due to the presence of several objects between the transmitter and receiver. The signal at the receiver is more or less distorted. Therefore, accurate channel modeling is required to determine the performance of the communication system and network realization [5]. The diffraction phenomenon of UWB signals from the non-perfectly conducting wedge is considered to gain signal strength in the shadow region [6].

1.2 High-frequency Phenomena

In high-frequency phenomena, the electromagnetic fields are being measured in a structure when the electromagnetic properties of the surrounding medium and scatterer size parameters vary somewhat over the gap of a wavelength. The engineering problems of such dimensions that these methods are valid at microwave frequencies and above; hence the term high-frequency [7]. Wave propagation mechanisms are quite multifaceted and diverse because of the parting between the receiver and the transmitter. Therefore, a reduction in signal strength happens [8]. Also, the signal in Fig. 1.1 spreads through reflection, diffraction, transmission, scattering, refraction, etc.

1.2.1 Diffraction

It arises after direct line-of-sight (LOS) transmission is blocked by an impervious barrier that is much greater than the signal wavelength. It happens at the edge of the barrier where radio waves scatter, and consequently, the signal strength is further reduced. This phenomenon

permits to receive of radio signals in case of non-line-of-sight (NLOS) communication, either in city or rural areas.

1.2.2 Scattering

It occurs when the propagation path contains obstacles with a size equal to the wavelength. The behaviour of this mechanism is like diffraction, but the radio waves are dispersed in many places. In all the reported results, scattering is very hard to measure.

1.2.3 Reflection

It happens when a radio wave introduces a barrier that is much larger than the wavelength. A reflected signal can decay or rise the signal strength at the receiver. For the cases of many reflected waves, the obtained signal is typically not stable. This mechanism is often stated as multipath fading. The radio signals are usually Rayleigh distributed in this case.

1.2.4 Transmission

It happens when a radio wave meets an obvious interference. This phenomenon permits the receiving of radio signals inside structures in circumstances when the real transmission points are outside.

1.2.5 Refraction

It is very significant in designing of macrocell radio system. Because of a variable refractive index of the atmosphere, radio waves propagate in a curve. Therefore, the area to cover the actual transmitter is usually large. However, due to fluctuations in atmospheric parameters, the received signal strength fluctuates again. The signal obtained in NLOS communication is the sum of the phenomenon that usually appears in numerous predefined cases. Consequently, the level of the signal received varies according to the time and especially about the displacement of the receiver or transmitter. Even a slight variation of the distance can cause the signal level to fluctuate above 30 dB. This fluctuation is identified as a short-term (or multipath) fading.

Instead, the signal level fluctuates slightly with the motion. These slow variations are highly dependent on natural factors, and they are identified as long-term fading.

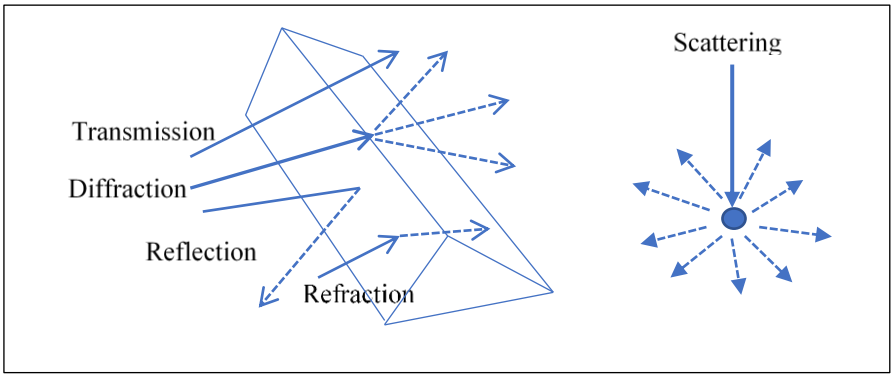

Fig. 1.1 Wave propagation mechanisms

1.3 Research Gaps

There's a great necessity to develop propagation solutions that measure the delay and amplitude of multipath repeats in city surroundings because of the placement of the fast digital communication systems. The high-frequency techniques have emerged as being well ideal for this task. These strategies inherently offer pulse delay records as a function of total ray path length in addition to predicting signal levels.

The High-frequency electromagnetic methods can be divided into two groups: ray-based techniques and induced-source-based techniques. The ray-based methods are Geometrical optics (GO) [9-19], Geometrical Theory of Diffraction (GTD) [20-25], and the Uniform Theory of Diffraction (UTD) [26-38]. The induced-source-based techniques are Physical Optics (PO) [39-50], the Physical Theory of Diffraction (PTD)[51-59], the Modified Theory of Physical Optics (MTPO) [60-70], the Uniform Asymptotic Theory of Diffraction (UAPO) [71-81], etc.

From the literature surveys, the growing attention in the ultrawideband communication system (UWB) is due to high-speed connectivity, high data rates, low equipment costs, and low system

complexity [82]. Therefore, the UWB is seen as a potential solution of 5G picocell and femtocells to fulfil the current requirements. The TD profile provides all required parameters in the UWB system, for example, multipath number, delay, power, and distortion of each path. It looks and works better in direct operation on TD than using a numerical inverse fast Fourier transform procedures to convert FD solutions to TD. The main physical phenomenon in radio propagation required to consider are reflections, transmissions through objects, and diffraction phenomena. In the case of diffraction, the uniform theory of diffraction (UTD) is most commonly used due to its simplicity and ray interpretation [83]. The following untouched areas of UWB applications are:

- In [84], the improvements to a UTD-based diffraction coefficient for non-perfectly conducting wedges have been presented in frequency-domain (FD). The improvements enable more accurate prediction of diffracted field for any observation angle for different wedge angles and for both the parallel and perpendicular polarizations. The improvements are based on reflection angles used in the calculation of the Fresnel reflection coefficient in some angular region and reconstructing the coefficient in other regions. However, the TD-UTD solutions of [84] for UWB applications were not addressed in [85-99].

- The transmitter may have such a position in a wedge scenario, where it can illuminate either single or both faces of the wedge structure. Therefore, the diffraction coefficients are defined for both the cases in [84] in frequency domain. In the works of literature [85-96], [99], the case of double diffraction in TD was presented for single face illumination. But, the case of both face illumination [84] has not been addressed for non-perfectly conducting wedges.

- The process of accounting for high order diffractions, especially for third and higher orders, can be very tedious. In the works of literature [85-96], [99], higher-order diffraction coefficients are used to obtain multiple diffractions. However, the self-consistent method [100] has been used to find the multiple order diffracted field in the frequency domain without using the higher-order diffraction coefficients. But the time domain solution using this method has not been done to find the double diffraction of all possible orders for UWB applications.

- In [104], a wedge angle of fewer than 20 degrees is considered, and a six-term diffraction formula is proposed which takes into account the transmission through the wedge. However, the following things are observed based on literature [85-103].

  1) The TD solution of [104] has not been presented for UWB applications.

  2) The proposed results in [104] have significant deviations from their FDTD results in the deep shadow region.

1.4 Research Objectives

Because of the above research opportunities, the following research decisions have been determined for UWB applications.

- To propose a new TD diffraction coefficient for non-perfectly conducting wedges operates in a situation where the source illuminates one or both sides of different wedge angles.

- To develop a TD double diffraction coefficient for the source illumination on one or both sides of non-perfectly conducting wedges.

- To compute the TD double diffraction of all possible orders for UWB application without using any higher-order diffraction coefficients.
- To propose a six-terms diffraction coefficient in TD for UWB applications that include transmission through obstacles.
- To find an improved six-terms diffraction coefficient in FD and TD for UWB applications that improves results in the deep shadow region of the obstacles.

1.5 Contribution

The contributions are as follows:

- The UWB signals suffer pulse distortion due to the frequency selectivity of the propagation path loss; hence, it is more efficient to study UWB propagation directly in the time domain (TD), where all the frequencies are treated simultaneously.
- In addition, all the necessary parameters of a UWB system, such as the number of multipath, the delay, the power, and the distortion of every path, can be easily obtained from the TD analysis.
- Moreover, it seems to be more efficient to work directly in the TD than applying the numerical inverse fast Fourier transform (IFFT) on each frequency separately.
- In TD, the channel's impulse response is calculated in closed form for each possible propagation path and then convolved with the input signal to obtain the received field.
- The proposed TD solution has the potential benefit of having very high computational efficiency as opposed to conventional FD method; thus, it can be integrated with the existing ray tracing tool, achieving higher speed without compromising accuracy.
- This signal is compared with the numerical inverse fast Fourier transform of the corresponding solution in the FD, so as to validate our method. The results show a very

good agreement between the two solutions with the TD solution offering much shorter computation times.

1.6 Scope of the Research

The major goal of this research is to provide new single-order and multiple-order Uniform Theory of Diffraction (UTD) coefficients in the time-domain (TD) for non-perfectly conducting wedges using the inverse Laplace transform of the frequency-domain (FD) solutions. Here, the source can illuminate on one or both sides of the wedge. The self-consistent approach is also applied to the case of multiple-order diffractions. By creating the six-terms UTD coefficients in TD and FD, the case of the transmission along with the diffraction phenomenon from the thin dielectric wedge has been investigated. Finally, the research is limited to a rectangular wedge structure with a maximum of two wedges. As part of a thorough and realistic design, some calculations, assumptions, and choices are made.

1.7 Organization of the Thesis

In the following, we present a summary of the thesis chapters based on research objectives for UWB applications.

Chapter 2 presents a new TD diffraction coefficient based on the direct convolution method by taking inverse Laplace transform of FD diffraction coefficients that apply to the case when the source illuminates either one or both sides of the non-perfectly conducting wedge with arbitrary internal angles. The Gaussian 2nd order pulse is used as an input pulse in direct TD-UTD solution and its spectrum is used as an input signal in the IFFT-FD method. The TD results are related to the IFFT of FD results for the various scenario to verify accuracy. Finally,

the computational efficiency of direct TD and IFFT-FD techniques are presented for hard polarization.

Chapter 3 deals with a TD double diffraction based on the direct convolution method by taking inverse Laplace transform of FD diffraction coefficients that apply to the case when the source illuminates either one or both sides of the non-perfectly conducting wedge with arbitrary internal angles. The different reflection angles and improved reflection coefficients are applied in the outside sections of the wedge for formulating TD double diffraction. The Gaussian 2nd order pulse is used as an input pulse in direct TD-UTD solution and its spectrum is used as an input signal in the IFFT-FD method. The TD results are related to the IFFT of FD results to ensure accuracy. Finally, the computational efficiency of direct TD and IFFT-FD techniques are presented for hard polarization.

In general, the higher-order diffraction coefficient is used to consider multiple diffractions. As a result, the calculation becomes more complex does not take into account all possible orders of diffraction between the wedges. **Chapter 4** presents TD multiple-order diffraction coefficients based on the direct convolution method by taking inverse Laplace transform of FD formulation applied to the dual dielectric wedge. Only, the first-order TD-UTD coefficient is applied for finding the higher-order diffraction without using any higher-order diffraction technique such as slope diffraction coefficients. Therefore, this technique is modest and calculates all possible orders of diffractions. The Gaussian 2nd order pulse is used as an input pulse in direct TD-UTD solution and its spectrum is used as an input signal in the IFFT-FD method. The TD results are related to the IFFT of FD results to verify accuracy.

In **chapter 5**, a new time-domain six-term heuristic diffraction coefficient is proposed to consider the effect of diffraction and transmission from the dielectric wedge with an arbitrary low wedge angle for UWB applications. The different scenarios are considered to test the

overall performance of the TD solution. The results of TD-UTD are confirmed by the inverse fast Fourier transform (IFFT) of frequency-based results in hard polarization. The computational efficiency of the proposed TD-UTD solutions is demonstrated by comparing the time they have taken with their IFFT-FD solutions.

In **chapter 6**, we present a novel heuristic diffraction coefficient in frequency-domain (FD) for non-perfectly conducting wedges and buildings. A six-term diffraction coefficient which is an extension of the four-term UTD coefficient is proposed to include the effect of transmitted ray for a lossy dielectric wedge with arbitrary low wedge angle, thus, attaining the continuity of the total field all around the structure. Further, a time-domain (TD) solution based on the classical frequency domain result is proposed for UWB applications in indoor environments. Finally, a case of double diffraction for two consecutive buildings scenario is presented based on slope diffraction and their corresponding TD solution is also presented. All the TD results are verified with IFFT of the FD solutions in both the soft and hard polarization and the results are found to be in very good agreement. The impulse response of the channel is also presented to determine the distortion on the input pulse. The computational efficiency of the presented TD solutions is demonstrated by comparing them with their IFFT-FD solutions.

Finally, some concluding remarks and other indications for future work are presented in **Chapter 7**.

Chapter 2

A New Time-Domain Diffraction Coefficient for Non-Perfectly Conducting Wedges

In this chapter, a new TD diffraction coefficient based on the direct convolution method by taking inverse Laplace transform of FD diffraction coefficients that apply to the case when the source illuminates either one or both sides of the non-perfectly conducting wedge with arbitrary internal angles. The Gaussian 2^{nd} order pulse is used as an input pulse in direct TD-UTD solution and its spectrum is used as an input signal in the IFFT-FD method. The TD results are related to the IFFT of FD results for the various scenario to verify accuracy. Finally, the computational efficiency of the direct TD and IFFT-FD techniques are presented for hard polarization.

2.1 Background

Ultra-wideband (UWB) transmission has been a main motivation of research in the current time because of its possible ability to deliver a high data rate at a short distance using low power with decent resolution competence, a low-cost system and great bandwidth. UWB communication is NLOS communication due to the presence of several objects between sender and receiver. Thus, the incident pulse is distorted at the receiver due to the diffraction, reflection and refraction from the objects. Hence, the correct depiction of the propagation channel is required for the performance and best plan of the UWB system. The diffraction phenomenon of UWB pulses from the obstacles has a significant effect on the modelling of the UWB indoor propagation channel. In many works of literature [105-108], the heuristic diffraction coefficients from dielectric wedges were discussed to incorporate the effect of diffraction with

their merits and drawbacks. In [84], the works showed improvements in Holm's proposed method [106] with different reflection angles in the illumination region applied in the transition functions. Here, an improved reflection coefficient is presented for the sectors, where the modified reflection angles fail resulting in different FD coefficients for different sectors of illumination. The TD model has merits for the UWB application presented in [91]. However, TD-UTD solutions of [84] for UWB applications were not addressed in [85-99]. Therefore, in this chapter, a new TD diffraction coefficient based on the direct convolution method by taking inverse Laplace transform of FD diffraction coefficients [84] that apply to the case when the source illuminates either one or both sides of the non-perfectly conducting wedge with arbitrary internal angles. The Gaussian 2nd order pulse is used as an input pulse in direct TD-UTD solution and its spectrum is used as an input signal in the IFFT-FD method. The TD results are related to the IFFT of FD results for the various scenario to verify accuracy. Finally, the computational efficiency of direct TD and IFFT-FD techniques are presented for hard polarization.

2.2 Propagation Scenario

Fig. 2.1 shows the propagation path of diffraction with single side illumination (SSI) and double side illumination (DSI) from a non-perfectly conducting wedge. The edge of the wedge is representing the z-axis of polar coordinates. The incident angle ϕ' and diffracted angle ϕ are measured with the 0-face of the wedge. The interior angle φ is the wedge angle. 0-face and n-face of the wedge are defined at $\phi = 0$ and $\phi = n\pi$ with $\varphi = 2\pi - n\pi$. The spherical source is used to illuminate the faces of the wedge at a distance r_1. The transmitting and receiving points are represented by (r_1, ϕ') and (r_2, ϕ), respectively. There are three cases of illumination of wedge faces by the different positions of the transmitting antenna.

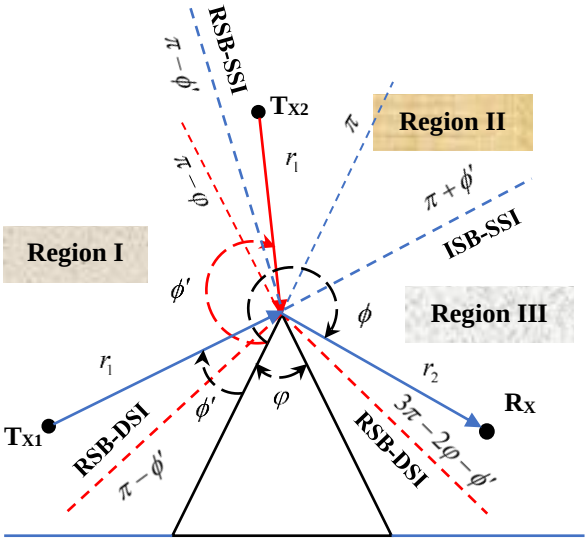

Fig. 2.1 The propagation path of diffraction with single side illumination (SSI) and double side illumination (DSI).

Case1: 0-face illumination $(\phi' < \pi - \varphi)$

In this case, 0-face is only illuminated. There may be three regions around the wedge due to different wave propagation. All the wave components (Incident, reflected and diffracted waves) exist in Region-I $(0 < \phi < \pi - \phi')$. The limiting boundary $(\phi = \pi - \phi')$ of the reflected wave is the reflection shadow boundary (RSB) in Region-I. Only incident and diffracted waves are in Region-II $(\pi - \phi' < \phi < \pi + \phi')$. The limiting boundary $(\phi = \pi + \phi')$ of the incident wave is the incident shadow boundary (ISB) in Region-II. Only diffracted waves exist in Region-III $(\pi + \phi' < \phi < 3\pi - \varphi - \phi')$. Region-III is the shadow region.

Case 2: 0-face and n-face illumination $(\pi - \varphi < \phi' < \pi)$

In this case, both the faces of the wedge are always illuminated. There may also be three regions around the wedge for different wave propagation. Region-I $(0 < \phi < \pi - \phi')$ consists of all the wave components (Incident, reflected and diffracted waves). It has a limiting boundary (reflection shadow boundary: RSB-DSI-I) at the angle $\phi = \pi - \phi'$. Region-II

$(\pi - \phi' < \phi < 3\pi - 2\varphi - \phi')$ consists of the only incident and diffracted waves. Region-III $(3\pi - 2\varphi - \phi' < \phi < 2\pi - \varphi)$ consists of all the wave components similar to Region-I. It has a limiting boundary (Reflection shadow boundary: RSB-DSI-II) at the angle $(\phi = 3\pi - 2\varphi - \phi')$.

Case 3: n-face illumination $(\phi' > \pi)$

In this case, the n-face is only illuminated. There may also be three regions around the wedge for different wave propagation. Region-I consists of only diffracted waves. It is the shadow region. It has a limiting boundary (incident shadow boundary: ISB-SSI (n face)) at the angle $\phi = \phi' - \pi$. Region-II$(\phi' - \pi < \phi < 2\pi - \phi')$ consists of the incident and diffracted waves. Region-III $(2\pi - \phi' < \phi < 2\pi - \varphi)$consists of all the wave components (incident, reflected and diffracted waves). It has a limiting boundary (reflection shadow boundary: RSB-SSI) at the angle $\phi = 2\pi - \phi'$.

2.3 Single Diffraction

2.3.1 FD SOLUTION

Three types of rays (incident, reflected and diffracted rays) are used in the ray-based method UTD as shown in Fig. 2.1. The received signal after single diffraction from non-perfectly conducting wedge under spherical wave propagation is given by [91]

$$E_{Rx} = \frac{E_i}{r_1} \cdot D_{s,h}(\omega) \cdot A(\mathrm{r}_2) \cdot \mathrm{e}^{-jk(r_1 + r_2)} \qquad (2.1)$$

where E_{Rx} is the received field. E_i is the transmitted field. r_1 is the distance from the transmitter to the diffracted point. r_2 is the distance from the diffracted point to the receiver. $k = \omega/c$ is the wavenumber. c is the speed of light. ω is the angular frequency. $A(r_2) = \sqrt{r_1 / (r_2 (r_1 + r_2))}$ is the

spreading factor. $j=\sqrt{(-1)}$ is an imaginary number. $D_{s,h}(\omega)$ is the diffraction coefficient for soft and hard polarization respectively. It is given by [84]

Case 1: Only 0-face illumination (i.e., incidence angle $\phi' \le (n-1)\pi$ with $n=2-\varphi/\pi$) as shown in Fig. 1,

$$D_{s,h}(\omega) = D_1 + R_0 R_n D_2 + R_0 D_3 + R_n D_4 . \qquad (2.2)$$

Case 2: Both face illumination (i.e., incidence angle $\phi' > (n-1)\pi$) as shown in Fig. 2.1, diffraction at $\phi > \left|(2n-1)\pi - \phi'\right|$

$$D_{s,h}(\omega) = D_1 + R_0 R_n D_2 + R_0 D_3 + R_n D_4 \qquad (2.3)$$

and diffraction at $\phi \le \left|(2n-1)\pi - \phi'\right|$

$$D_{s,h}(\omega) = D_1 + D_2 + \Upsilon_{s,h}(D_3 + D_4). \qquad (2.4)$$

Case 3: Only n-face illumination (i.e., incidence angle $\phi' > \pi$) as shown in Fig. 2.1,

$$D_{s,h}(\omega) = R_0 R_n D_1 + D_2 + R_n D_3 + R_0 D_4 \qquad (2.5)$$

where D_i with $i=1-4$ is given as in [106]

$$D_i = \frac{-e^{j\pi/4}}{2n\sqrt{2\pi k}} \cot(a_i) F\left[2kLn^2 \sin^2(a_i)\right] \qquad (2.6)$$

where $a_1 = \left[\pi - (\phi - \phi')\right]/(2n)$, and $a_2 = \left[\pi + (\phi - \phi')\right]/(2n)$ are defined for n-face and 0-face of the wedge related to the incident shadow boundary (ISB). While, $a_3 = \left[\pi - (\phi + \phi')\right]/(2n)$, and $a_4 = \left[\pi + (\phi + \phi')\right]/(2n)$ are defined for 0-face and n-face of the wedge related to the reflected shadow boundary (RSB). $L = r_1 r_2/(r_1 + r_2)$ is the distance parameter. $F(X)$ is the transition function which is given as in [91]

$$F[X] = 2j\sqrt{X}e^{jX}\int_{u=\sqrt{X}}^{u=\infty} e^{-ju^2}du = \sqrt{j\pi X}e^{jX}erfc\left(\sqrt{jX}\right) \qquad (2.7)$$

where $erfc(X)$ is the complementary error function with $X = 2kLn^2\sin^2(a_i)$ and $j = \sqrt{-1}$. The R_0 and R_n are the Fresnel reflection coefficient for $0-$ face and $n-$face which are given by [109]

$$R_{s,h} = \frac{\sin\theta_n - (1,1/\varepsilon)\sqrt{\varepsilon - \cos^2\theta_n}}{\sin\theta_n + (1,1/\varepsilon)\sqrt{\varepsilon - \cos^2\theta_n}} \qquad (2.8)$$

where θ_n is the reflection angles for $0-$ face and $n-$face as defined in [11]. $\varepsilon = \varepsilon_r - j\sigma/\omega\varepsilon_0$ is the complex permittivity. σ is the conductivity in S/m. $\varepsilon_0 = 8.854\times10^{-12}$ f/m is the permittivity of free space. ε_r is the relative permittivity. $\Upsilon_{s,h}$ is the modified reflection coefficient given in [84]

$$\Upsilon_{s,h} = \frac{(1,\varepsilon)\alpha - \sqrt{\varepsilon - 1 + \alpha^2}}{(1,\varepsilon)\alpha - \sqrt{\varepsilon - 1 + \alpha^2}} \qquad (2.9)$$

where

$$\alpha = \begin{cases} 2\sin\left(\frac{\phi}{2}\right)\sin\left(\frac{\phi'}{2}\right), & for\ \varphi < n\pi - \phi' \\ 2\sin\left(\frac{n\pi-\phi}{2}\right)\sin\left(\frac{n\pi-\phi'}{2}\right), & otherwise \end{cases}. \qquad (2.10)$$

2.3.2 TD SOLUTION

The impulse response of a single diffracted ray as shown in Fig. 2.1 can be given by taking Inverse Laplace Transform and setting $E_i = 1$ (with impulsive excitation) in (2.1). Therefore, the impulse response

$$h(t) = \frac{A(\mathrm{r}_2)}{r_1} \cdot \left[d_{s,h}(t) * \delta\left(t - (r_1 + r_2)/c\right) \right] \qquad (2.11)$$

where the delta function $\delta\left(t - (r_1 + r_2)/c\right)$ is related to a time shift. This is equal to the time that the transmitted signal requires to pass through the path to the receiver. The $d_{s,h}(t)$ is the TD diffraction coefficient for a non-perfectly conducting wedge which is given for different cases in (2.2-2.5) as

Case 1: Only 0-face illumination (i.e., incidence angle $\phi' \le (n-1)\pi$) as shown in Fig. 2.1,

$$d_{s,h}(t) = d_1 + r_0 * r_n * d_2 + r_0 * d_3 + r_n * d_4 . \qquad (2.12)$$

Case 2: Both face illumination (i.e., incidence angle $\phi' > (n-1)\pi$) as shown in Fig. 2.1, diffraction at $\phi > \left|(2n-1)\pi - \phi'\right|$

$$d_{s,h}(t) = d_1 + r_0 * r_n * d_2 + r_0 * d_3 + r_n * d_4 \qquad (2.13)$$

and diffraction at $\phi \le \left|(2n-1)\pi - \phi'\right|$

$$d_{s,h}(t) = d_1 + d_2 + \gamma_{s,h}(t) * (d_3 + d_4) . \qquad (2.14)$$

Case 3: Only n-face illumination (i.e., incidence angle $\phi' > \pi$) as shown in Fig. 2.1,

$$d_{s,h}(t) = r_0 * r_n * d_1 + d_2 + r_n * d_3 + r_0 * d_4 \qquad (2.15)$$

where $d_i(t)$ with $i = 1-4$ is given as in [108]

$$d^{(i)}(t) = -\frac{Ln}{2\pi\sqrt{2c}} \times \frac{\sin(2a_i)}{\sqrt{t}\left(t + 2Ln^2 \sin^2(\mathrm{a}_i)/c\right)} \cdot u(t) \qquad (2.16)$$

with $u(t)$ is the Heaviside step function. $r_{0,n,s,h}(t)$ is the TD Fresnel reflection coefficient of (2.8) for the $0-$ and $n-$ face respectively. This is given by [109]

$$r_{s,h}(t) = \mp\left[P\,\delta(t) + \frac{4p}{1-p^2}\frac{e^{-at}}{t}\sum_{q=1}^{\infty}(-1)^{q+1} qP^q I_q(at) \right] \qquad (2.17)$$

where $P_{s,h} = \left(1 - p_{s,h}\right)/\left(1 + p_{s,h}\right)$, $p_s = \sin\theta_n \Big/ \sqrt{\left(\varepsilon_r - \cos^2\theta_n\right)}$,

$p_h = \sqrt{\left(\varepsilon_r - \cos^2\theta_n\right)}\Big/\left(\varepsilon_r \cdot \sin\theta_n\right)$, $\delta(t)$ is the Dirac delta function, $I_q(t)$ is the modified Bessel function of order q, $a = \sigma/\left(2\varepsilon_r\varepsilon_0\right)$, and the leading $-(+)$ sign is for soft (hard) polarization. $\gamma_{s,h}(t)$ is the modified TD reflection coefficient which is given by taking inverse Laplace transform of (2.9)

$$\gamma_{s,h}(t) = \mp\left[\begin{array}{l} P'\,\delta(t) + \\ \dfrac{4p'}{1-\left(p'\right)^2}\dfrac{e^{-at}}{t}\displaystyle\sum_{q=1}^{\infty}(-1)^{q+1} q\left(P'\right)^q I_q(at) \end{array} \right] \qquad (2.18)$$

where $P'_{s,h} = \left(1 - p'_{s,h}\right)/\left(1 + p'_{s,h}\right)$, $p'_s = \alpha \Big/ \sqrt{\left(\alpha^2 + \varepsilon_r - 1\right)}$, and $p'_h = \sqrt{\left(\alpha^2 + \varepsilon_r - 1\right)}\Big/\left(\alpha \cdot \varepsilon_r\right)$.

In the next section, the TD outcomes are discussed for arbitrary internal angles of the wedge with the Gaussian doublet pulse [91] having a pulse length of 0.1 ns shown in Fig. 2.2 as an input pulse and its Gaussian spectrum is shown in Fig. 2.3 which is used in IFFT-FD solution as the input signal.

2.4 Results and Discussions

Considering hard polarization, Figs. 2.4-2.9 display the diffracted field at Rx that is located in the deep shadow region of the scenario with the wedge material of [109]. Three cases of the source illumination are applied as only 0-face, only n-face, or both sides of a wedge of Fig 2.1. In Fig. 2.1, $\varepsilon_r = 5$, $\sigma = 0.016$ S/m, receiver height=1m, wedge height=2m and distance from the centre of the wedge= 2m. Here, the results are presented for different incident angles and wedge angles concerning the cases of face illuminations. The attenuation and waveform

distortion in received signals is achieved due to the only diffraction phenomenon in the shadow region of the structure and frequency dependence behaviour of UWB signals.

Gaussian doublet pulse [91] shown in Fig. 2.2 is used to test the TD solutions proposed. This pulse is crossing the zero line two times with a Gaussian shape. Hence, it is called the 2nd order Gaussian pulse. It has the time-scaling factor $\tau = 0.1$ ns .

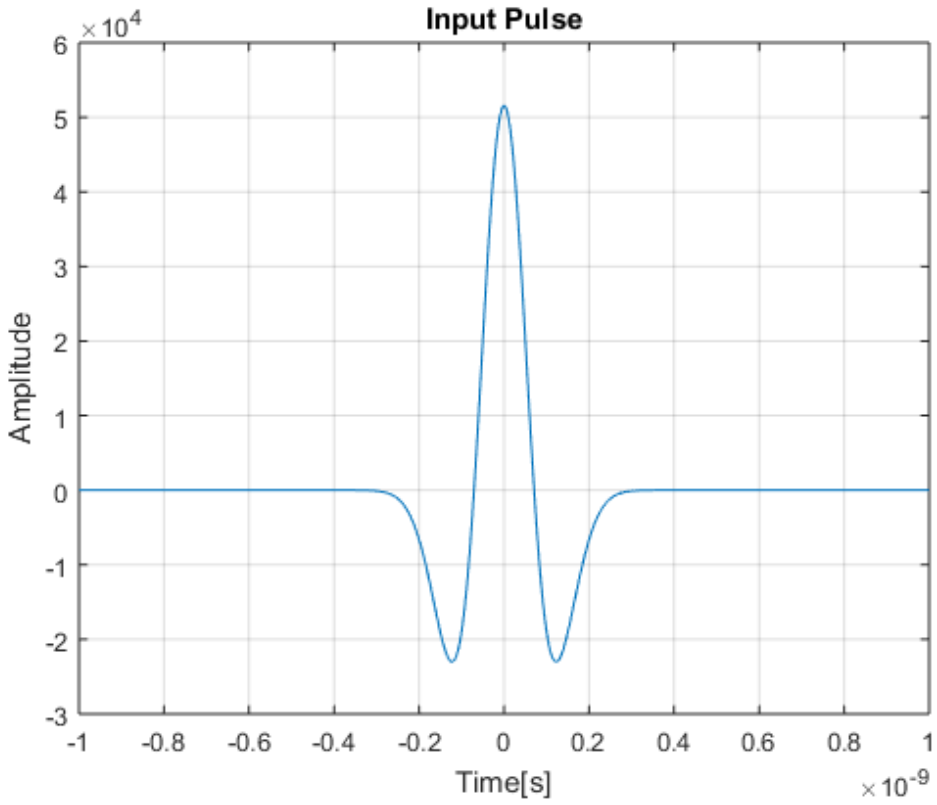

Fig. 2.2 The 2nd order Gaussian input pulse.

The Gaussian doublet pulse spectrum shown in Fig. 2.3 is used in IFFT-FD solutions as input pulse in FD. This spectrum has a frequency range of UWB signals. Therefore, the pulse is used as a transmitted pulse of UWB signals with a short duration in ns.

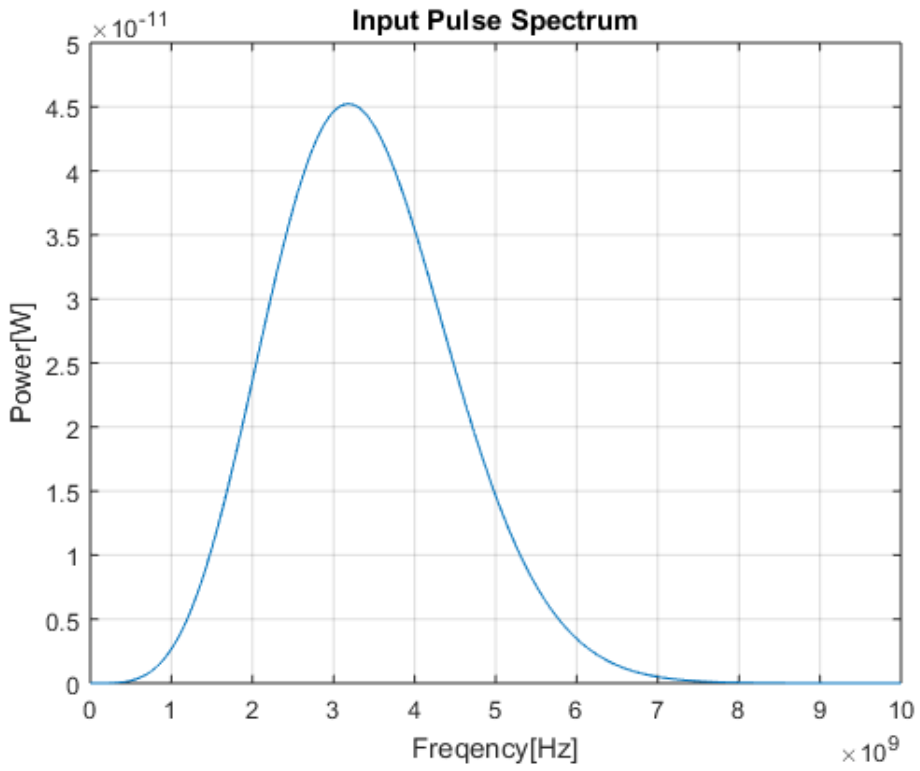

Fig. 2.3 Gaussian doublet pulse spectrum.

Figs. 2.4 and 2.5 are the case of 0-face illumination for different wedge angles. In this case, there is a reflection and incidence shadow boundary. Both the TD and IFFT-FD solutions are matching to each other. Therefore, it confirms the accuracy of the proposed TD solution. The incident pulses are attenuated and distorted after the diffraction from the non-perfectly conducting wedges. This attenuation is due to the lossy behaviour of wedges. While this distortion is due to the frequency dependence of the TD diffraction coefficients.

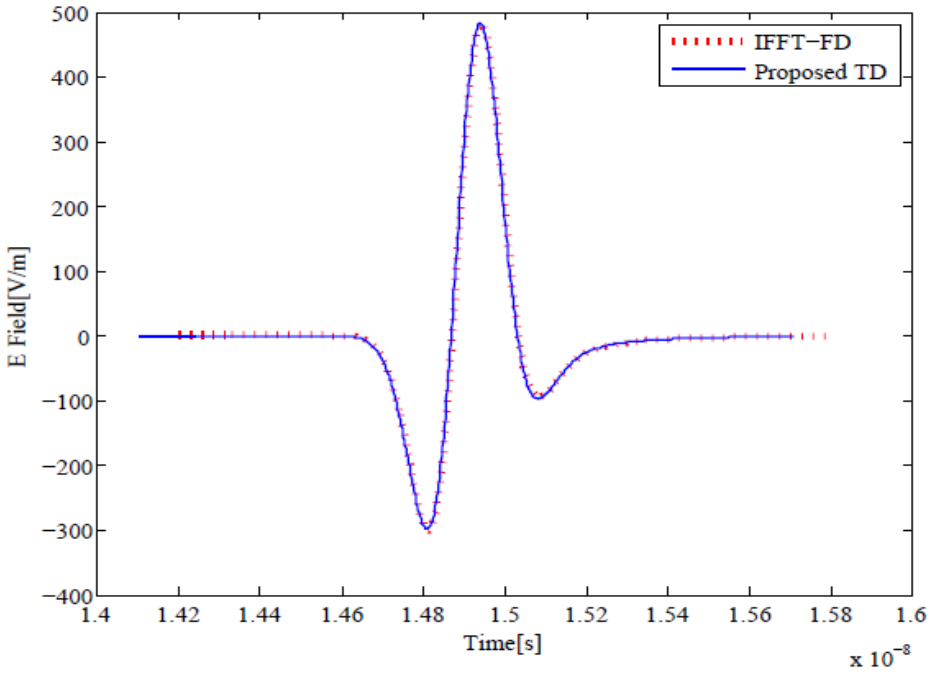

Fig. 2.4 The IFFT-FD and direct TD diffracted fields with wedge internal angle $\varphi = 50°$ and incidence angle $\phi' = 5°$.

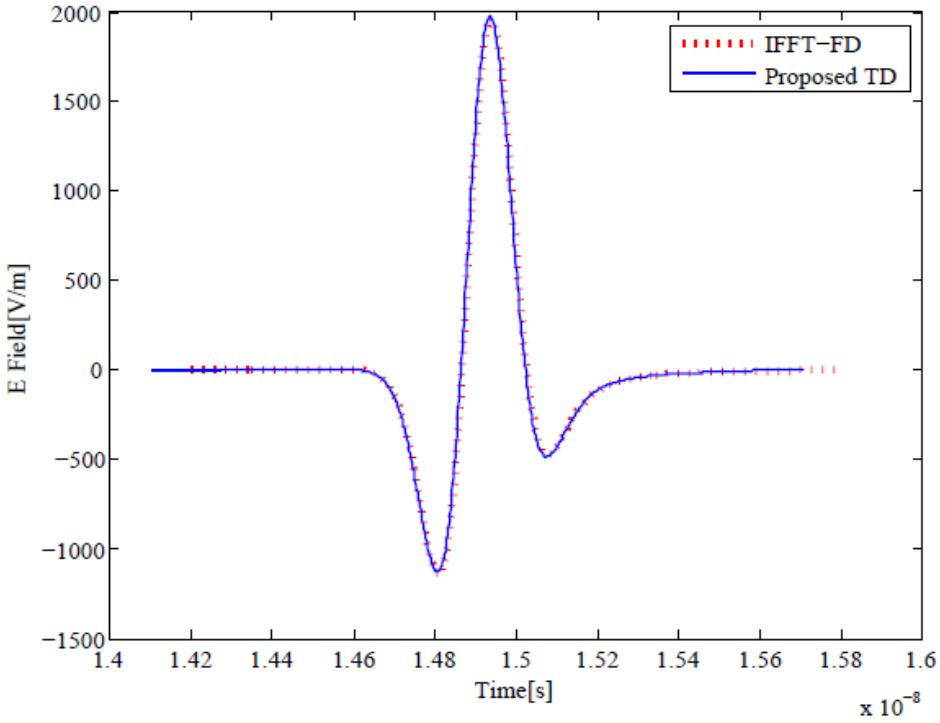

Fig. 2.5 The IFFT-FD and direct TD diffracted fields with wedge internal angle $\varphi = 150°$ and incidence angle $\phi' = 5°$.

Figs. 2.6 and 2.7 are the case of both-face illumination of the wedges of different internal angles. In this case, no incidence shadow boundary exists and only, two reflection shadow boundary exists. Therefore, the incident pulses are highly attenuated and distorted. But, the TD response is completely matching with the IFFT-FD response. Hence, the accuracy of the proposed TD solution is confirmed.

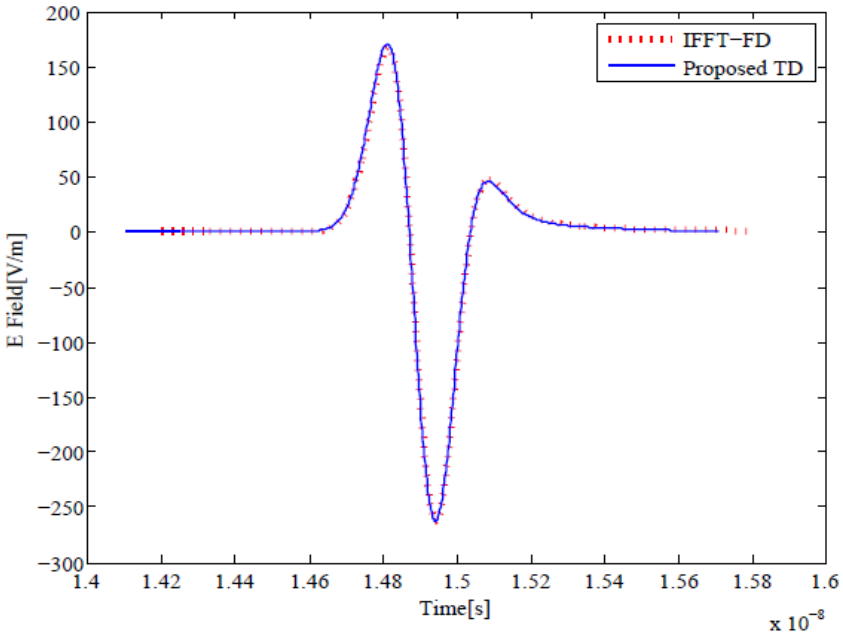

Fig. 2.6 The IFFT-FD and direct TD diffracted fields with wedge internal angle $\varphi = 50°$ and incidence angle $\phi' = 145°$.

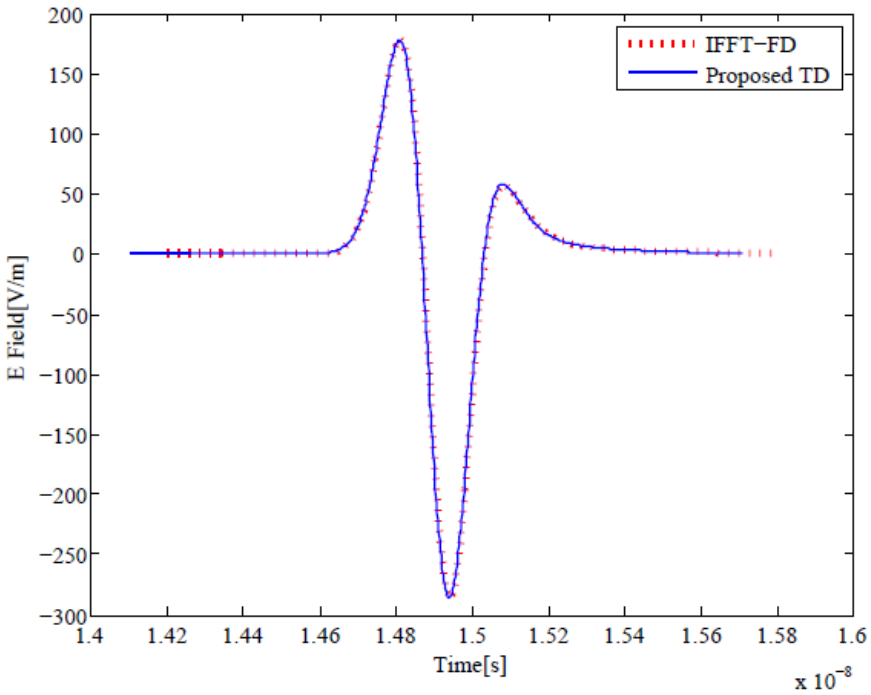

Fig. 2.7 The IFFT-FD and direct TD diffracted fields with wedge internal angle $\varphi = 150°$ and incidence angle $\phi' = 145°$.

Figs. 2.8 and 2.9 are the case of n-face illumination of the non-perfectly conducting wedges of different internal angles. In this case, there is an incidence and reflection shadow boundary. Here, the incidence angle is very high. Therefore, the Gaussian doublet pulse is extremely attenuated and distorted due to the same reason stated earlier. Both the TD response and IFFT-FD response are matching to each other. Hence, the proposed method is accurate.

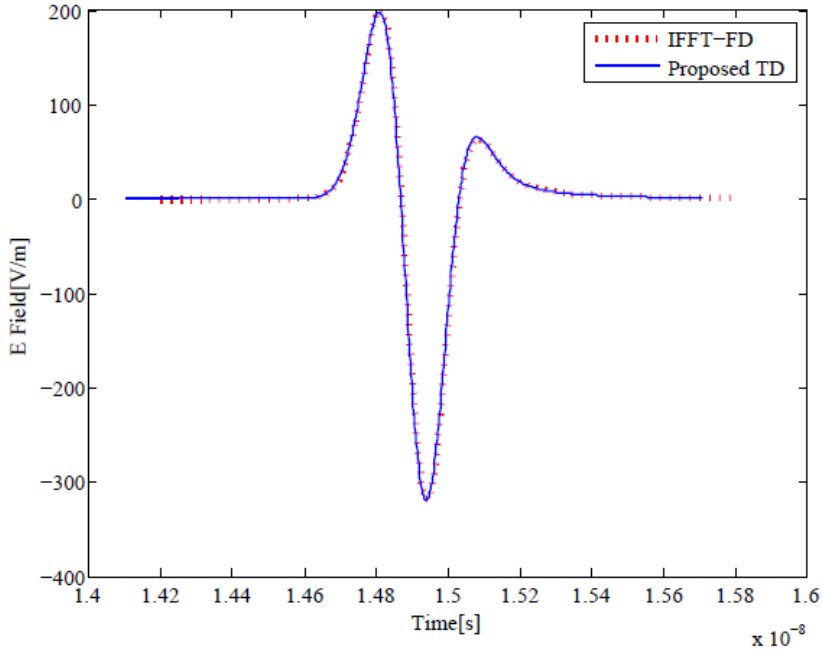

Fig. 2.8 The IFFT-FD and direct TD diffracted fields with wedge internal angle $\varphi = 50°$ and incidence angle $\phi' = 225°$.

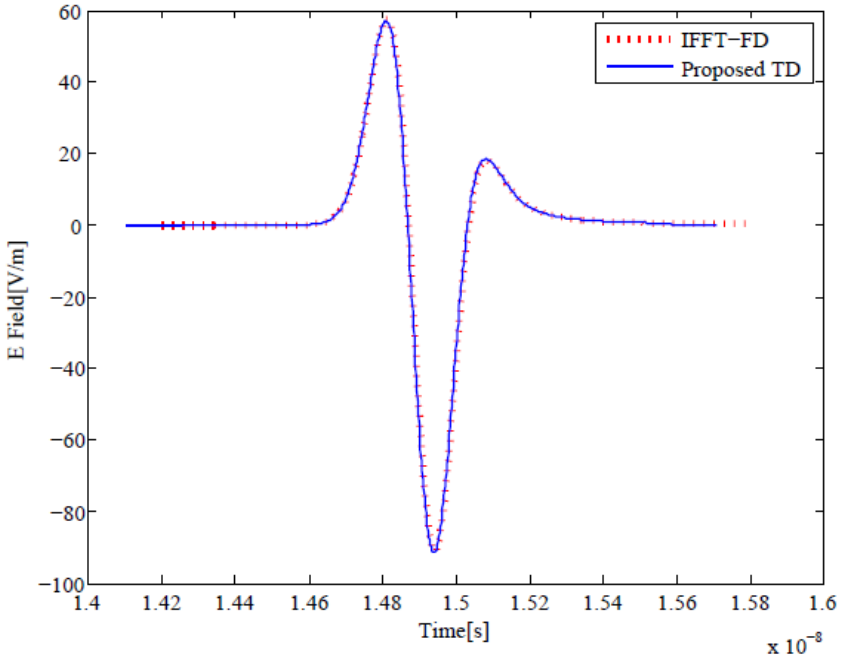

Fig. 2.9 The IFFT-FD and direct TD diffracted fields with wedge internal angle $\varphi = 150°$ and incidence angle $\phi' = 225°$.

The benefit of the proposed algorithm is the saving on the computation time when the prediction of the received waveform is carried out directly in the time-domain rather than calculating the numerical inverse Fourier transform of the corresponding FD received signal. This can be seen in Table 2.1, where the average ratios of the computation times of the two methods $T_{IFFT-FD}/T_{TD}$ are presented, for the scenarios similar to Fig. 2.1 with only 0-face, 0- and n-face, and only n-face illumination from the source. This is due to the direct TD method based on convolution technique, where all the frequencies are treated simultaneously. Whereas, the IFFT-FD method would involve the calculation of the radio propagation effects for each frequency separately, which is very inefficient for very large bandwidths particularly for UWB applications. Hence, TD is the preferred domain, as long as we can employ simple closed forms for the prediction of the radio wave propagation for every path.

Table 2.1 Computational efficiency of proposed TD solution

Illumination face	Wedge angle	Incident angle	$T_{IFFT-FD}/T_{TD}$ (Ratio of time taken by the IFFT-FD method and the direct TD method)
0-face	50°	5°	17.1210
0-face	150°	5°	30.3229
0-and n-face	50°	145°	17.8972
0-and n-face	150°	145°	16.9206
n-face	50°	225°	17.2395
n-face	150°	225°	22.1955

2.5 Conclusion

In this chapter, a new TD diffraction coefficient based on the direct convolution method by taking inverse Laplace transform of FD diffraction coefficients that apply to the case when the source illuminates either one or both sides of the non-perfectly conducting wedge with arbitrary

internal angles is presented. The Gaussian 2nd order pulse is used as an input pulse in direct TD-UTD solution and its spectrum is used as an input signal in the IFFT-FD method. The TD results are related to the IFFT of FD results for the various scenario and the accuracy is verified. Finally, the computational efficiency of the direct TD and the IFFT-FD techniques are presented for hard polarization. It proves that the direct TD technique is efficient than the IFFT-FD technique.

Chapter 3

A Time-domain Double Diffraction for Non-perfectly Conducting Wedges

This chapter deals with a TD double diffraction based on the direct convolution method by taking inverse Laplace transform of FD diffraction coefficients that apply to the case when the source illuminates either one or both sides of the non-perfectly conducting wedge with arbitrary internal angles. The different reflection angles and improved reflection coefficients are applied in the outside sections of the wedge for formulating TD double diffraction. The Gaussian 2nd order pulse is used as an input pulse in direct TD-UTD solution and its spectrum is used as an input signal in the IFFT-FD method. The TD results are related to the IFFT of FD results to ensure accuracy. Finally, the computational efficiency of direct TD and IFFT-FD techniques are presented for hard polarization.

3.1 Background

The key features of growing attention in the ultrawideband communication system (UWB) are due to high-speed connectivity, high data rates, low equipment costs, and low system complexity [110]. Very short pulse time (impulse-like signals), usually a fraction of 1 ns are used in such systems for transmission and reception. Short pulse time is defined in the frequency range as a signal with very large bandwidth. It is natural to work in the TD due to the consideration of all the frequency components at the same time. The parameters required in the UWB system, for example, the number of multipath signals, power, delay and distortion of each path are readily available in the TD profile. This looks and works better in direct operation on TD than using numerical inverse fast Fourier transform procedures to convert FD

solutions into TD. The latter will include calculating the effects of radio propagation on each frequency range, which does not work well on very large bandwidths. The resulted impulse response is treated as a standard solution, regardless of the bandwidth, which is convolved by any incident signal.

Few heuristic FD models for dielectric wedges were introduced in [105-108]. The model [84] delivers enhancement over the model in [106] in the case of both face illumination. The emphasis on multiple diffractions among the wedges was presented in [111-112]. The field because of the multiple diffractions has a great impact on the shadow region. The TD radio channel models are favoured over the FD models for UWB applications. In TD models, the study of transient scattering performance of UWB signals is possible and all the frequency components are dealt with simultaneously. In the works of literature [85-96], [99], the case of double diffraction in TD was presented for single face illumination. But, the case of both face illumination [84] has not been addressed for non-perfectly conducting wedges. Therefore, this chapter presents a TD double diffraction based on the direct convolution method by taking inverse Laplace transform of FD diffraction coefficients of [84] that apply to the case when the source illuminates either one or both sides of the non-perfectly conducting wedge with arbitrary internal angles. The different reflection angles and improved reflection coefficients are applied in the outside sections of the wedge for formulating TD double diffraction. The Gaussian 2nd order pulse is used as an input pulse in direct TD-UTD solution and its spectrum is used as an input signal in the IFFT-FD method. The TD results are related to the IFFT of FD results to ensure accuracy. Finally, the computational efficiency of direct TD and IFFT-FD techniques are presented for hard polarization.

3.2 TD Techniques and Calculation of Singularity

Wireless systems are tested on measurements and simulations. However, a simulation-based approach is preferred to a measurement-based approach as the latter is site-specific and time-consuming. The time-domain (TD) solution of UWB systems is more efficient and less time consuming than the FD solutions due to the greater operating frequency of UWB signals [103]. There are the following ways to get a time-domain response:

3.2.1 Convolution Technique

If $x(t)$ is the transmitted UWB pulse, $h(t)$ is the channel response, then the output response $y(t)$ is represented mathematically as [113]

$$y(t) = x(t) * h(t) = \int_0^t x(\tau) \cdot h(t-\tau) \cdot d\tau \tag{3.1}$$

where $*$ and $\cdot$ are the sign of convolution and multiplication.

3.2.2 Inverse Fourier Transform (IFT)

The Inverse Fourier Transform can be used to obtain a TD solution $y(t)$ from a given FD solution $Y(\omega)$ [114],i.e.,

$$y(t) = \frac{1}{2\pi} \cdot \int_{-\infty}^{\infty} Y(\omega) e^{j\omega t} d\omega \tag{3.2}$$

where the angular frequency is ω. One side of the Fourier transform can be described as

$$y^{+}(t) = \frac{1}{\pi} \cdot \int_{0}^{\infty} Y(\omega) e^{j\omega t} d\omega \tag{3.3}$$

where TD solution $y^{+}(t)$ is a complex solution and a causal function. The real and imaginary part of the same is even and an odd function. Therefore, the analytic solution can be written as

$$y^{+}(t) = y(t) + jH\left[y(t)\right] \tag{3.4}$$

where $H\left[y(t)\right]$ is Hilbert's transform of $y(t)$ and can be provided as

$$\begin{aligned} H\left[y(t)\right] &= \frac{1}{\pi} \cdot \mathrm{pv} \int_{-\infty}^{\infty} y(\tau)(t-\tau)^{-1} d\tau \\ &= \frac{1}{2\pi} \cdot \int_{-\infty}^{\infty} (-j)\,\mathrm{sgn}(\omega) Y(\omega) e^{j\omega t} d\omega \end{aligned} \tag{3.5}$$

where the pv and the $\mathrm{sgn}(\omega)$ are Cauchy principal value integration and signum function. The exact TD solution y(t) in (3.4) is the real part of the analytic solution in (3.3).

3.2.3 Inverse Laplace Transform (ILT)

Alternative inverse Laplace transform may make it easier to obtain a TD solution from the FD solution provided in most cases. Equation (3.2) can be replaced by substituting $j\omega$ with s as

$$y(t) = \frac{1}{2\pi} \cdot \int_{-\infty}^{\infty} Y(s) e^{st} ds \tag{3.6}$$

where $Y(s)$ is the Laplace transform of $y(t)$. The left-hand side of the imaginary axis of the s-plane should have all the poles of $Y(s)$.

3.2.4 Inverse Fast Fourier Transform (IFFT)

Usually, we get a discrete FD solution after simulation. In this case, a higher angular frequency is preferred than the transmitted angular frequency without loss of generality. Thereafter, IFFT is used to obtain the TD solution from the FD solution.

3.2.5 Calculation of Singularity in the System Response

The system response $y(0)$ is evaluated at $t = 0$ in (3.1). But in some cases, there is a singularity at $t = 0$ when $t \to 0, 1/\sqrt{t} \to \infty$. As a result, the waveform of the system response is distorted. Let, $h(t)$ has a singularity in the time domain in (3.1). An effective method is used to remove this singularity from [12-13] as follows:

$$x(t) * \int_0^t h(t)\,dt = \int_0^t \left(x(t) * h(t)\right) dt \tag{3.7}$$

In (3.7), the singularity of $h(t)$ was removed by the integration $\int_0^t h(t)\,dt$. The evaluation of the integral is performed in numerically or closed form.

3.3 Propagation Scenario

Fig. 3.1 shows the propagation path of double diffraction with single side illumination (SSI) and double side illumination (DSI) from a non-perfectly conducting wedge.

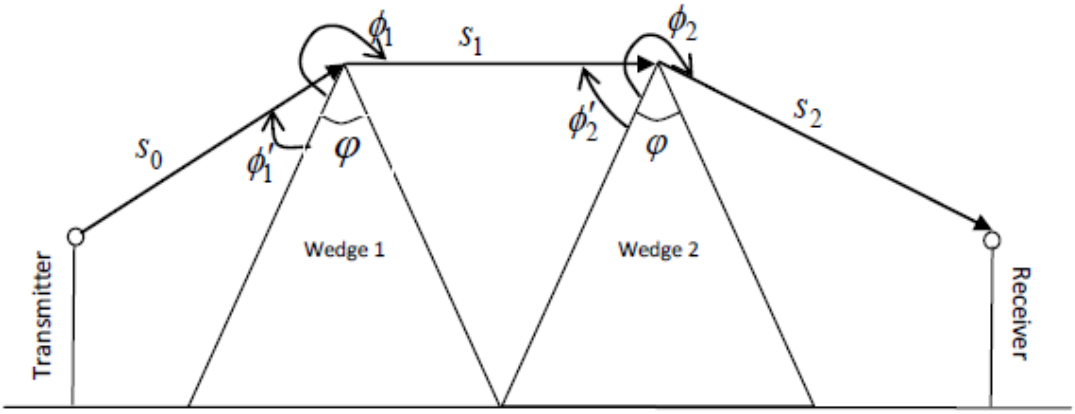

Fig. 3.1 The propagation path of the double-diffracted signal.

The edge of the wedge is representing the z-axis of polar coordinates. The incident angle ϕ_1' and diffracted angle ϕ_1 are measured with the 0-face of wedge 1. The incident angle ϕ_2' and diffracted angle ϕ_2 are measured with the 0-face of wedge 2. The interior angle φ is the wedge angle. The spherical source is used to illuminate the faces of wedge 1 at a distance s_0. The distance between the wedges is s_1. The transmitting and receiving points are represented by (s_0, ϕ_1') and (s_2, ϕ_2), respectively. There are three cases of illumination of wedge 1 faces by the different positions of the transmitting antenna.

3.4 Formulation of Double Diffraction

3.4.1 Frequency-domain Formulation

The FD single diffraction coefficients for a single wedge structure is given by [84]

$$D^{s,h} = \begin{cases} R_0 R_n D^{(1)} + D^{(2)} + R_0 D^{(3)} + R_n D^{(4)}, \\ for\ \phi' \le (n-1)\pi \cup \left(\phi' > (n-1)\pi \cap \phi > \left|(2n-1)\pi - \phi'\right|\right). \\ \\ D^{(1)} + R_0 R_n D^{(2)} + R_n D^{(3)} + R_n D^{(4)}, \\ for\ \phi' > \pi \\ \\ D^{(1)} + D^{(2)} + \Gamma^{s,h}\left(D^{(3)} + D^{(4)}\right), \\ for\ \phi' > (n-1)\pi \cap \phi \le \left|(2n-1)\pi - \phi'\right| \end{cases} \tag{3.8}$$

where $D^{(i)}$ with $i = 1-4$ given as in [106]. The R_0 and R_n are the Fresnel reflection coefficient for 0 − face and n – face same as (2.8) of Chapter 2. ϕ and ϕ' are the diffracted angle and incident angle for a single wedge structure. $\Gamma^{s,h}$ is the modified reflection coefficient same as (2.9) of Chapter 2.

$$\Gamma^{s,h} = \frac{(1,\varepsilon)\alpha - \sqrt{\varepsilon - 1 + \alpha^2}}{(1,\varepsilon)\alpha - \sqrt{\varepsilon - 1 + \alpha^2}} \tag{3.9}$$

where, $\varepsilon = \varepsilon_r - j\sigma/\omega\varepsilon_0$ and

$$\alpha = \begin{cases} 2\sin\left(\frac{\phi}{2}\right)\sin\left(\frac{\phi'}{2}\right), & for\ \varphi < n\pi - \phi' \\ 2\sin\left(\frac{n\pi - \phi}{2}\right)\sin\left(\frac{n\pi - \phi'}{2}\right), & otherwise \end{cases} \tag{3.10}$$

with φ is the wedge angle. The received field afterwards the double diffraction is specified by [106]

$$E_{RD} = \frac{E_0 e^{-jk(s_0+s_1+s_2)}}{\sqrt{s_0 s_1 s_2 (s_0+s_1+s_2)}} \times \left[D_1 D_2 - \frac{1}{jks_1} \frac{\partial D_1(\phi_1, \phi_1')}{\partial \phi_1} \frac{\partial D_2(\phi_2, \phi_2')}{\partial \phi_2'} \right] \tag{3.11}$$

In (3.11), only the first and second-order field has been considered for simplicity. $D_1(\phi_1, \phi_1')$ and $D_2(\phi_2, \phi_2')$ are the first-order diffraction coefficients of the first and second wedge. $\frac{\partial D_1(\phi_1, \phi_1')}{\partial \phi_1}$ and $\frac{\partial D_2(\phi_2, \phi_2')}{\partial \phi_2'}$ are the slope diffraction coefficients and they can be defined as [62,79].

3.4.2 Time-domain Formulation

Taking inverse Laplace transform of (3.8), the TD solution is given as in [115]

$$d^{s,h}(t) = \begin{cases} r_0(t) * r_n(t) * d^{(1)}(t) + d^{(2)}(t) + \\ r_0(t) * d^{(3)}(t) + r_n(t) * d^{(4)}(t), \\ for\ \phi' \le (n-1)\pi \cup \\ \left(\phi' > (n-1)\pi \cap \phi > \left|(2n-1)\pi - \phi'\right|\right). \\ \\ d^{(1)}(t) + r_0(t) * r_n(t) * d^{(2)}(t) + \\ r_n(t) * d^{(3)}(t) + r_0(t) * d^{(4)}(t), \quad for\ \phi' > \pi. \\ \\ d^{(1)}(t) + d^{(2)}(t) + \gamma(t) * \left(d^{(3)}(t) + d^{(4)}(t)\right), \\ for\ \phi' > (n-1)\pi \cap \phi \le \left|(2n-1)\pi - \phi'\right|. \end{cases} \tag{3.12}$$

$d^{(i)}(t), \quad (i = 1-4)$ in the above formulations is specified as in [91]

$$d^{(i)}(t) = -\frac{Ln}{2\pi\sqrt{2c}} \times \frac{\sin(2\varsigma_i)}{\sqrt{t\left(t + 2Ln^2 \sin^2(\varsigma_i)/c\right)}} \cdot u(t) \tag{3.13}$$

$\gamma(t)$ is given by taking inverse Laplace transform of (3.9) as

$$\gamma(t) = \mp\left[\frac{1-k}{1+k}\delta(t) + \frac{4k}{1-k^2}\frac{e^{-xt}}{t} \times \sum_{n=1}^{\infty}(-1)^{n+1} n k^n I_n(xt)\right] \tag{3.14}$$

with $k = \left(\frac{\sqrt{\alpha^2 + \varepsilon_r - 1}}{\alpha}\right)^{-1}$ for soft polarization, $k = \left(\frac{\sqrt{\alpha^2 + \varepsilon_r - 1}}{\alpha \cdot \varepsilon_r}\right)$ for hard polarization and $x = \frac{\sigma}{2\varepsilon_0 \varepsilon_r}$. The leading $-(+)$ sign is for soft (hard) polarization. $I_n(t)$ is the modified Bessel function n. Taking inverse Laplace transform of (3.11), the field in TD

$$e_{RD}(t) = e_0(t) * \left[\begin{array}{l} \sqrt{\frac{1}{(s_0 + s_1 + s_2)s_0 s_1 s_2}} \times \\ \left[d_1(t) * d_2(t) - \frac{1}{s_1} d_1^f(t) * d_2^f(t)\right] \\ * \delta\left(t - \frac{s_0 + s_1 + s_2}{c}\right) \end{array}\right] \tag{3.15}$$

where, $d_1(t)$ and $d_2(t)$ are the single order diffraction coefficients in TD from wedge 1 and wedge 2 as (3.12). In (3.15), the derivatives of TD reflection coefficients are made simple by the early time estimate as in [92] assuming that the derivatives of FD reflection coefficients do not fluctuate ω. Thus, the R_0 and R_n in (3.8) are revised by substituting $\varepsilon \approx \varepsilon_r$ as follows

$$R^{s,h} = \frac{\sin\psi - (1,1/\varepsilon_r)\sqrt{\varepsilon_r - \cos^2\psi}}{\sin\psi + (1,1/\varepsilon_r)\sqrt{\varepsilon_r - \cos^2\psi}} \tag{3.16}$$

where the reflection angle ψ is stated as in [84]. The (3.9) is also revised by substituting $\varepsilon \approx \varepsilon_r$. Then, the $d_1^f(t)$ and $d_2^f(t)$ of (3.15) are defined using the concept of [92]

$$d_1^{\,f}(t) = L^{-1}\left\{\frac{1}{\sqrt{jk}}\frac{\partial D_1}{\partial \phi_1}\right\}$$

$$= \frac{-L}{\sqrt{2\pi}}\begin{bmatrix} R_0 R_n F_s^{(1)}(t) - F_s^{(2)}(t) + R_0 F_s^{(3)}(t) - \\ R_n F_s^{(4)}(t), \quad for\ \phi' \le (n-1)\pi \cup \\ \left(\phi' > (n-1)\pi \cap \phi > \left|(2n-1)\pi - \phi'\right|\right). \\ \\ F_s^{(1)}(t) - R_0 R_n F_s^{(2)}(t) + R_n F_s^{(3)}(t) - \\ R_0 F_s^{(4)}(t), \quad for\ \phi' > \pi. \\ \\ F_s^{(1)}(t) - F_s^{(2)}(t) + \Gamma\left(F_s^{(3)}(t) - F_s^{(4)}(t)\right), \\ for\ \phi' > (n-1)\pi \cap \phi \le \left|(2n-1)\pi - \phi'\right|. \end{bmatrix} \tag{3.17}$$

$$+ \frac{c}{2n\sqrt{2\pi}} \times$$

$$\begin{bmatrix} R_0 \dfrac{\partial R_n}{\partial \psi}\cot(\varsigma_1)\dfrac{\sqrt{a_1}}{\sqrt{t+a_1}} + \dfrac{\partial R_n}{\partial \psi}\cot(\varsigma_4)\dfrac{\sqrt{a_4}}{\sqrt{t+a_4}} \\ R_0 \dfrac{\partial R_n}{\partial \psi}\cot(\varsigma_2)\dfrac{\sqrt{a_2}}{\sqrt{t+a_2}} + \dfrac{\partial R_n}{\partial \psi}\cot(\varsigma_3)\dfrac{\sqrt{a_3}}{\sqrt{t+a_3}} \\ \dfrac{\partial \Gamma}{\partial \varphi_1}\left[\cot(\varsigma_3)\dfrac{\sqrt{a_3}}{\sqrt{t+a_3}} + \cot(\varsigma_4)\dfrac{\sqrt{a_4}}{\sqrt{t+a_4}}\right] \end{bmatrix}$$

and

$$d_2^f(t) = L^{-1}\left\{\frac{1}{\sqrt{jk}}\frac{\partial D_2}{\partial \varphi_2'}\right\}$$

$$= \frac{-L}{\sqrt{2\pi}}\begin{bmatrix} -R_0R_nF_s^{(1)}(t) + F_s^{(2)}(t) + R_0F_s^{(3)}(t) - R_nF_s^{(4)}(t), \\ for\ \phi' \le (n-1)\pi \cup \\ \left(\phi' > (n-1)\pi \cap \phi > \left|(2n-1)\pi - \phi'\right|\right). \\ \\ -F_s^{(1)}(t) + R_0R_nF_s^{(2)}(t) + R_nF_s^{(3)}(t) - R_0F_s^{(4)}(t), \\ for\ \phi' > \pi. \\ \\ -F_s^{(1)}(t) + F_s^{(2)}(t) + \Gamma\left(F_s^{(3)}(t) - F_s^{(4)}(t)\right), \\ for\ \phi' > (n-1)\pi \cap \phi \le \left|(2n-1)\pi - \phi'\right|. \end{bmatrix} \tag{3.18}$$

$$+ \frac{-c}{2n\sqrt{2\pi}}\begin{bmatrix} \frac{\partial R_0}{\partial \psi}R_n\cot(\varsigma_1)\frac{\sqrt{a_1}}{\sqrt{t+a_1}} + \frac{\partial R_0}{\partial \psi}\cot(\varsigma_3)\frac{\sqrt{a_3}}{\sqrt{t+a_3}} \\ \frac{\partial R_0}{\partial \psi}R_n\cot(\varsigma_2)\frac{\sqrt{a_2}}{\sqrt{t+a_2}} + \frac{\partial R_0}{\partial \psi}\cot(\varsigma_4)\frac{\sqrt{a_4}}{\sqrt{t+a_4}} \\ \frac{\partial \Gamma}{\partial \varphi_2'}\left[\cot(\varsigma_3)\frac{\sqrt{a_3}}{\sqrt{t+a_3}} + \cot(\varsigma_4)\frac{\sqrt{a_4}}{\sqrt{t+a_4}}\right] \end{bmatrix}$$

where, $F_s^{(i)}(t) = \frac{\sqrt{a_i}}{2(t+a_i)^{3/2}} \cdot u(t)$ and $a_i = 2Ln^2\sin^2(\varsigma_i)/c$.

In the following section, the TD results are deliberated for different face illumination. The incident pulse [91] having full width half maximum pulse duration of 0.1 *ns* shown in Fig. 2.2 as an input pulse and its Gaussian spectrum is shown in Fig. 2.3 which is used in the IFFT-FD solution as the input signal. Fig. 3.1 consists of two wedges and its parameters are given in Table 3.1.

3.5 Results Analysis

Fig. 3.2 - Fig. 3.4 display the TD electric fields at the receiver due to double diffraction in hard polarization. The wedge material has $\varepsilon_r = 10$ and $\sigma = 0.001\,S/m$. Now, three cases of face illumination are considered for wedge structure as in [109]. The good agreement of TD and IFFT-FD results proves the accuracy of the TD solution.

In Fig. 3.2, only the 0-face of the wedge is illuminated by the spherical source. It can be observed that the double diffracted field has been extremely attenuated and distorted in comparison to the input 2nd order Gaussian pulse due to the double diffraction and frequency dependence of UWB signals.

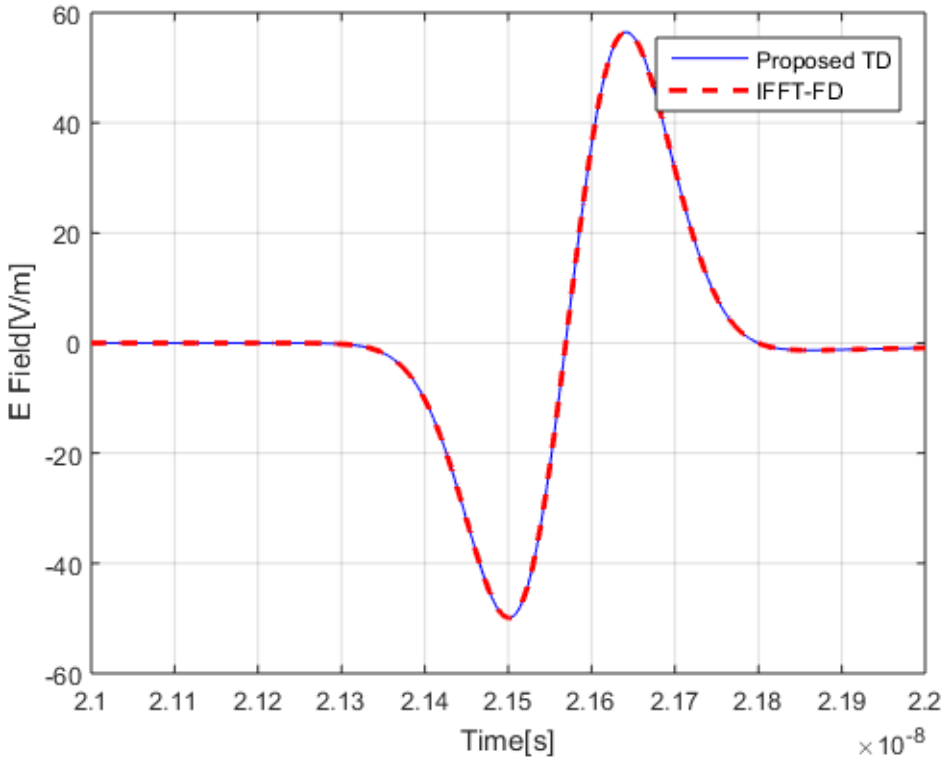

Fig. 3.2 TD double diffracted fields at the receiver for $\varphi = 30°$, $\phi_1' = 10°$, $\phi_1 = 255°$, $s_1 = 2\,\text{m}$, $s_2 = 2\,\text{m}$, Receiver Height=2m, and Wedge Height= 3m.

In Fig. 3.3, the source illuminates both faces of the wedge. In this case, the received pulse is similar to the source pulse in shape but highly attenuated due to double diffraction.

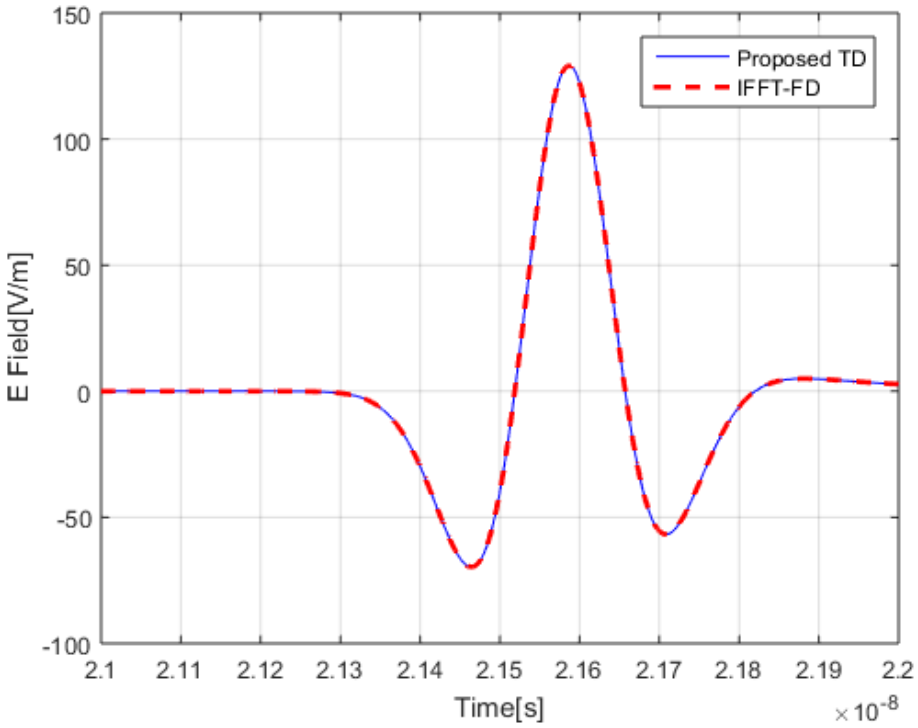

Fig. 3.3 TD double diffracted fields at the receiver for $\varphi = 30°$, $\phi_1' = 155°$, $\phi_1 = 327°$, $s_1 = 2$ m, $s_2 = 2$ m, Receiver Height=2m, and Wedge Height= 3m.

In Fig. 3.4, only the n-face is illuminated by the source. In this case, again the received pulse is highly attenuated and distorted due to the same reason stated earlier in case 1. The direct TD result and the equivalent IFFT-FD result are completely matching to each other. Hence, the accuracy of the stated techniques is confirmed.

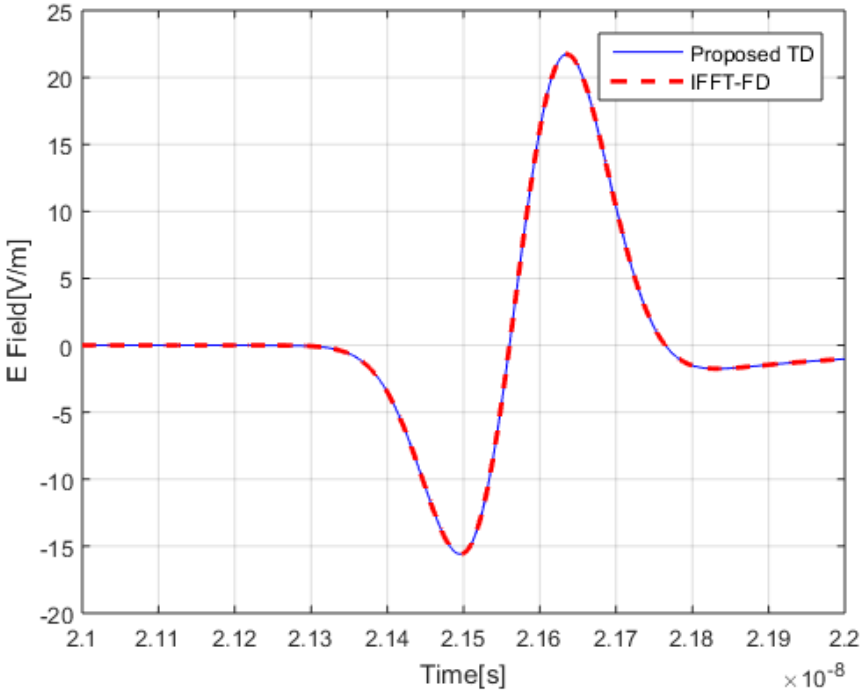

Fig. 3.4 TD double diffracted fields at the receiver for $\varphi = 30°$, $\phi_1' = 190°$, $\phi_1 = 255°$, $s_1 = 2$ m, $s_2 = 2$ m, Receiver Height=2m, and Wedge Height= 3m.

Finally, Table 3.1 shows the comparison of the computational times taken by IFFT-FD and proposed TD solutions. Clearly, it can be observed that the TD solution takes less computation time to provide the simulation results and so outperforms the IFFT-FD method. This significant time saving is because of the efficient convolution technique used in TD method. This is also due to the fact that the short duration Gaussian pulses directly correspond to very huge bandwidth in FD and will require the computations for each frequency component separately that is a time consuming process.

Table 3.1 Computational Efficiency

Illumination face	Wedge angle φ	Incident angle ϕ_1'	Diffracted angle ϕ_1	$T_{IFFT\text{-}FD}/T_{TD}$ (Ratio of time taken by the IFFT-FD method and time taken by the direct TD method)
0-face	30°	10°	255°	15.1230
0-and n-face	30°	155°	327°	16.7982
n-face	30°	190°	255°	16.2593

3.6 Conclusion

In this Chapter, a TD double diffraction based on the direct convolution method by taking inverse Laplace transform of FD diffraction coefficients that apply to the case when the source illuminates either one or both sides of the non-perfectly conducting wedge with arbitrary internal angles is presented. The different reflection angles and improved reflection coefficients are applied in the outside sections of the wedge for formulating TD double diffraction. The Gaussian 2nd order pulse is used as an input pulse in direct TD-UTD solution and its spectrum

is used as an input signal in the IFFT-FD method. The direct TD results are related to the IFFT of FD results that ensure accuracy. Finally, It proves that the direct TD technique is efficient than the IFFT-FD technique.

Chapter 4

Time-domain Multiple-order Diffraction for Two Wedges of Arbitrary Angles

In general, the higher-order diffraction coefficient is used to consider multiple diffractions. As a result, the calculation becomes more complex does not take into account all possible orders of diffraction between the wedges. This chapter presents a TD multiple-order diffraction coefficient based on the direct convolution method by taking inverse Laplace transform of FD formulation applied to the dual dielectric wedge. Only, the first-order TD-UTD coefficient is applied for finding the higher-order diffraction without using any higher-order diffraction technique such as slope diffraction coefficients. Therefore, this technique is modest and calculates all possible orders of diffractions. The Gaussian 2nd order pulse is used as an input pulse in direct TD-UTD solution and its spectrum is used as an input signal in the IFFT-FD method. The TD results are related to the IFFT of FD results to verify accuracy.

4.1 Background

The request for high data rates is growing pointedly in wireless communication over the previous periods. The signal features fluctuate over the wireless medium and are subject to several factors such as the distance, paths and objects between transmitter and receiver. The fields at the receiver are attained by the convolution of the input signal with the impulse response of the channel. Hence, channel modelling is significant to know the performance of communication systems. Lately, Ultra-wideband transmission has paid the attention of research scholars from all over the world for communication at high data rates on short distances using low power. The UWB pulse distortion is the main problem because of its high bandwidth and

NLOS communication [116]. This distortion arises mainly due to the diffraction phenomena from the obstacle edges. The TD study is more effective to obtain this distortion as it calculates all frequencies of UWB signals instantaneously. The FD solution is transformed into a TD solution applying the inverse fast Fourier transform (IFFT). But, this technique requires extra time to consider each frequency component distinctly. Thus, the direct TD technique based on the efficient convolution method is favoured over the IFFT of the FD solution [91,117-118].

The TD model of multiple diffractions was presented in [91]. In [119], a hybrid UTD-PO TD model of multiple diffractions was presented.

The process of accounting for high order diffractions, especially for third and higher orders, can be very tedious. In the works of literature [85-96], [99], higher-order diffraction coefficients are used to obtain multiple diffractions. However, the self-consistent method [100] has been used to find the multiple order diffracted field in the frequency domain without using the higher-order diffraction coefficients. But the time domain solution using this method has not been done to find the double diffraction of all possible orders for UWB applications. This chapter presents a TD multiple-order diffraction coefficient based on the direct convolution method by taking inverse Laplace transform of FD formulation of [100] applied to the dual dielectric wedge. Only, the first-order TD-UTD coefficient is applied for finding the higher-order diffraction without using any higher-order diffraction technique such as slope diffraction coefficients. Therefore, this technique is modest and calculates all possible orders of diffractions. The Gaussian 2nd order pulse is used as an input pulse in direct TD-UTD solution and its spectrum is used as an input signal in the IFFT-FD method. The TD results are related to the IFFT of FD results to verify accuracy.

4.2 Propagation Scenario

Fig. 4.1 shows the propagation path of multiple diffractions from non-perfectly conducting wedges. Here, the diffracted signal from wedge 1 is again diffracted by wedge 2 and vice versa. Therefore, this is a case of multiple order diffraction. The edge of the wedge is representing the z-axis of polar coordinates. The incident angle ϕ_1' and diffracted angle ϕ_1 are measured with the 0-face of wedge 1. The incident angle ϕ_2' and diffracted angle ϕ_2 are measured with the 0-face of wedge 2. The interior angle φ is the wedge angle. The spherical source is used to illuminate the face of wedge 1 at a distance s_0. The distance between the wedges is d. The transmitting and receiving points are represented by (s_0, ϕ_1') and (s_2, ϕ_2), respectively.

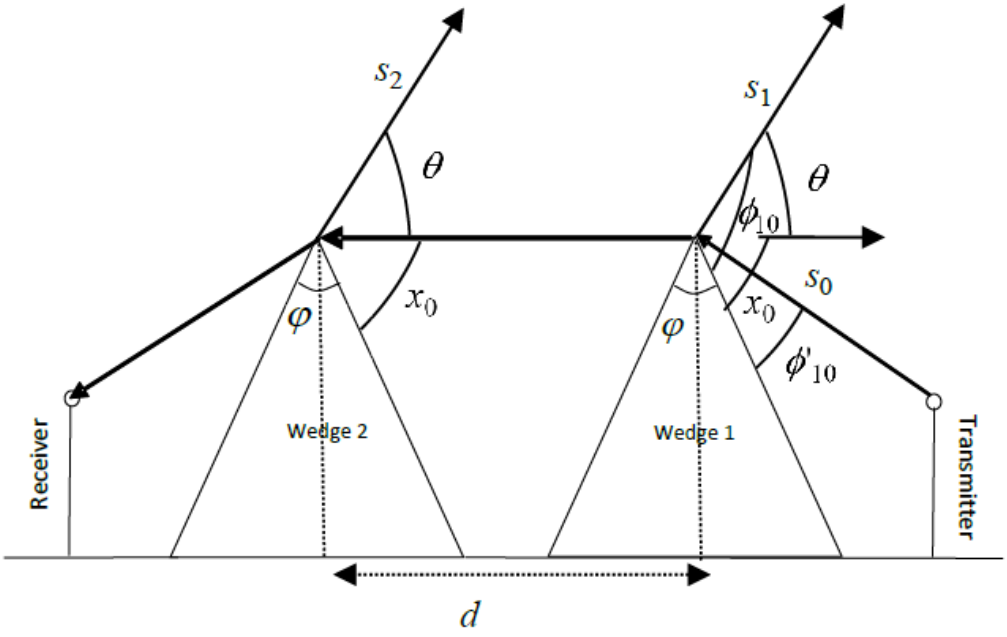

Fig. 4.1 Multiple order diffraction between two wedges.

4.3 Problem Formulation

4.3.1 FD Solution

Here, a consistent approach [100] used for multiple diffractions in Fig. 4.1 is defined. The diffractions by wedge 1 because of the radiation from the source and because of all orders of diffraction from wedge 2 can be written as

$$\begin{aligned} E_1^{s,h}(s_1,\theta) = E_0^{s,h} &\times D_{10}^{s,h} \\ &\times \left(L_{10}, \phi_{10} = x_0 + \theta, \phi'_{10}, n_1\right) \\ &\times A_{10}(s_1) e^{-jks_1} \\ &+ E_2^{s,h}(s_2 = d, \theta = 0) \\ &\times D_{12}^{s,h}\left(L_{12}, \phi_{12} = x_0, \phi'_{12}, n_1\right) \\ &\times A_{12}(s_1) e^{-jks_1} \end{aligned} \tag{4.1}$$

where

$E_1^{s,h}(s_1,\theta)$ =Total diffracted field by wedge 1 in soft and hard polarization,

$E_0^{s,h}$ = Field from the source at wedge 1,

$E_2^{s,h}(s_2 = d, \theta = 0)$ = Entire diffracted field by wedge 2 next to wedge 1 with all orders of diffraction,

$D_{10}^{s,h}$ = Diffraction coefficient for wedge 1 due to radiation from the source,

$D_{12}^{s,h}$ = Diffraction coefficient for wedge 1 due to radiation from wedge 2,

ϕ_{10} = Diffracted angle of wedge 1 due to radiation from the source,

ϕ_{12} = Diffracted angle of wedge 1 due to radiation from wedge 2,

ϕ'_{10} = Incident angle of wedge 1 due to radiation from the source,

ϕ'_{12} = Incident angle of wedge 1 due to radiation from wedge 2,

L_{10} =Distance parameter of the first wedge as a result of radiation by the Transmitter,

L_{12} =Distance parameter of the first wedge as a result of radiation by the second wedge,

n_1 = Angle parameter of the first wedge,

A_{10} = Spreading factor of wedge 1 as a result of radiation by the Transmitter,

A_{12} = Spreading factor of wedge 1 as a result of radiation by the second wedge, and

$E_2^{s,h}(s_2 = d, \theta = 0)$ is the unknown component in (4.1). A consistent method will be used to determine it.

Similarly, a total diffracted field by wedge 2 for all orders of diffraction from wedge 1 can be given as

$$\begin{aligned} E_2^{s,h}(s_2, \theta) = & E_1^{s,h}(s_1 = d, \theta = \pi) \\ & \times D_{21}^{s,h}\left(L_{21}, \phi_{21} = x_0 + \theta, \phi'_{21} = x_0, n_2\right) \\ & \times A_{21}(s_2) e^{-jks_2} \end{aligned} \tag{4.2}$$

where $E_2^{s,h}(s_2, \theta)$ = Total diffracted field by wedge 2,

$E_1^{s,h}(s_1 = d, \theta = \pi)$ = The entire diffracted field with the first wedge facing the second wedge with all orders of diffraction,

$D_{21}^{s,h}$ = Diffraction coefficient of wedge 2 due to radiation from wedge 1,

L_{21} = Distance parameter of wedge 2 due to radiation from wedge 1,

ϕ_{21} = Diffracted angle of wedge 2 due to radiation from wedge 1,

ϕ'_{21} = Incident angle of wedge 2 due to radiation from wedge 1,

n_2 = Angle parameter of the second wedge,

A_{21} = Spreading factor of the second wedge as a result of radiation by the first wedge, and

$E_1^{s,h}(s_1 = d, \theta = \pi)$ is an unknown component in (4.2). It will be determined using the consistent method.

(4.1) and (4.2) form a fixed pair for two unknown components, namely $E_2^{s,h}(s_2 = d, \theta = 0)$ and $E_1^{s,h}(s_1 = d, \theta = \pi)$. If these two terms are found, then they are applied to measure the diffracted fields from each wedge considering all diffraction orders. The two unknown ones can be found as follows.

The total diffracted field by wedge 1 in place of wedge 2 $(s_1 = d, \theta = \pi)$, as given by (4.1), can be reduced to

$$\begin{aligned} E_1^{s,h}(s_1 = d, \theta = \pi) = E_0^{s,h} \times D_{10}^{s,h}\left(L_{10}, \phi_{10} = x_0 + \pi, \phi'_{10}, n_1\right) \\ \times A_{10}(s_1 = d) e^{-jkd} \\ + E_2^{s,h}(s_2 = d, \theta = 0) \\ \times D_{12}^{s,h}\left(L_{12}, \phi_{12} = x_0, \phi'_{12}, n_1\right) \\ \times A_{12}(s_1 = d) e^{-jkd} \end{aligned} \quad . \qquad (4.3)$$

Similarly, the total diffracted field by wedge 2 in place of wedge 1 $(s_2 = d, \theta = 0)$, as given by (4.2), can be reduced to

$$\begin{aligned} E_2^{s,h}(s_2 = d, \theta = 0) = E_1^{s,h}(s_1 = d, \theta = \pi) \\ \times D_{21}^{s,h}\left(L_{21}, \phi_{21} = x_0, \phi'_{21} = x_0, n_2\right). \\ \times A_{21}(s_2 = d) e^{-jkd} \end{aligned} \qquad (4.4)$$

A simplified form of (4.3) and (4.4)

$$\begin{aligned} E_1^{s,h}(s_1 = d, \theta = \pi) = E_0^{s,h} \times T_{10}^{s,h} \\ + E_2^{s,h}(s_2 = d, \theta = 0) \times R_{12}^{s,h} \end{aligned} \qquad (4.5)$$

Where $T_{10}^{s,h} = D_{10}^{s,h}\left(L_{10}, \phi_{10} = x_0 + \pi, \phi'_{10}, n_1\right) \times A_{10}(s_1 = d) e^{-jkd}$

$$R_{12}^{s,h} = D_{12}^{s,h}\left(L_{12}, \phi_{12} = x_0, \phi'_{12}, n_1\right) \times A_{12}(s_1 = d) e^{-jkd}$$

and

$$E_2^{s,h}(s_2 = d, \theta = 0) = E_1^{s,h}(s_1 = d, \theta = \pi) \times R_{21}^{s,h} \tag{4.6}$$

where, $R_{21}^{s,h} = D_{21}^{s,h}\left(L_{21}, \phi_{21} = x_0, \phi'_{21} = x_0, n_2\right) \times A_{21}(s_2 = d) e^{-jkd}$

Writing in matrix form to the (4.5) and (4.6), we have

$$\begin{bmatrix} 1 & -R_{12} \\ -R_{21} & 1 \end{bmatrix} \times \begin{bmatrix} E_1^{s,h} \\ E_2^{s,h} \end{bmatrix} = \begin{bmatrix} E_0^{s,h} T_{10} \\ 0 \end{bmatrix} \tag{4.7}$$

or

$$\begin{bmatrix} E_1^{s,h} \\ E_2^{s,h} \end{bmatrix} = \begin{bmatrix} 1 & -R_{12} \\ -R_{21} & 1 \end{bmatrix}^{-1} \times \begin{bmatrix} E_0^{s,h} T_{10} \\ 0 \end{bmatrix} \tag{4.8}$$

The above-explained method does not use any higher-order diffraction coefficients for the calculation of multiple diffractions and it can be extended as well as applied to the interactions between a large number of edges. However, the order of the system of equations to be answered is also rising and will be identical to the number of communications amid the numerous edge groupings. Using this method, the double diffracted field in TD at the receiver is calculated by a single order diffraction coefficient than in other works [91] for multiple diffractions.

4.3.2 TD Solution

Taking inverse Laplace transform of (4.1), (4.2) and (4.8), we have total fields in the time domain by wedge1 and wedge 2 as follows

$$\begin{aligned} e_1^{s,h}(s_1,\theta,t) &= A_{10}(s_1) \\ &\times\begin{bmatrix} e_0^{s,h}(t) * d_{10}^{s,h}\left(L_{10},\phi_{10}=x_0+\theta,\phi'_{10},n_1,t\right) \\ *\delta(t-s_1/c) \end{bmatrix} \\ &+ A_{12}(s_1)\times\begin{bmatrix} e_2^{s,h}(s_2=d,\theta=0,t) \\ *d_{12}^{s,h}\left(L_{12},\phi_{12}=x_0,\phi'_{12},n_1,t\right) \\ *\delta(t-s_1/c) \end{bmatrix} \end{aligned} \tag{4.9}$$

$$\begin{aligned} e_2^{s,h}(s_2,\theta,t) &= A_{21}(s_2) \\ &\times\begin{bmatrix} e_1^{s,h}(s_1=d,\theta=\pi,t) \\ *d_{21}^{s,h}\left(L_{21},\phi_{21}=x_0+\theta,\phi'_{21}=x_0,n_2,t\right) \\ *\delta(t-s_2/c) \end{bmatrix} \end{aligned} \tag{4.10}$$

In the matrix form

$$\begin{aligned} \begin{bmatrix} e_1^{s,h}(s_1=d,\theta=\pi,t) \\ e_2^{s,h}(s_2=d,\theta=0,t) \end{bmatrix} &= \begin{bmatrix} 1 & -r_{12}(t) \\ -r_{21}(t) & 1 \end{bmatrix}^{-1} \\ &* \begin{bmatrix} e_0^{s,h}(t) * \tau_{10}(t) \\ 0 \end{bmatrix} \end{aligned} \tag{4.11}$$

where

$$\begin{aligned} r_{12}(t) &= A_{12}(s_1=d)\times\begin{bmatrix} d_{12}^{s,h}\left(L_{12},\phi_{12}=x_0,\phi'_{12},n_1,t\right) \\ *\delta(t-d/c) \end{bmatrix} \\ r_{21}(t) &= A_{21}(s_2=d)\times\begin{bmatrix} d_{21}^{s,h}\left(L_{21},\phi_{21}=x_0,\phi'_{21}=x_0,n_2,t\right) \\ *\delta(t-d/c) \end{bmatrix} \\ \tau_{10}(t) &= A_{10}(s_1=d)\times\begin{bmatrix} d_{10}^{s,h}\left(L_{10},\phi_{10}=x_0+\pi,\phi'_{10},n_1,t\right) \\ *\delta(t-d/c) \end{bmatrix} \end{aligned} \tag{4.12}$$

and

$$d^{s,h}(t) = d^{(1)}(t) + r_0(t) * r_n(t) * d^{(2)}(t) + r_n(t) * d^{(3)}(t) + r_0(t) * d^{(4)}(t) \tag{4.13}$$

where, $d^{(i)}(t), \quad (i = 1-4)$ are defined as [91]

$$d^{(i)}(t) = -\frac{Ln}{2\pi\sqrt{2c}} \frac{\sin(2\varsigma_i)}{\sqrt{t}\left(t + 2Ln^2 \sin^2(\varsigma_i)/c\right)} \cdot u(t) \tag{4.14}$$

The $r_0(t)$ and $r_n(t)$ are the reflection coefficients in TD for 0-face and n-face which are given as in [91].

$$r_{s,h}(t) = \mp\left[P\,\delta(t) + \frac{4p}{1-p^2} \frac{e^{-at}}{t} \sum_{q=1}^{\infty} (-1)^{q+1} q P^q I_q(at) \right] \tag{4.15}$$

where $P_{s,h} = (1 - p_{s,h})/(1 + p_{s,h})$, $p_s = \sin\theta_n \Big/ \sqrt{(\varepsilon_r - \cos^2\theta_n)}$,

$p_h = \sqrt{(\varepsilon_r - \cos^2\theta_n)}\Big/(\varepsilon_r \cdot \sin\theta_n)$, $\delta(t)$ is the Dirac delta function, $I_q(t)$ is the modified Bessel function of order q, $a = \sigma/(2\varepsilon_r\varepsilon_0)$, and the leading $-(+)$ sign is for soft (hard) polarization. θ_n is the reflection angles for $0-$ face and $n-$face.

4.4 Results and Discussion

In this section, the time domain solutions are discussed for different scenarios. The 2nd order Gaussian pulse as in [92] is applied as the incident pulse shown in Fig. 4.2 and its Gaussian spectrum is shown in Fig. 4.3 which is used in the IFFT-FD solution as the input signal. Fig. 4.1 consists of two wedges and its parameters are $\varepsilon_r = 10$ and $\sigma = 0.001\,\text{S/m}$.

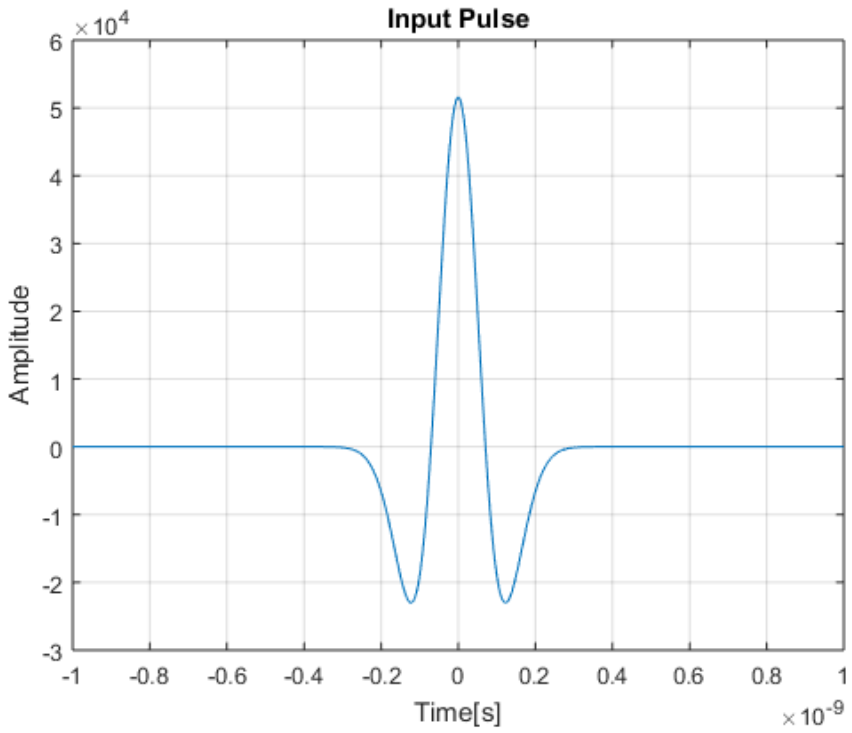

Fig. 4.2 The 2nd order Gaussian input pulse.

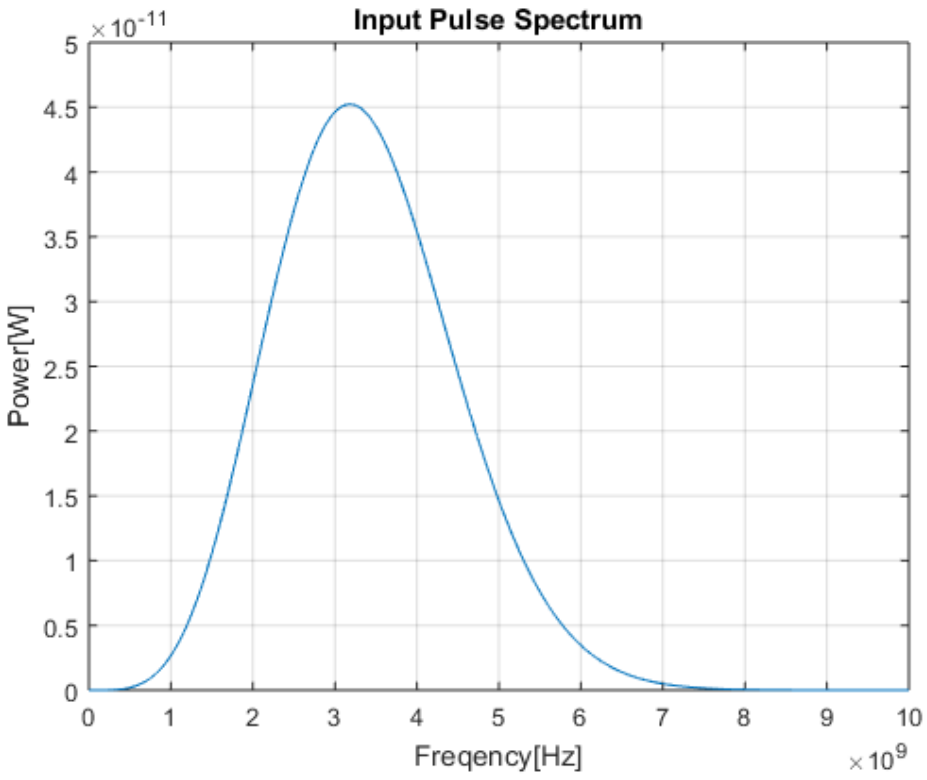

Fig. 4.3 Gaussian doublet pulse spectrum.

From Fig. 4.4-4.6, we see that the proposed TD solutions are matching with their corresponding IFFT-FD solutions but are highly attenuated and distorted due to the multiple order diffraction and frequency dependence behaviour of UWB signals. In Fig. 4.5, a grazing incidence case has also been considered in a building scenario. In this case, the received field is obtained without using any slope diffraction terms in (4.11). Hence, it proves that the proposed technique has merits over the techniques introduced in numerous works of literature [85-96, 99]. Therefore, the proposed method is suitable for UWB applications where the distance between wedges is small and requires considering all possible orders of diffraction for accurate prediction of the signal at the receiver.

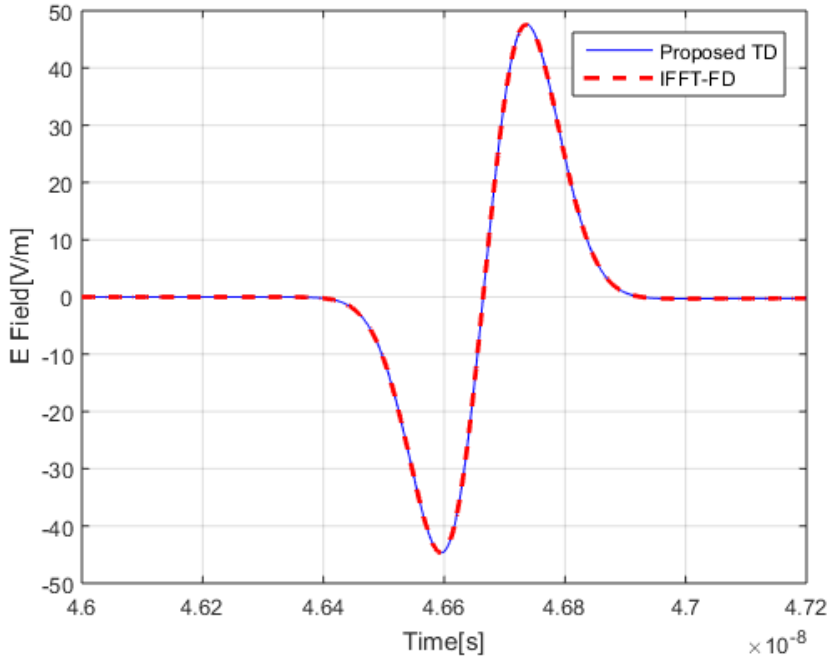

Fig. 4.4 TD received fields. TX height= 1m, Rx height=1m, wedge height= 4m, d=4m and $\varphi = 45^{\circ}$.

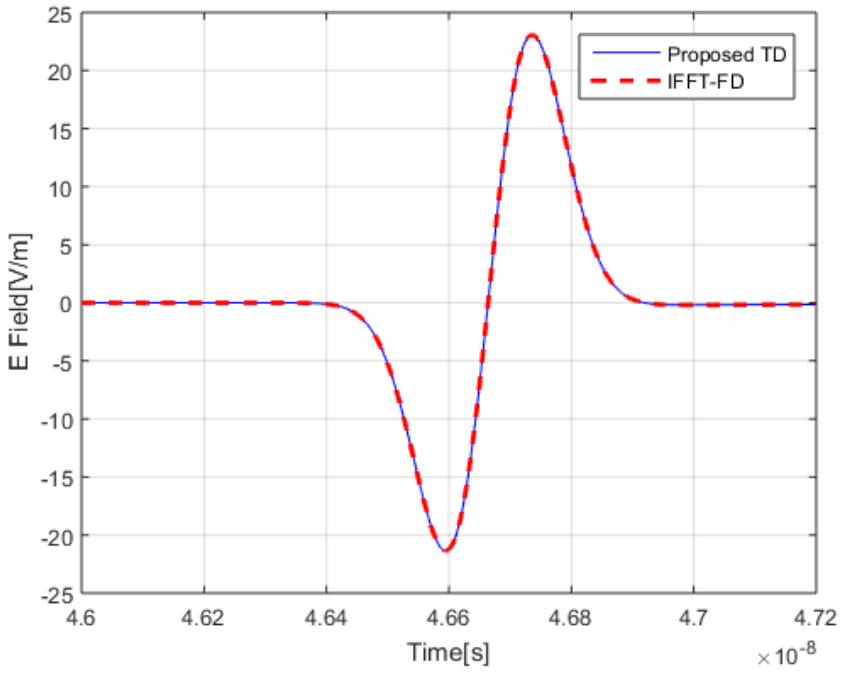

Fig. 4.5 TD received fields. Tx height= 1m, Rx height=1m , wedge height= 4m, d=4m and $\varphi = 90^{\circ}$.

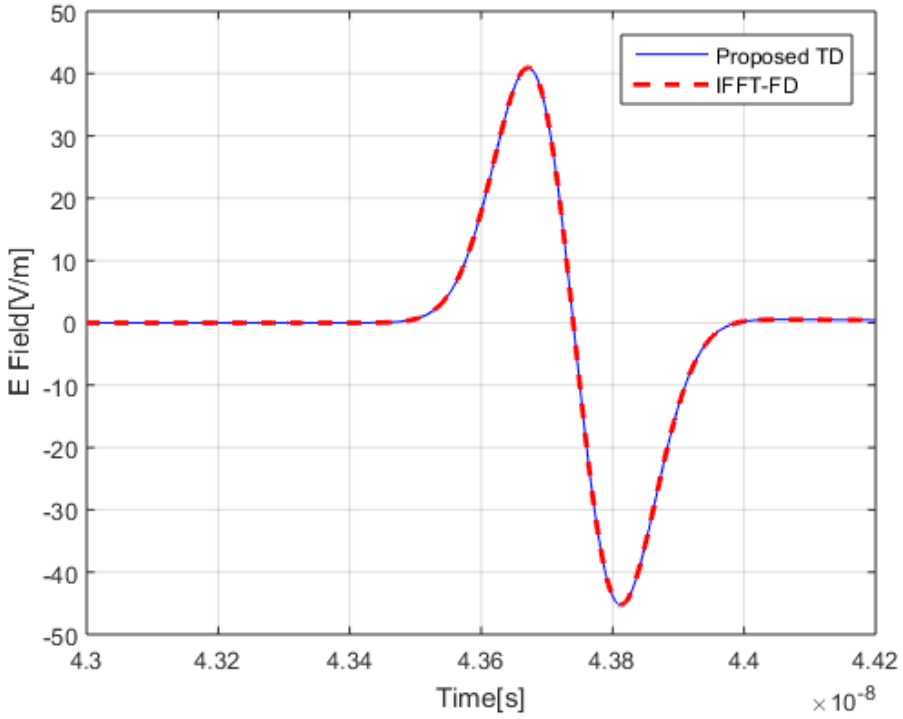

Fig. 4.6 TD received fields. Tx height= 5m, Rx height=1m , wedge height= 4m, d= 4m and $\varphi = 55^{\circ}$.

In Fig. 4.7, the received field is decreasing because the wedge angle is increasing. Even for the case of Fig. 4.6 wherever transmitter height is more than the wedge height, the received field has attenuated significantly due to the multiple order diffraction.

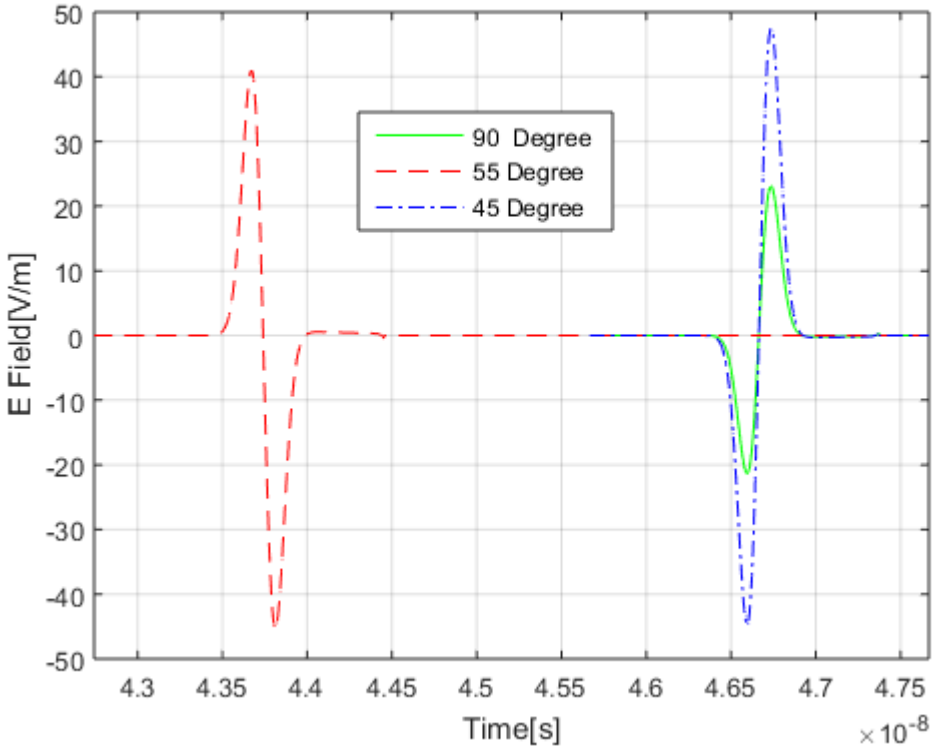

Fig. 4.7 Comparison of TD received fields for the wedge scenarios Fig. 4.4-4.6.

4.5 Conclusion

In this chapter, the TD multiple-order diffraction coefficients are presented. Only, the first-order TD-UTD coefficient is applied for finding the higher-order diffraction without using any higher-order diffraction technique such as slope diffraction coefficients. Therefore, this technique is modest and calculates all possible orders of diffractions. The Gaussian 2nd order pulse is used as an input pulse in direct TD-UTD solution and its spectrum is used as an input signal in the IFFT-FD method. The direct TD results are related to the IFFT of FD results that verify the accuracy.

Chapter 5

A Novel TD-UTD Coefficients for Evaluation of Diffraction and Transmission from Dielectric Wedges

In this chapter, a new time-domain six-term heuristic diffraction coefficient is proposed to consider the effect of diffraction and transmission from the dielectric wedge with an arbitrary low wedge angle for UWB applications. The different scenarios are considered to test the overall performance of the TD solution. The results of TD-UTD are confirmed by the inverse fast Fourier transform (IFFT) of frequency-based results in hard polarization. The computational efficiency of the proposed TD-UTD solutions is demonstrated by comparing the time they have taken with their IFFT-FD solutions.

5.1 Background

The Ultra-Wideband (UWB) communication (3.1-10.6 GHz) is the most emerging wireless technology as a potential solution for 5G picocells and femtocells. It is capable to operate in an unlicensed band with high data rates for short-range using very low power parallelly with current radio communications without creating interference [4]. The propagated pulse through the UWB channel is distorted due to its frequency selective nature resulting in performance degradation [116]. Therefore, accurate UWB channel modeling is required to determine the performance of the communication system and network arrangement [5]. It is since the UWB channel has a large bandwidth and thus, working for the entire range of UWB signal in frequency-domain (FD) is difficult. Therefore, many works of literature have a time-domain solution of various propagation scenarios with UWB applications [91,99,103]. The time-domain analysis of the UWB channel can be done in two ways. 1) Taking the IFFT of the

conventional FD solution in the entire UWB frequency range, and 2) directly converting the FD formula into the TD formula using Inverse Laplace transform. The second method is more convenient and less time-consuming than its IFFT counterpart. There are three important phenomena to characterize the behaviour of UWB channels: (i) Reflection, (ii) Diffraction, and (iii) Transmission.

The diffraction phenomenon is considered by the most popular theory known as the Uniform Theory of Diffraction (UTD) [6]. In [104], a six-term UTD formula has been proposed in FD to consider the transmission through the dielectric wedge. However, the TD solution has not been presented for this case [85-103]. There are various papers where an emphasis on considering transmission through lossy electromagnetic materials has been given [121-123].

In this work, the analytical TD-UTD formulations are obtained by taking the inverse Laplace transform of the FD solutions in [104]. The TD results are verified with the IFFT for the FD solutions and the results are found to be very consistent with IFFT solutions. Section-5.2 of the paper explains the propagation scenario with single-order diffraction by a dielectric wedge. In Section 5.3, the formulations for the TD-UTD diffraction coefficient is derived. Finally, Section-5.4 presents a detailed discussion of the proposed outcomes.

5.2 Propagation Scenario with a Dielectric Wedge

Fig. 5.1 shows the propagation path of diffraction and transmission with single side illumination (SSI) from a dielectric wedge. The edge of the wedge is representing the z-axis of polar coordinates. The incident angle ϕ' and diffracted angle ϕ are measured with the 0-face of the wedge. The interior angle φ is the wedge angle. A line source is used to illuminate the face of the wedge at a distance r_1. The transmitting and receiving points are represented by (r_1, ϕ') and (r_2, ϕ), respectively. There are four

regions of observation with 0-face illumination $\left(\phi' < \pi - \varphi\right)$. Region-I $\left(0 < \phi < \pi - \phi'\right)$ has incident, reflected, and diffracted fields. The limiting boundary $\left(\phi = \pi - \phi'\right)$ of the reflected wave is the reflection shadow boundary (RSB). Only incident and diffracted fields exist in Region-II $\left(\pi - \phi' < \phi < \pi + \phi'\right)$. The limiting boundary $\left(\phi = \pi + \phi'\right)$ of the incident wave is the incident shadow boundary (ISB). Region-III $\left(\pi + \phi' < \phi < \pi + g_0\left(\phi'\right)\right)$ has diffracted fields only. The limiting boundary $\left(\phi = \pi + g_0\left(\phi'\right)\right)$ of the transmitted ray is the transmission shadow boundary (TSB). Region-IV $\left(\pi + g_0\left(\phi'\right) < \phi < 3\pi - \varphi - \phi'\right)$ has the diffracted and the transmitted fields. This is the shadow region of the scenario. The $g_0\left(\phi'\right)$ is defined in [104].

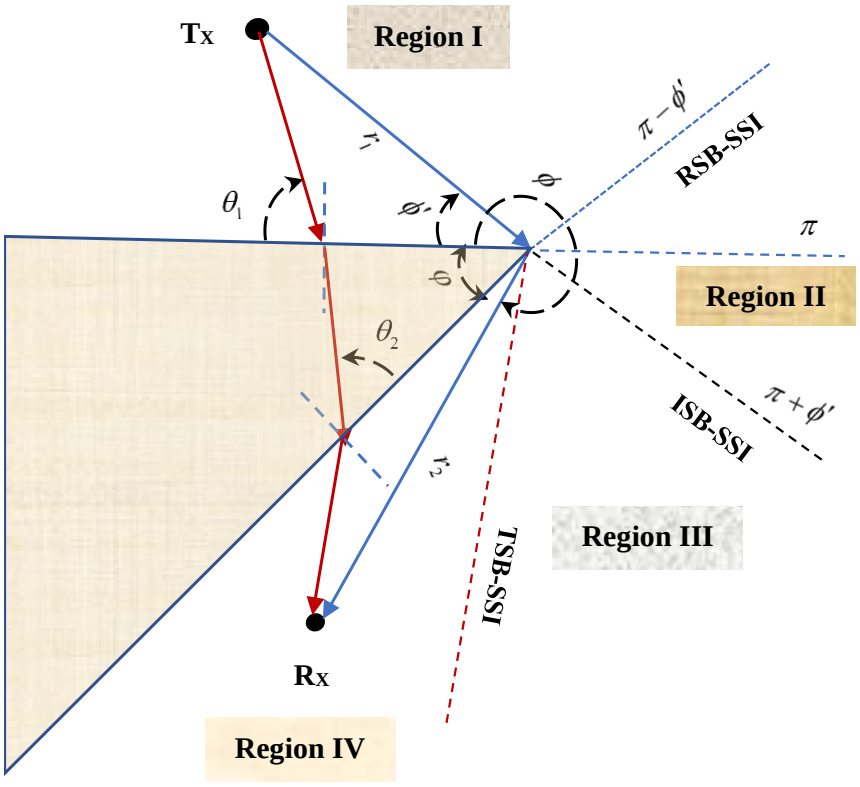

Fig. 5.1 Propagation scenario by a dielectric wedge.

5.3 Formulation of the Proposed TD-UTD Coefficient

The diffraction and transmission phenomena show a vital role in the modeling of the wireless channel. The diffracted and transmitted fields compensate for the discontinuities of each geometrical optics (GO) field at ISB, RSB, and TSB by adding antisymmetric discontinuities, so that the entire field is continuous around the structure. The impulse response of the received field in the shadow region of Fig. 5.1 can be obtained by taking the inverse Laplace transform of (1) in [104] with impulse input. Hence, the impulse response

$$u_d(t) = A(\mathrm{r}_2) \cdot \left[d_{s,h}(t) * \delta\left(t - (r_1 + r_2)/c\right) \right] \tag{5.1}$$

where $A(\mathrm{r}_2)$ is the amplitude spreading factor, and the delta function $\delta\left(t - (r_1 + r_2)/c\right)$ is the time delay that occurs between transmitter and receiver. The $d_{s,h}(t)$ is the diffraction coefficient in TD for a dielectric wedge which is obtained by taking the inverse Laplace transform of (3) in [104]

$$d_{s,h}(t) = d_1 + d_2 + r_0 * d_3 + r_n * d_4 + t_0 * t_0' * d_5 + t_n * t_n' * d_6 \tag{5.2}$$

where $d_i(t)$ with $i = 1-4$ is given as in [91]

$$d_i(t) = -\frac{Ln}{2\pi\sqrt{2c}} \times \frac{\sin(2a_i)}{\sqrt{t}\left(t + 2Ln^2 \sin^2(\mathrm{a}_i)/c\right)} \cdot u(t) \tag{5.3}$$

$r_{s,h}(t)$ is the Fresnel reflection coefficient in TD. This is obtained from [109]

$$r_{s,h}(t) = \mp\left[P\,\delta(t) + \frac{4p}{1-p^2} \frac{e^{-at}}{t} \sum_{q=1}^{\infty} (-1)^{q+1} q P^q I_q(at) \right] \tag{5.4}$$

where $P_{s,h} = \left(1 - p_{s,h}\right)/\left(p_{s,h} + 1\right)$, $p_s = \sin\theta_1 \Big/ \sqrt{\left(\varepsilon - \cos^2\theta_1\right)}$,

$p_h = \sqrt{\left(\varepsilon - \cos^2\theta_1\right)} \Big/ \left(\varepsilon \cdot \sin\theta_1\right)$, the modified Bessel function of order q is $I_q(t)$,

$a = \sigma/\left(2\varepsilon_r \varepsilon_0\right)$, and soft (hard) polarizations represented by the leading $-(+)$ sign.

Taking inverse Laplace transform of (7) and (14) in [104], d_5 and d_6 of (5.2) can be given as

$$d_5(t) = -\frac{L^i n}{2\pi\sqrt{2v}} \times \frac{\sin(2a_5)}{\sqrt{t}\left(t + 2L^i n^2 \sin^2(\mathrm{a}_5)/v\right)} \cdot u(t) \qquad (5.5)$$

and

$$d_6(t) = -\frac{L^i n}{2\pi\sqrt{2v}} \times \frac{\sin(2a_6)}{\sqrt{t}\left(t + 2L^i n^2 \sin^2(\mathrm{a}_6)/v\right)} \cdot u(t) \qquad (5.6)$$

The $t_{s,h}(t) = \delta(t) + r_{s,h}(t)$ and $t'_{s,h}(t) = \delta(t) + r'_{s,h}(t)$ in (2) are the transmission coefficients in TD on the first interface (air/dielectric), and the second interface (dielectric/air) with $r'_{s,h}(t)$ as in (5.4)

$$r'_{s,h}(t) = \mp\left[P''\delta(t) + \frac{4p''}{1-p''^2}\frac{e^{-at}}{t}\sum_{q=1}^{\infty}(-1)^{q+1}qP''^{q}I_q(at)\right] \qquad (5.7)$$

where $P''_{s,h} = \left(1 - p''_{s,h}\right)/\left(p''_{s,h} + 1\right)$, $p''_s = \cos\theta_2 \Big/ \sqrt{\left(1/\varepsilon - \sin^2\theta_2\right)}$,

$p''_h = \varepsilon\sqrt{\left(1/\varepsilon - \sin^2\theta_2\right)}\Big/\left(\cos\theta_2\right)$, and $v = c/\sqrt{\varepsilon_r}$. All the other terms are defined as in [104].

5.4 Results and Discussions

The 2nd order Gaussian pulse [103] shown in Fig. 5.2 is used to test the TD solutions proposed in Section-5.3. This pulse is crossing the zero line two times with a Gaussian shape. Hence, it is called the 2nd order Gaussian pulse. It has the time-scaling factor $\tau = 0.1$ *ns* .

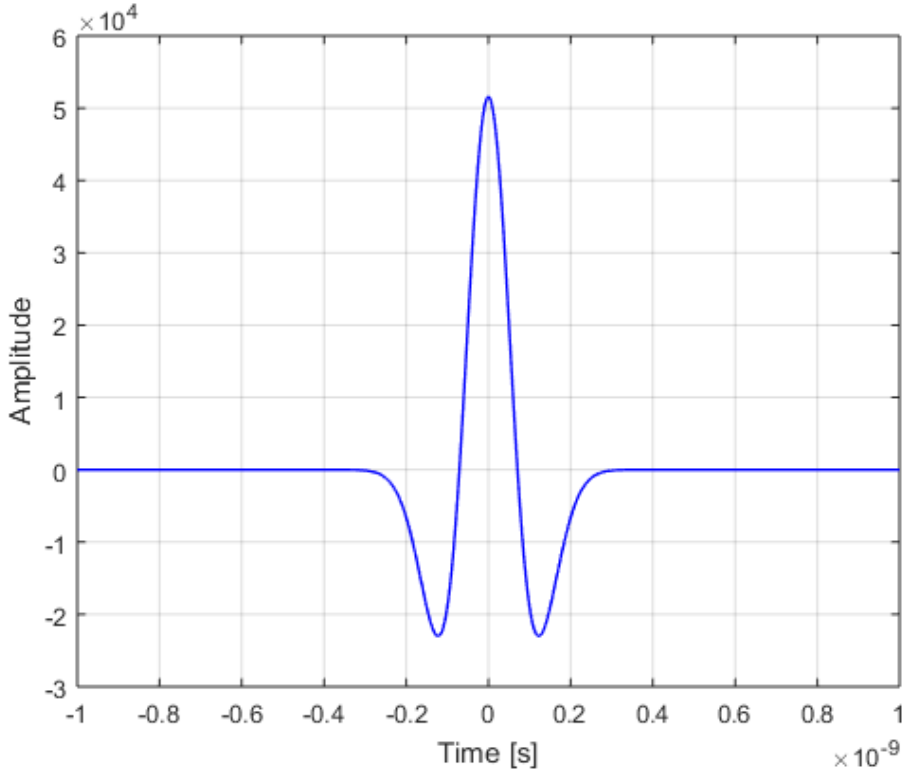

Fig. 5.2 2nd-order Gaussian pulse.

The 2nd order Gaussian pulse spectrum shown in Fig. 5.3 is used in IFFT-FD solutions. This spectrum has a frequency range of UWB signals. Therefore, the pulse is used as a transmitted pulse of UWB signals with a short duration in *ns*.

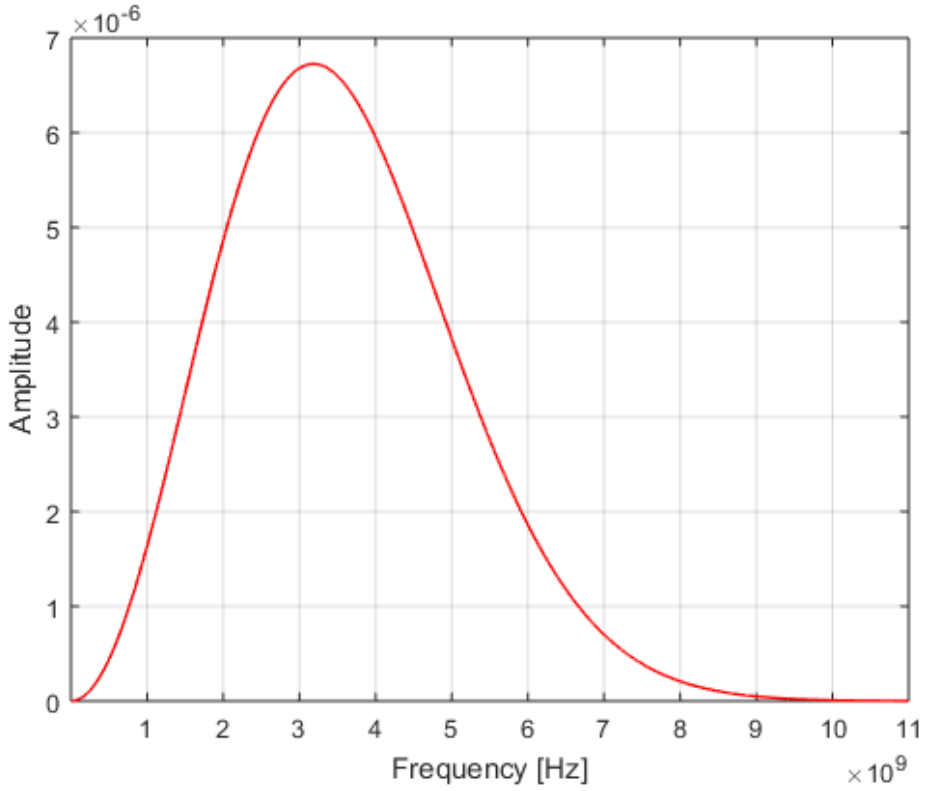

Fig. 5.3 2nd-order Gaussian pulse spectrum.

In Fig. 5.4, the TD response is compared with its corresponding IFFT-FD response and both have very good matching. Therefore, the proposed method is verified. Here, the incidence angle is $\phi' = 15°$ and wedge angle is $\varphi = 17°$ which is selected as in [10] to have transmitted fields. The received pulse is attenuated and distorted in comparison to the input pulse due to the lossy behaviour of the dielectric wedge and frequency dependence nature of the UWB signal in the shadow region of the structure.

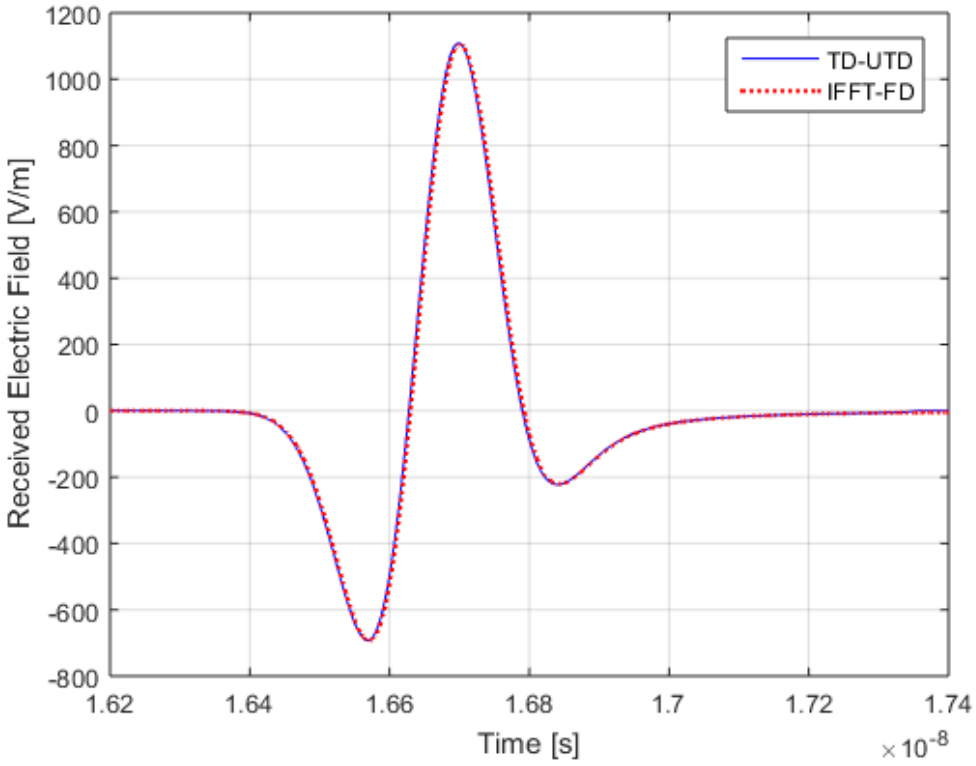

Fig. 5.4 TD received fields. $\phi' = 15°$, $\phi = 335°$, $r_1 = 3\,\text{m}, r_2 = 2\,\text{m}$, $\varphi = 17°$, relative permittivity $\varepsilon_r = 10$, conductivity $\sigma = 0.001\,\text{S/m}$.

In Fig. 5.5, the TD received pulse is also matching with its corresponding IFFT-FD solution for a different scenario where incidence angle is $\phi' = 75°$. In this case, the received pulse is strongly attenuated and distorted due to the only transmitted and diffracted fields available in the shadow region. The received pulse is also subject to the frequency dependence of UWB signals.

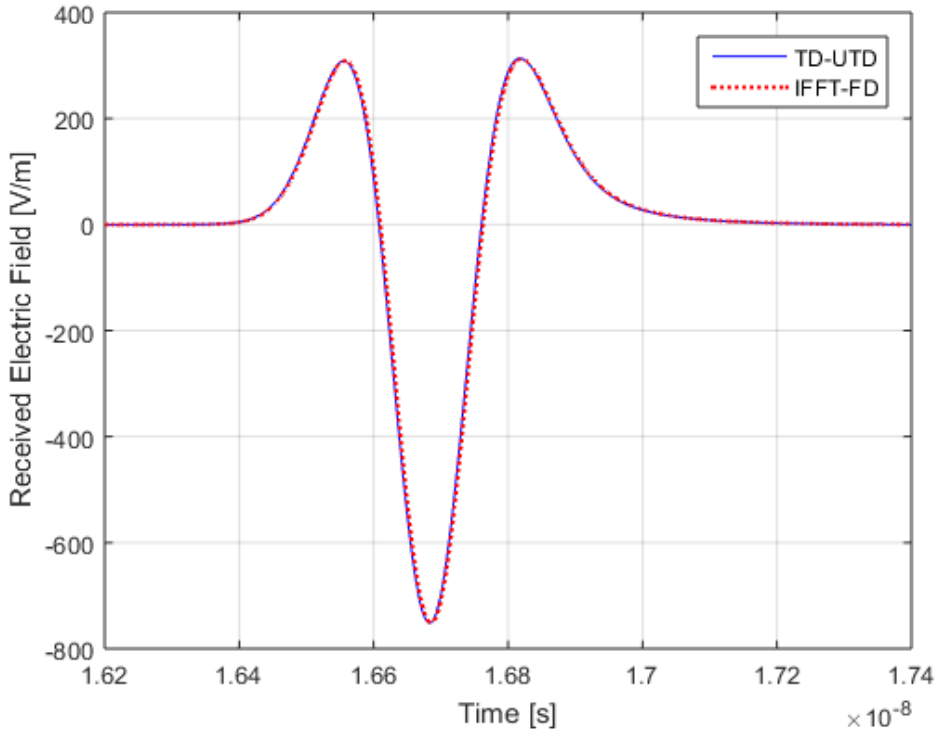

Fig. 5.5 TD received fields. $\phi' = 75°$, $\phi = 335°$, m, $r_1 = 3$ $r_2 = 2$ m, $\varphi = 17°$, relative permittivity $\varepsilon_r = 10$, conductivity $\sigma = 0.001$ S/m.

In Fig. 5.6, a different scenario is selected where the incidence angle is $\phi' = 115°$. Here, the received pulse is less attenuated and distorted than in the earlier cases. This is due to the only diffracted fields available in the shadow region. Here, both the TD-UTD and IFFT-FD solutions are matching each other. Therefore, it confirms the accuracy of the proposed method.

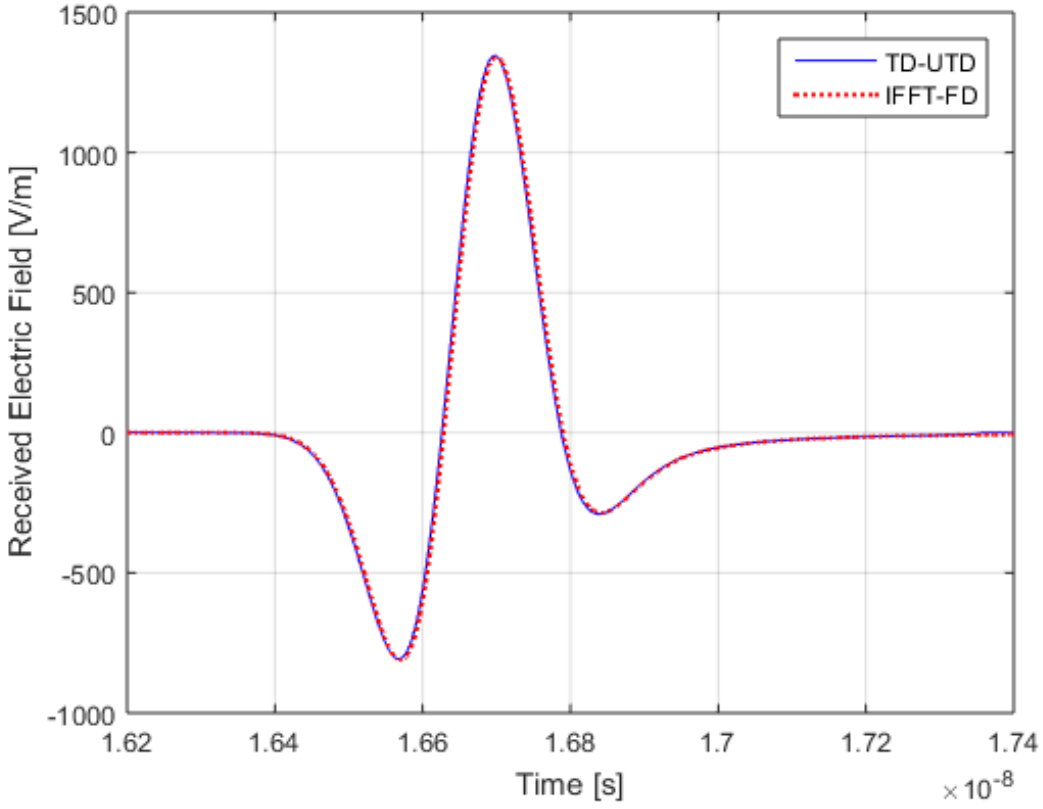

Fig. 5.6 TD received fields. $\phi' = 115°$, $\phi = 335°$, $r_1 = 3\,\text{m}, r_2 = 2\,\text{m}$, $\varphi = 17°$, relative permittivity $\varepsilon_r = 10$, conductivity $\sigma = 0.001\,\text{S/m}$.

In Fig. 5.7, a very thin wedge structure is selected with a wedge angle $\varphi = 13°$. In this case, the TD-UTD and IFFT-FD solutions are also similar. Therefore, the proposed TD solution is guaranteed to be accurate. The received pulse is strong due to the high transmission fields. Minor distortions are caused by the frequency dependence of the proposed TD-UTD coefficients.

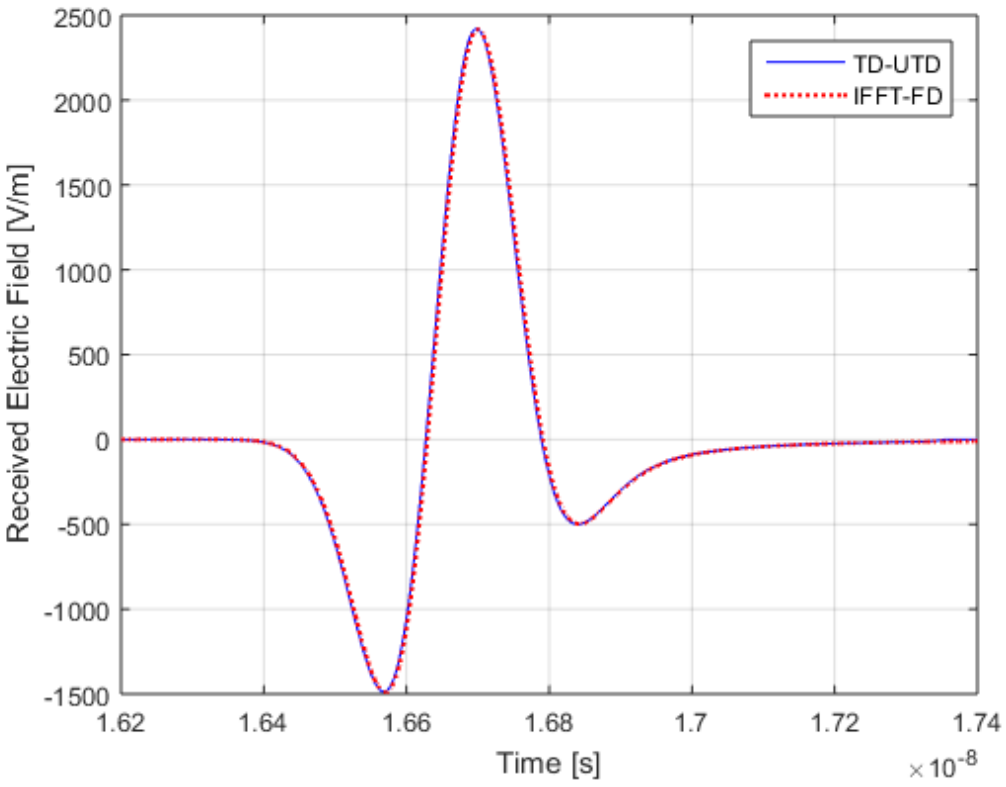

Fig. 5.7 TD received fields. $\phi' = 75°$, $\phi = 335°$, $r_1 = 3\,\text{m}, r_2 = 2\,\text{m}$, $\varphi = 13°$, relative permittivity $\varepsilon_r = 10$, conductivity $\sigma = 0.001\,\text{S/m}$.

Table 5.1 and Fig. 5.8 present the computational efficiency of the proposed TD technique with its corresponding IFFT-FD technique. It is quite clear that the TD-UTD solution works much better than the IFFT-FD method. It is because the TD-UTD method is based on the effective convolution method. While the IFFT-FD method takes longer to convert each frequency component of UWB signals to TD due to a shorter Gaussian pulse.

Table 5.1 Details of the time taken in simulation by the TD-UTD and IFFT-FD techniques.

Dielectric Wedge Structure	Time (TD-UTD) in (Sec.)	Time (IFFT-FD) in (Sec.)	Time (IFFT-FD) / Time (TD-UTD)
$\phi' = 15°, \varphi = 17°$	0.670283	28.794093	42.95
$\phi' = 75°, \varphi = 17°$	0.562310	16.318998	29.02
$\phi' = 115°, \varphi = 17°$	2.512664	58.093214	23.12
$\phi' = 75°, \varphi = 13°$	0.217421	26.213103	120.56

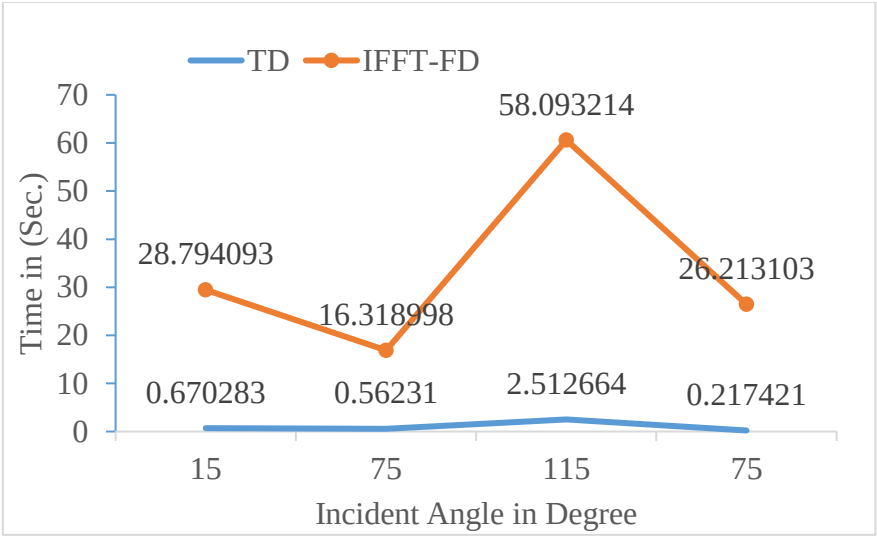

Fig. 5.8 Time taken by the direct TD-UTD method and the IFFT-FD method.

5.5 Conclusion

In this chapter, novel six-terms UTD diffraction coefficients in TD has been presented to consider transmission and diffraction phenomena from a thin dielectric wedge. The TD-UTD results are compared with its corresponding IFFT-FD results in hard polarization showing excellent matching. Various scenarios have been selected to test the proposed TD solutions. Finally, the TD-UTD process is more effective than the IFFT-FD method.

Chapter 6

Characterization of Diffracted and Transmitted Field with UWB Applications

One of the foremost propagation phenomena based on the ray concept is diffraction. The classical frequency-domain model of Uniform Theory of Diffraction (UTD) is used to evaluate the signal diffracted in the shadow region of the scenario as well as to determine the cell coverage of the wireless communication system. The Time-domain formulation of UTD is used to analyze the UWB channel characteristics in the time-domain. In this chapter, a novel heuristic diffraction coefficient in frequency-domain (FD) for non-perfectly conducting wedges and buildings is proposed. A six-term diffraction coefficient which is an extension of the four-term UTD coefficient is proposed to include the effect of transmitted ray for a lossy dielectric wedge with arbitrary low wedge angle, thus, attaining the continuity of the total field all around the structure. This new six-terms UTD diffraction coefficient is verified with a finite difference time domain (FDTD) based on a numerical method. Further, a time-domain (TD) solution based on the classical frequency domain result is proposed for UWB applications in indoor environments. Finally, a case of double diffraction for two consecutive buildings scenario is presented based on slope diffraction and their corresponding TD solution is also presented. The different input pulses and building materials are considered to test the overall behaviour of the TD model. All the TD results are verified with inverse fast Fourier transform (IFFT) of the FD results in both the soft and hard polarization and the results are found to be in very good agreement. The impulse response of the channel is also presented to determine the distortion on the input pulse. The computational efficiency of the proposed TD solutions is demonstrated by comparing them with IFFT-FD solutions.

6.1 Background

The wireless systems are assessed through measurements and simulations. But, the simulation-based method is preferred over the measurement-based approach as the latter is site-specific and time-consuming. Moreover, the wave propagation calculation is required repeatedly. Hence, it is appropriate to use the high-frequency asymptotic methods i.e. the geometrical theory of diffraction (GTD) and its improvement in the uniform theory of diffraction (UTD). These techniques were developed for perfectly conducting wedges where reflection and diffraction effects in an urban environment are evaluated. Many researchers proposed heuristic methods to study dielectric wedges [84, 106]. The time-domain (TD) solution of UWB systems is more efficient and less time consuming than the FD solutions due to the large operating frequency of UWB signals [103]. In [99, 124], the reflected fields are specified in TD. In [116], the TD solutions are presented in closed form for ultra-wideband applications where both the perfectly conducting and dielectric wedges are considered. The TD results are compared with their corresponding IFFT-FD solutions in the urban environment. The impulse response is derived from Bertoni's propagation model and a case of pulse distortion is also investigated to explain the performance of the UWB system. In [91], the TD multiple-diffraction solutions are investigated for metallic and dielectric wedges. The TD results are validated with their IFFT-FD results. An algorithm is also proposed to measure the TD diffracted field after an arbitrary number of wedges of different shapes and types. In [103], A TD diffraction solution is presented for lossy wedges and buildings which is pertinent for different wedge face illumination by the source. A new time-domain (TD) solution is proposed for analyzing the diffraction of ultra-wideband (UWB) signals in three dimensional (3-D) scenarios [120]. But, the above TD solutions do not consider the transmitted ray in the diffraction coefficient due to the thick wedge size.

In [121-123], the transmitted field along with the diffracted field is considered to predict the total field at the receiver in the urban environment. The transmitted fields become very significant in UWB communication due to the non-line-of-sight (NLOS) communications where the diffracted and reflected fields are very weak in the deep shadow regions. In [99], the TD model based on FD solutions is presented to consider the transmission phenomenon through the dielectric wedge and building made of low-loss materials. The results are validated with IFFT-FD solutions. In [124], the TD pulse distortion is analyzed due to the multiple reflections and transmissions of the UWB signal from the lossy dielectric walls. In [104], the author has presented a heuristic diffraction coefficient including the transmitted field when the dielectric wedge angle is less than 20˚. In this case, the diffracted field in the shadow region has significant improvement and the total field is continuous all around the wedge. Also, the UTD results confirmed with the FDTD method where a significant alteration is detected between ISB and TSB except other parts of the wedge geometry.

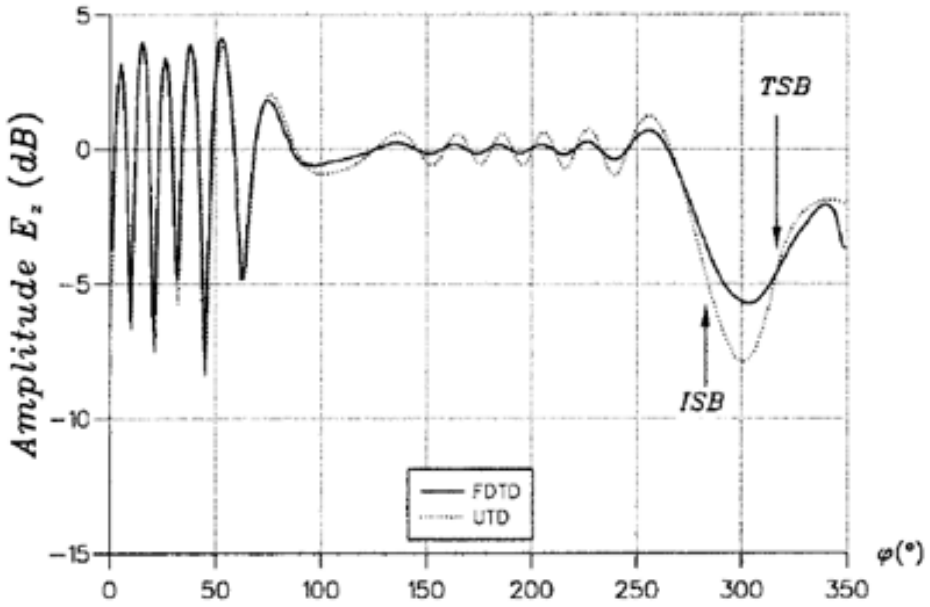

Fig. 6.1. Dielectric wedge. $f = 900$ MHz, $\phi' = 105°$, $r_2 = 1\,\text{m}$, $\varphi = 10°$, $\sigma = 0.001\,\text{S/m}$.

In this work, a heuristic four terms UTD is presented in frequency-domain (FD). Then, a novel six-terms UTD is established to consider the transmitted ray in the diffraction coefficient as (3) of [104] where two more terms are added in four terms UTD. It predicts a better response between ISB and TSB than the result given in Fig. 6 of [104] shown in Fig. 6.1. Further, it is validated with FDTD. Subsequently, we present the formulation for multiple diffraction cases with two successive wedge vertices and a building structure. Here, the doubly diffracted field by the slope diffraction is calculated behind the structure when the refracted field doesn't occur. Moreover, the TD solution is proposed through the above FD solution for UWB applications which contemplates the transmitted ray. As we know that the TD solutions are favoured over the FD solutions due to the high operating frequency range of UWB signals [103]. The TD double diffraction solution is also presented by the TD slope diffraction coefficient in the case of grazing incidence.

Section-6.2 of this chapter explains the propagation scenario with single-order diffraction by a lossy wedge. In Section 6.3, the formulation for single-order FD-UTD and TD-UTD diffraction coefficient is specified. Here, we describe the implementation of UTD for lossy dielectric wedges with an additional transmission coefficient. In Section 6.4, the case of multiple diffractions is stated in both the FD and TD. There, slope diffraction is used to interpret grazing incidence or double diffraction. Section-6.5 deals with results and discussion. There, the proposed FD and TD results are represented for both the polarization soft and hard. Results obtained by the six-terms UTD coefficient are good and the same has been verified with FDTD. Further, the TD outcomes are verified with the IFFT of the alike FD solutions. Various input pulses and wedge materials are used to check the overall performance of the TD solutions. Improvement of the results due to double diffraction is also presented in the shadow region of the structure. UWB pulse distortion is evaluated by exploring the channel impulse response.

The computational effectiveness of TD and IFFT-FD solution is also projected. Finally, conclusions are presented in Section-6.6.

6.2 Propagation Scenario with Single-order Diffraction by a Lossy Wedge

Fig. 6.2 shows the propagation path of diffraction and transmission with single side illumination (SSI) from a non-perfectly conducting wedge.

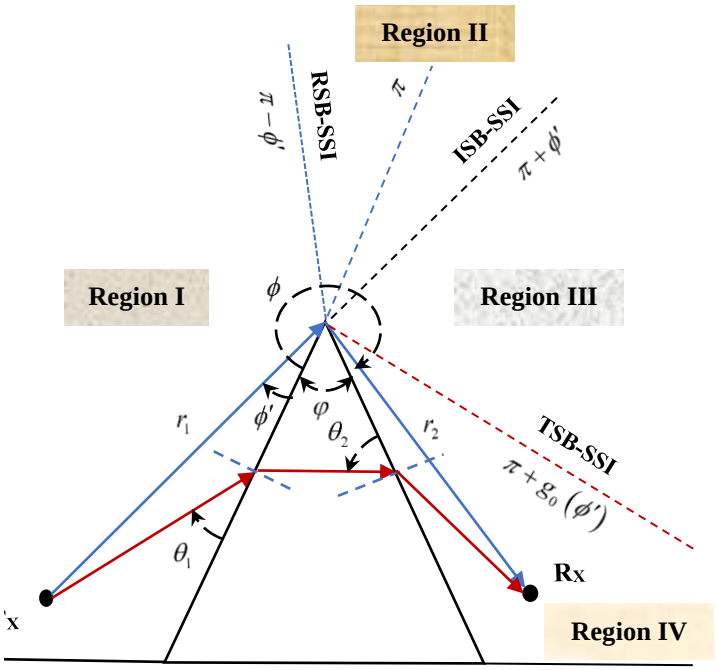

Fig. 6.2 Propagation scenario by a lossy wedge.

The edge of the wedge is representing the z-axis of polar coordinates. The edge of the wedge is representing the z-axis of polar coordinates. The incident angle ϕ' and diffracted angle ϕ are measured with the 0-face of the wedge. The interior angle φ is the wedge angle. A plane

wave source is used to illuminate the face of the wedge at a distance r_1. The transmitting and receiving points are represented by (r_1, ϕ') and (r_2, ϕ), respectively. There are four regions of observation due to different wave propagation when 0-face illumination $(\phi' < \pi - \varphi)$ of a wedge is considered.

Region-I $(0 < \phi < \pi - \phi')$ is having wave components (incident, reflected, and diffracted waves). The limiting boundary $(\phi = \pi - \phi')$ of the reflected wave is the reflection shadow boundary (RSB) in Region-I. Only incident and diffracted waves exist in Region-II $(\pi - \phi' < \phi < \pi + \phi')$. In Region-II, the limiting boundary $(\phi = \pi + \phi')$ of the incident wave is the incident shadow boundary (ISB). Region-III $(\pi + \phi' < \phi < \pi + g_0(\phi'))$ is having diffracted waves only. In Region-III, the limiting boundary $(\phi = \pi + g_0(\phi'))$ of the transmitted wave is the transmission shadow boundary (TSB). Region-IV $(\pi + g_0(\phi') < \phi < 3\pi - \varphi - \phi')$ is having diffracted and transmitted waves. This is the shadow region of the wedge. $g_0(\phi')$ is defined in (6.14).

6.3 Proposed Heuristic Diffraction Coefficient

6.3.1 FD-UTD

The diffraction phenomenon occurs when an electromagnetic wave falls on a metallic or dielectric edge as shown in Fig. 6.2. It has an important role in the modeling of wireless communications links with mobiles. The diffracted field compensates for the discontinuity of each geometrical optics (GO) field at the ISB and RSB by adding anti-symmetrical discontinuity. Thus, the total field is continuous around the structure. One of the fast well-

known asymptotic ray-based methods is the uniform theory of diffraction (UTD). The received signal after single diffraction from non-perfectly conducting wedge under plane wave propagation is given by [91]

$$E_{Rx} = E_i \cdot D_{s,h}(\omega) \cdot A(\mathrm{r}_2) \cdot \mathrm{e}^{-jk(r_1+r_2)} \tag{6.1}$$

where E_{Rx} is the received field. E_i is the transmitted field. r_1 is the distance from the transmitter to the diffracted point. r_2 is the distance from the diffracted point to the receiver. $k = \omega/c$ is the wavenumber. c is the speed of light. ω is the angular frequency. $A(r_2) = 1/\sqrt{r_2}$ is the spreading factor. $D_{s,h}(\omega)$ is the diffraction coefficient for soft and hard polarization correspondingly. It is proposed as

$$D_{s,h}(\omega) = D_1 + D_2 + R_0 D_3 + R_0 R_n D_4 \tag{6.2}$$

where D_i with $i = 1-4$ is given as in [91]

$$D_i = \frac{-e^{j\pi/4}}{2n\sqrt{2\pi k}} \cot(a_i) F\left[2kLn^2 \sin^2(a_i)\right] \tag{6.3}$$

with $a_1 = \left[\pi - (\phi - \phi')\right]/(2n)$, $a_2 = \left[\pi + (\phi - \phi')\right]/(2n)$, $a_3 = \left[\pi - (\phi + \phi')\right]/(2n)$, and $a_4 = \left[\pi + (\phi + \phi')\right]/(2n)$. $L = r_2$ is the distance parameter. The transition function is $F(X)$ which is given as in [91]

$$F[X] = 2j\sqrt{X}e^{jX} \int_{\sqrt{X}}^{\infty} e^{-ju^2} du = \sqrt{j\pi X}e^{jX} erfc\left(\sqrt{jX}\right) \tag{6.4}$$

where $erfc(X)$ is the complementary error function. The Fresnel reflection coefficient for soft and hard polarization is given by [109]

$$R_{s,h}(\theta_1) = \frac{\sin\theta_1 - (1,1/\varepsilon)\sqrt{\varepsilon - \cos^2\theta_1}}{\sin\theta_1 + (1,1/\varepsilon)\sqrt{\varepsilon - \cos^2\theta_1}} \tag{6.5}$$

where $\theta_{1,0} = \phi'$ and $\theta_{1,n} = n\pi - \phi'$ are the reflection angles for $0-$ and $n-$face respectively, $\varepsilon = \varepsilon_r - j\sigma/\omega\varepsilon_0$ is the complex permittivity, σ is the conductivity in S/m, $\varepsilon_0 = 8.854\times10^{-12}$ f/m is the permittivity of free space, and ε_r is the relative permittivity.

An incident wave penetrates the wall of the dielectric wedge if the interior angle is less than $\varphi = 20°$ [104]. A refracted ray occurs across the dielectric wedge in this case. Due to this, an extra shadow boundary exists in the shadow region of the structure that is called transmitted shadow boundary (TSB). In this case, the above four terms UTD (6.2) is not able to end the discontinuity at the TSB. Thus, two more terms are added to the four-terms UTD to confirm the continuity at the TSB [104]. Now, the proposed six-terms UTD is stated as

$$D_{s,h}(\omega) = D_1 + D_2 + R_0 D_3 + R_0 R_n D_4 + T_0 T_0' D_5 + T_n T_n' D_6 \qquad (6.6)$$

where $T_{s,h}(\theta_1) = 1 + R_{s,h}(\theta_1)$ is the transmission coefficients for soft and hard polarization distinctly on the first interface (air/dielectric), and $T'_{s,h}(\theta_2) = 1 + R'_{s,h}(\theta_2)$ is the transmission coefficients on the second interface (dielectric/air) with

$$R'_{s,h}(\theta_2) = \left(\frac{\cos\theta_2 - (1,\varepsilon)\sqrt{1/\varepsilon - \sin^2\theta_2}}{\cos\theta_2 + (1,\varepsilon)\sqrt{1/\varepsilon - \sin^2\theta_2}} \right) \qquad (6.7)$$

$$\theta_{2,0,n} = \varphi - \arcsin\left(\cos\left(\phi', n\pi - \phi\right)/\varepsilon_r\right) \qquad (6.8)$$

Here, D_5 and D_6 are defined as the (14) and (7) of [104].

$$D_5 = \frac{-e^{-j(\pi/4)}}{2n\sqrt{2\pi k_d}} \cot\left(\left(2\pi - \left(\phi - g_0(\phi')\right)\right)/(2n)\right) F\left[k_d L^i b_5\right] \qquad (6.9)$$

$$b_5 = 2\cos^2\left\{\frac{2\pi n N_5 + \left(\phi - \left(\pi + g_0(\phi')\right)\right)}{2}\right\} \qquad (6.10)$$

N_5 is the nearest integer solution of

$$2\pi nN_5 + \left(\phi - \left(\pi + g_0\left(\phi'\right)\right)\right) = -\pi \tag{6.11}$$

b_5 of (6.10) can also be simplified using the (13) of [125] to remove the integer N_5 as $b_5 = 2n^2 \sin^2\left(a_5\right)$. Hence, D_5 can be written in simple form as follows

$$D_5 = \frac{-e^{-j(\pi/4)}}{2n\sqrt{2\pi k_d}} \cot\left(a_5\right) F\left[2k_d L^i n^2 \sin^2\left(a_5\right)\right] \tag{6.12}$$

$$a_5 = \left[2\pi - \left(\phi - g_0\left(\phi'\right)\right)\right] / \left(2n\right) \tag{6.13}$$

$$g_0\left(\phi'\right) = \frac{\pi}{2} - \varphi - \arcsin\left\{\sqrt{\varepsilon_r}\,\sin\left[\arcsin\left(\frac{\cos\left(\phi'\right)}{\sqrt{\varepsilon_r}}\right) - \varphi\right]\right\} \tag{6.14}$$

and

$$D_6 = \frac{-e^{-j(\pi/4)}}{2n\sqrt{2\pi k_d}} \cot\left(\left(2\pi + \left(\phi + g_n\left(\phi'\right)\right)\right) / \left(2n\right)\right) F\left[k_d L^i b_6\right] \tag{6.15}$$

$$b_6 = 2\cos^2\left\{\frac{2\pi nN_6 + \left(\phi + \left(\pi + g_n\left(\phi'\right)\right)\right)}{2}\right\} \tag{6.16}$$

N_6 is the nearest integer solution of

$$2\pi nN_6 + \left(\phi + \left(\pi + g_n\left(\phi'\right)\right)\right) = \pi \tag{6.17}$$

b_6 of (6.16) can also be simplified using the (13) of [125] to remove the integer N_6 as $b_6 = 2n^2 \sin^2\left(a_6\right)$. Hence, D_6 can be written in simple form as follows

$$D_6 = \frac{-e^{-j(\pi/4)}}{2n\sqrt{2\pi k_d}} \cot\left(a_6\right) F\left[2k_d L^i n^2 \sin^2\left(a_6\right)\right] \tag{6.18}$$

$$a_6 = \left[2\pi + \left(\phi + g_n\left(\phi'\right)\right)\right] / \left(2n\right) \tag{6.19}$$

$$g_n(\phi') = -\frac{\pi}{2} - \arcsin\left\{\sqrt{\varepsilon_r}\sin\left[\varphi - \arcsin\left(\frac{\cos(\varphi+\phi')}{\sqrt{\varepsilon_r}}\right)\right]\right\} \qquad (6.20)$$

where $k_d = k\sqrt{\varepsilon_r}$.

6.3.2 TD-UTD

The impulse response of a single diffracted ray shown in Fig. 6.2 can be given by setting $E_i = 1$ (with impulsive excitation) in (6.1). Therefore, the impulse response

$$h(t) = A(\mathrm{r}_2)\cdot\left[d_{s,h}(t) * \delta\left(t-(r_1+r_2)/c\right)\right] \qquad (6.21)$$

where the delta function $\delta\left(t-(r_1+r_2)/c\right)$ is related to a shift in time that the transmitted signal takes to traverse the path to the receiver. The $d_{s,h}(t)$ is the TD-UTD for a non-perfectly conducting wedge which is expressed as

$$d_{s,h}(t) = d_1 + d_2 + r_0 * d_3 + r_0 * r_n * d_4 \qquad (6.22)$$

where $d_i(t)$ with $i = 1-4$ is given as in [91]

$$d_i(t) = -\frac{Ln}{2\pi\sqrt{2c}} \times \frac{\sin(2a_i)}{\sqrt{t}\left(t + 2Ln^2\sin^2(\mathrm{a}_i)/c\right)}\cdot u(t) \qquad (6.23)$$

The Heaviside step function is $u(t)$. $r_{s,h}(t)$ is the TD Fresnel reflection coefficient of (6.5). This is given by [109]

$$r_{s,h}(t) = \mp\left[P\,\delta(t) + \frac{4p}{1-p^2}\frac{e^{-at}}{t}\sum_{q=1}^{\infty}(-1)^{q+1}qP^qI_q(at)\right] \qquad (6.24)$$

where $P_{s,h} = \left(1-p_{s,h}\right)/\left(p_{s,h}+1\right)$, $p_s = \sin\theta_1\Big/\sqrt{\left(\varepsilon-\cos^2\theta_1\right)}$,

$p_h = \sqrt{\left(\varepsilon-\cos^2\theta_1\right)}\Big/\left(\varepsilon\cdot\sin\theta_1\right)$, $\delta(t)$ is the Dirac delta function, the modified Bessel function

of order q is $I_q(t)$, $a=\sigma/(2\varepsilon_r\varepsilon_0)$, and soft (hard) polarizations represented by the leading $-(+)$ sign.

Considering the refracted rays from the dielectric interface, the (6.6) can be written in the time-domain as

$$d_{s,h}(t)=d_1+d_2+r_0*d_3+r_0*r_n*d_4+t_0*t_0'*d_5+t_n*t_n'*d_6 \qquad (6.25)$$

where

$$d_5(t)=-\frac{L^i n}{2\pi\sqrt{2v}}\times\frac{\sin(2a_5)}{\sqrt{t}\left(t+2L^i n^2\sin^2(\mathrm{a}_5)/v\right)}\cdot u(t) \qquad (6.26)$$

and

$$d_6(t)=-\frac{L^i n}{2\pi\sqrt{2v}}\times\frac{\sin(2a_6)}{\sqrt{t}\left(t+2L^i n^2\sin^2(\mathrm{a}_6)/v\right)}\cdot u(t) \qquad (6.27)$$

Where $t_{s,h}(t)=\delta(t)+r_{s,h}(t)$ is the time-domain transmission coefficients on the first interface (air/dielectric), and $t'_{s,h}(t)=\delta(t)+r'_{s,h}(t)$ is the TD transmission coefficients on the second interface (dielectric/air) with $r'_{s,h}(t)$ as in (6.24)

$$r'_{s,h}(t)=\mp\left[P''\delta(t)+\frac{4p''}{1-p''^2}\frac{e^{-at}}{t}\sum_{q=1}^{\infty}(-1)^{q+1}qP''^{q}I_q(at)\right] \qquad (6.28)$$

where $P''_{s,h}=(1-p''_{s,h})/(p''_{s,h}+1)$, $p''_s=\cos\theta_2/\sqrt{(1/\varepsilon-\sin^2\theta_2)}$,

$p''_h=\varepsilon\sqrt{(1/\varepsilon-\sin^2\theta_2)}/(\cos\theta_2)$, and $v=c/\sqrt{\varepsilon_r}$.

6.4 Multiple Diffraction

Figs. 6.3 (a) and (b) show the multiple diffractions by two consecutive wedge structures and a lossy building structure respectively.

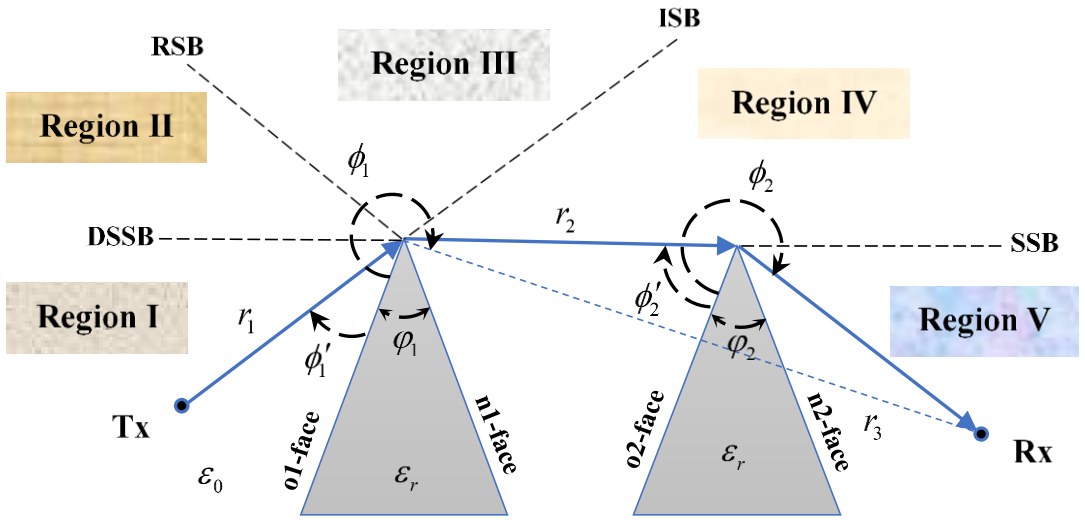

(a)

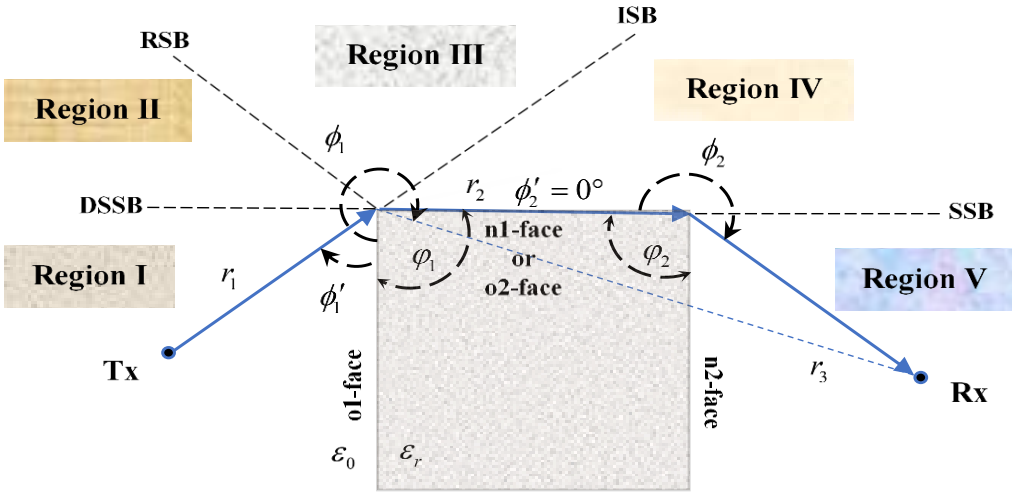

(b)

Fig. 6.3 Double diffraction. (a) by two consecutive wedges. (b) by a lossy building.

The transmitting and receiving points are represented by (r_1, ϕ_1') and (r_3, ϕ_1) respectively. In Fig. 6.3 (b), the case of grazing incidence is considered where the incident angle ϕ_2' is $0°$. In this

case, slope diffraction is used to find a doubly diffracted field. There are five regions in Fig. 6.3 and each region has the following fields for an incident wave on the 01-face of the wedge:

Region I Total Field=Reflected Field + Incident Field + Diffracted Field. The limiting boundary is the double scattered shadow boundary (DSSB).

Region II Total Field=Reflected Field + Incident Field + Diffracted Field + Doubly Diffracted Field. The limiting boundary is RSB.

Region III Total Field=Incident Field + Diffracted Field + Doubly Diffracted Field. The limiting boundary is ISB.

Region IV Total Field=Diffracted Field + Doubly Diffracted Field. The limiting boundary is the scattered shadow boundary (SSB).

Region V Total Field=Doubly Diffracted Field. This region is limited by the wedge structure.

6.4.1 FD Solution

The doubly diffracted field at the receiver for plane wave incidence is expressed as [106]

$$E_{DRx} = \frac{E_i e^{-jk(r_1+r_2+r_4)}}{\sqrt{r_2 r_4}} \times \left[D^1 D^2 - \frac{1}{jkr_2} \frac{\partial D^1(\phi_1, \phi_1')}{\partial \phi_1} \frac{\partial D^2(\phi_2, \phi_2')}{\partial \phi_2'} \right] \tag{6.29}$$

where $D^1(\phi_1, \phi_1')$ and $D^2(\phi_2, \phi_2')$ are the FD-UTD coefficient on the first and second wedge. $\frac{\partial D^1(\phi_1, \phi_1')}{\partial \phi_1}$ and $\frac{\partial D^2(\phi_2, \phi_2')}{\partial \phi_2'}$ are the slope diffraction coefficients. It can be given as in [91,106].

6.4.2 TD Solution

The TD doubly diffracted field can be given by taking inverse Laplace transform of (6.29) as

$$e_{DRx}(t) = \frac{e_i(t)}{\sqrt{r_2 r_4}} * \left[\left\{ d^1(t) * d^2(t) - \frac{1}{r_2} d^{1f}(t) * d^{2f}(t) \right\} * \delta\left(t - \frac{r_1 + r_2 + r_4}{c} \right) \right] \tag{6.30}$$

where, $d^1(t)$ and $d^2(t)$ are the TD-UTD diffraction for wedge 1 and wedge 2. They are derived similarly to (6.22). The $d^{1f}(t)$ and $d^{2f}(t)$ are expressed as [92]

$$\begin{aligned} d^{1f}(t) &= L^{-1}\left\{ \frac{1}{\sqrt{jk}} \frac{\partial D^1}{\partial \phi_1} \right\} \\ &= \frac{-L}{\sqrt{2\pi}} \left[F^{(1)}(t) - F^{(2)}(t) + r_0 * F^{(3)}(t) - r_0 * r_n * F^{(4)}(t) \right] \\ &\quad + \frac{c}{2n\sqrt{2\pi}} \left[\cot(\mathrm{a}_2) \cdot \left\{ r_0 * \frac{\partial r_n}{\partial \phi_1} * \frac{\sqrt{\varsigma_2}}{\sqrt{t+\varsigma_2}} \right\} + \cot(\mathrm{a}_4) \cdot \left\{ \frac{\partial r_n}{\partial \phi_1} * \frac{\sqrt{\varsigma_4}}{\sqrt{t+\varsigma_4}} \right\} \right] \end{aligned} \tag{6.31}$$

and

$$\begin{aligned} d^{2f}(t) &= L^{-1}\left\{ \frac{1}{\sqrt{jk}} \frac{\partial D^2}{\partial \phi_2'} \right\} \\ &= \frac{-L}{\sqrt{2\pi}} \left[-F^{(1)}(t) + F^{(2)}(t) + r_0 * F^{(3)}(t) - r_0 * r_n * F^{(4)}(t) \right] \\ &\quad - \frac{c}{2n\sqrt{2\pi}} \left[\cot(\mathrm{a}_2) \cdot \left\{ \frac{\partial r_0}{\partial \phi_2'} * r_n * \frac{\sqrt{\varsigma_2}}{\sqrt{t+\varsigma_2}} \right\} + \cot(\mathrm{a}_3) \cdot \left\{ \frac{\partial r_0}{\partial \phi_2'} * \frac{\sqrt{\varsigma_3}}{\sqrt{t+\varsigma_3}} \right\} \right] \end{aligned} \tag{6.32}$$

where $F^{(i)}(t) = \frac{\sqrt{\varsigma_i}}{2(t+\varsigma_i)^{3/2}} \cdot u(t)$ and $\varsigma_i = 2Ln^2 \sin^2(\mathrm{a}_i)/c$ with a_i as defined earlier. The derivative terms $\frac{\partial r_0}{\partial \phi_2'}$ and $\frac{\partial r_n}{\partial \phi_1}$ can be given as [91].

The simulation results are projected in the following section to check the exactness of proposed FD and TD solutions as discussed in section 6.3 and 6.4. The TD solutions will also be tested for different types of excitation pulses and wedge materials.

6.5 Results and Discussions

A heuristic four-terms UTD and its extended formulation of six-terms UTD are proposed in this paper. Our work shows how the six terms UTD performs in the case of a lossy wedge with an internal angle that is small enough. In Figs. 6.4 (a) and (b), the total field around a lossy wedge is irregular on the transmission shadow boundary (TSB) in the case of the four-terms UTD coefficient (6.2) in both the polarization soft and hard. Subsequently, this irregularity vanishes by the six-terms UTD where two extra terms are included in the four-terms UTD coefficient.

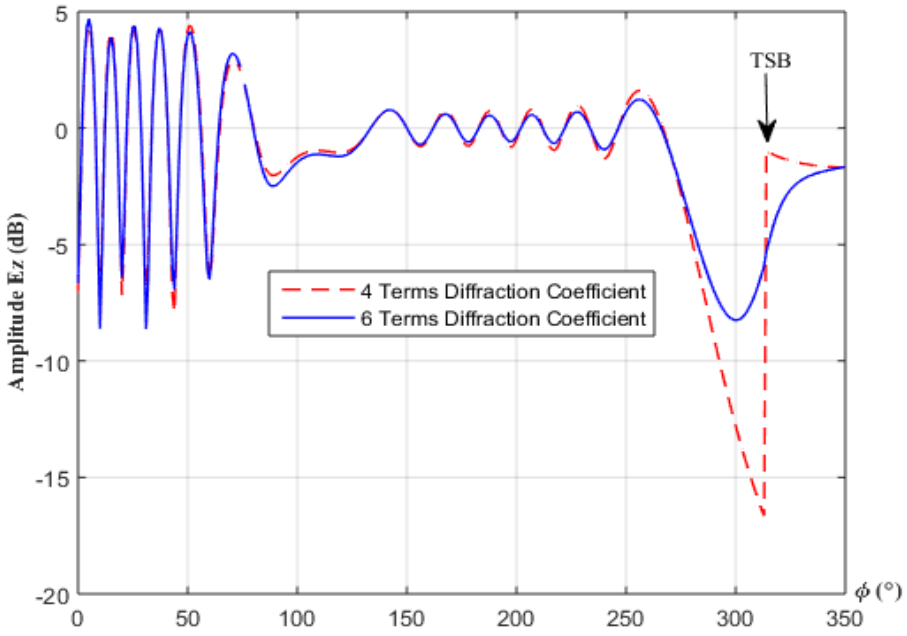

(a)

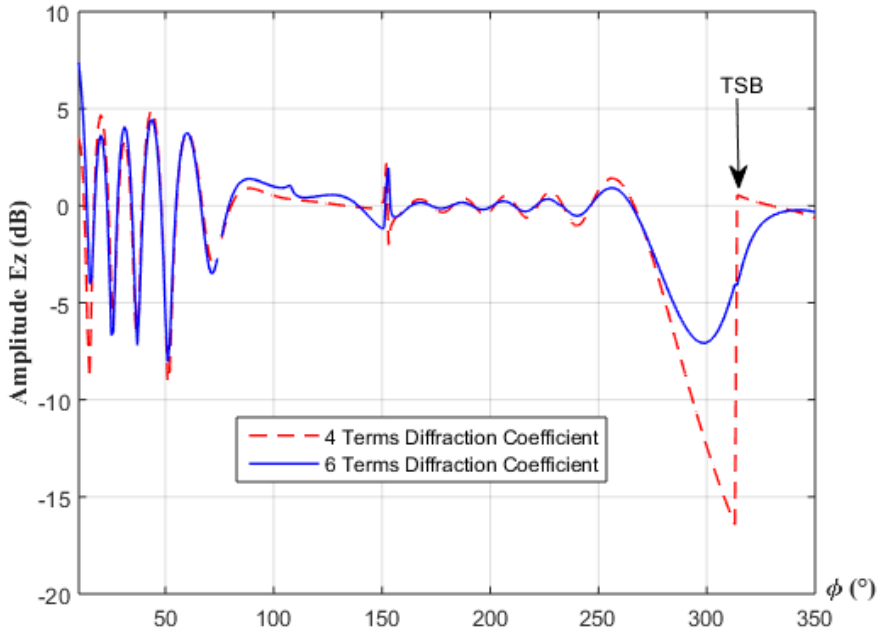

(b)

Fig. 6.4 Comparison of 4 Terms UTD and 6 Terms UTD using the scenario of Fig. 6.2. $f = 900$ MHz, $\phi' = 105°$, $r_2 = 1$m, $\varphi = 10°$, relative permittivity ($\varepsilon_r = 10$), and conductivity ($\sigma = 0.001$ S/m). (a) Soft polarization. (b) Hard polarization.

We represent the usefulness of the proposed six-terms UTD coefficient in Fig. 6.5 and Fig. 6.6. Here, the six-terms UTD [104] and the proposed six-terms UTD are compared with the FDTD method. A better agreement is obtained between the proposed UTD and FDTD than the results [104]. It is observed that there is an agreement between FDTD and the results of the proposed method in the regions where the GO field occurs. However, there is a significant difference between FDTD and the proposed method in the region between ISB and TSB where only diffracted field exists. This difference could be occurred due to ignorance of multipath between the two interfaces by the heuristic proposed method, while the same is considered in the full-wave FDTD approach.

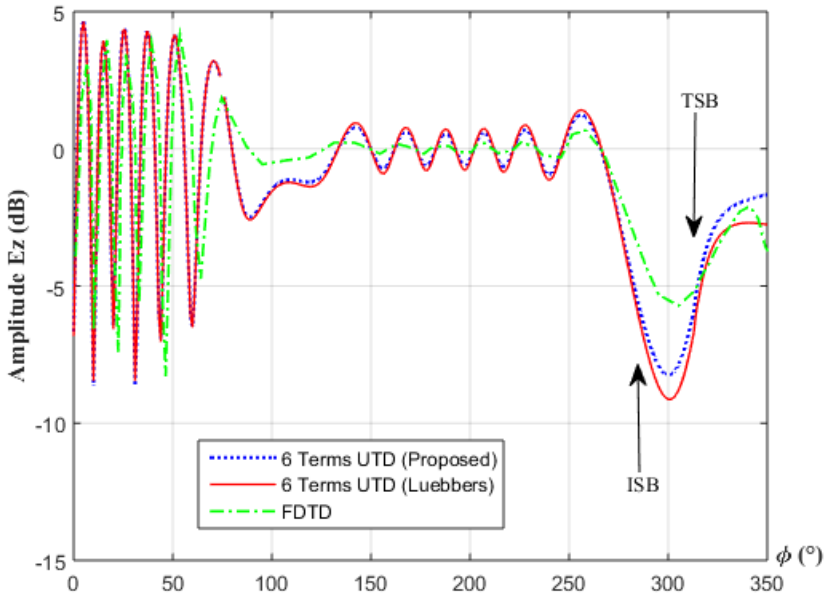

Fig. 6.5 Comparison of 6 Terms UTD (Proposed) and 6 Terms UTD (Luebbers) with FDTD using the scenario of Fig. 6.2. $f = 900$ MHz, $\phi' = 105°$, $r_2 = 1\,\text{m}$, $\varphi = 10°$, relative permittivity ($\varepsilon_r = 10$), and conductivity ($\sigma = 0.001\,\text{S/m}$).

Table 6.1 Various parameters from the simulated results of Fig. 6.5**.**

Parameter	**Value at** $\phi' = 305°$	**Value at** $\phi' = 313°$
Diffraction Coefficient, $D(\omega)$	0.2113- 0.1212i	0.1581-0.1119i
Amplitude of received electric field (*Ez*) by FDTD method	-5.7208 dB	-5.1729 dB
Ez by proposed method with respect to the FDTD result	-2.30 dB	-1.04 dB
Ez (Luebbers) [104] with respect to the FDTD result	-3.23 dB	-1.856 dB
Improvement of the proposed method over existing method [104] with respect to the FDTD result	0.93 dB	0.816 dB
% Improvement with respect to the FDTD result	16.24 %	14.88 %

From the Table 6.1, the value of diffraction coefficients between ISB and TSB are decreasing because the receiver moved from $\phi' = 305°$ to $\phi' = 313°$. The improvement of the proposed method over the existing method [104] with respect to the FDTD result is also decreasing due to the non-linear behaviour of the diffraction coefficient. Similarly, % of improvement has decreased in Fig 6.6.

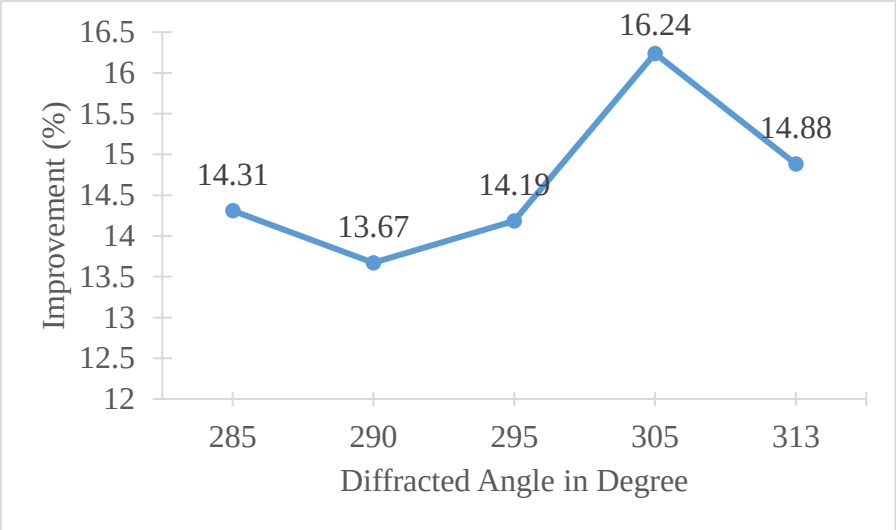

Fig. 6.6 Improvement (%) of 6 Terms UTD (Proposed) over 6 Terms UTD (Luebbers) of [104] in the deep shadow region (ISB-TSB)

Figs. 6.3 (a) and (b) show the scenario of multiple diffractions. We select a high lossy wedge material with a large thickness in Fig. 6.3 (b). The total field around the structure is calculated by applying UTD on two consecutive wedge vertices. Furthermore, we have calculated the doubly diffracted field using the slope diffraction all around the structure even in Region V. The results are presented in Figs. 6.7 and 6.8 show a good agreement with and without the slope diffraction before the SSB. Indeed, the diffracted field is the only field calculated after the ISB. Only, we get the doubly diffracted field in Region V. Thus, the results for both the soft and hard polarization are good in all the regions around the dielectric wedge.

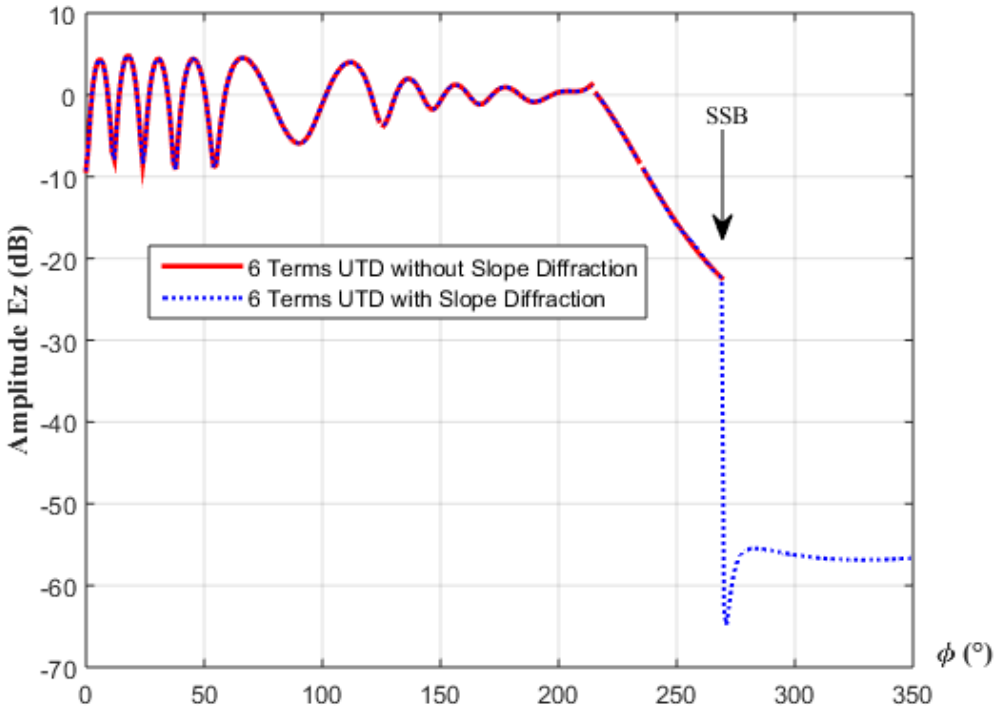

(a)

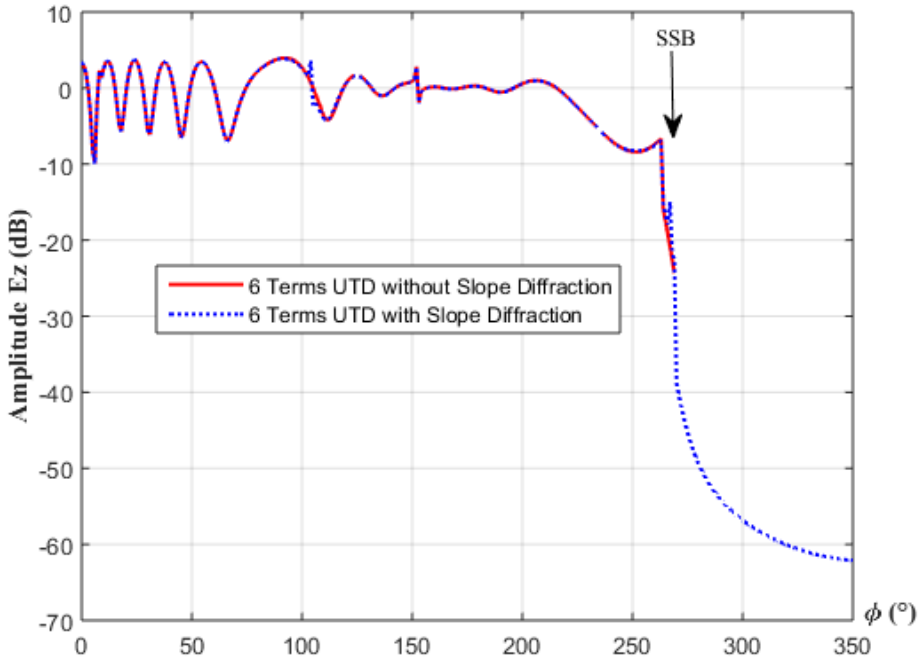

(b)

Fig. 6.7 Comparison of 6 Terms UTD without slope diffraction and 6 Terms UTD with slope diffraction using the scenario shown in Fig. 6.3 (a). $f = 900$ MHz, $\phi' = 55°$, $r_2 = 0.9$ m, $r_3 = 1$ m, $\varphi_1 = 10°$, $\varphi_2 = 10°$, $\varepsilon_r = 10$, $\sigma = 0.001$ S/m.

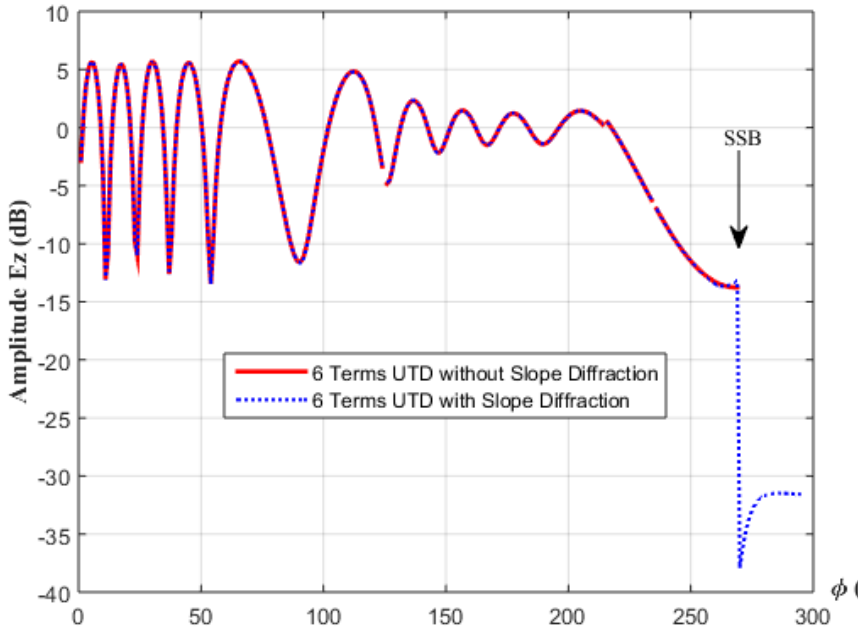

(a)

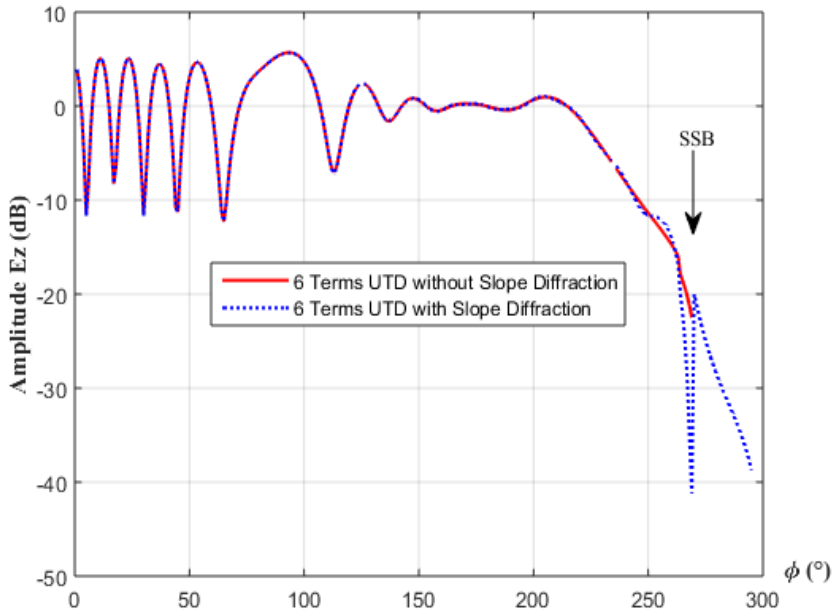

(b)

Fig. 6.8 Comparison of 6 Terms UTD without slope diffraction and 6 Terms UTD with slope diffraction using the scenario shown in Fig. 6.3 (b). $f = 900$ MHz, $\phi' = 55°$, $r_2 = 0.9$ m, $r_3 = 1\,\text{m}$, $\varphi_1 = 90°$, $\varphi_2 = 90°$, $\varepsilon_r = 10$, $\sigma = 0.001\,\text{S/m}$.

The Gaussian pulses [103] shown in Fig. 6.9 are used to test the TD solutions proposed in Sections 6.3 and 6.4. Here, the time-scaling factor $\tau = 0.1$ ns is selected. It is seen that the first-order Gaussian pulse is crossing the zero line only once. However, its next derivatives are crossing the zero line twice and thrice. It means each derivative is producing extra zero crossings.

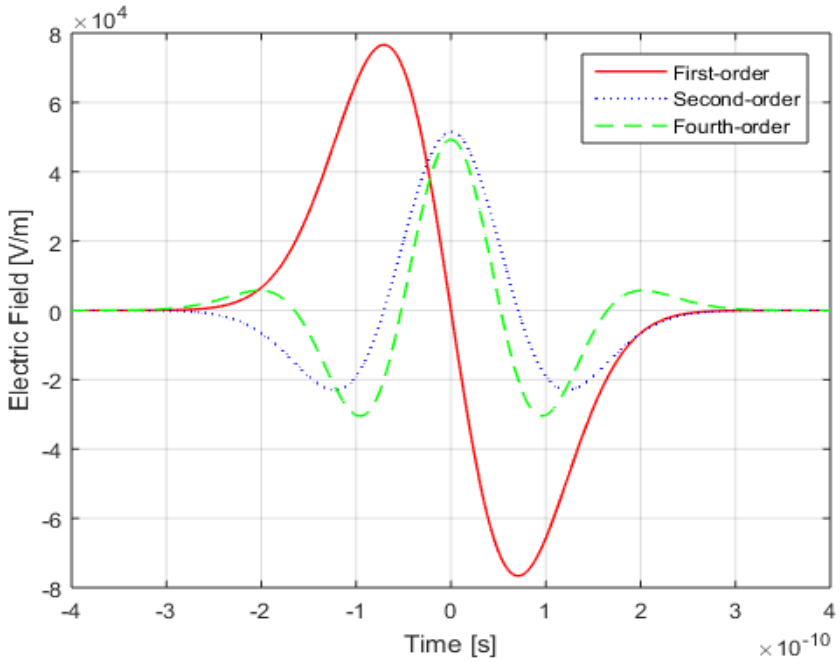

Fig. 6.9 Input Gaussian pulses.

The second-order Gaussian pulse is shown in Fig. 6.9 is the most common pulse stated in many works of literature [109,124]. The TD received signal due to diffraction by a dielectric wedge is shown in Fig. 6.10. It is seen that the TD-UTD results are matching with the IFFT-FD results in both the soft and hard polarization. Hence, the proposed TD-UTD is right. From Figs. 6.9 and 6.10, It is also observed that the input pulse has been extremely attenuated and distorted due to diffraction by a dielectric wedge. This attenuation and shape distortion is resulted due to the lossy nature of dielectric materials and frequency dependence of the TD-UTD coefficient.

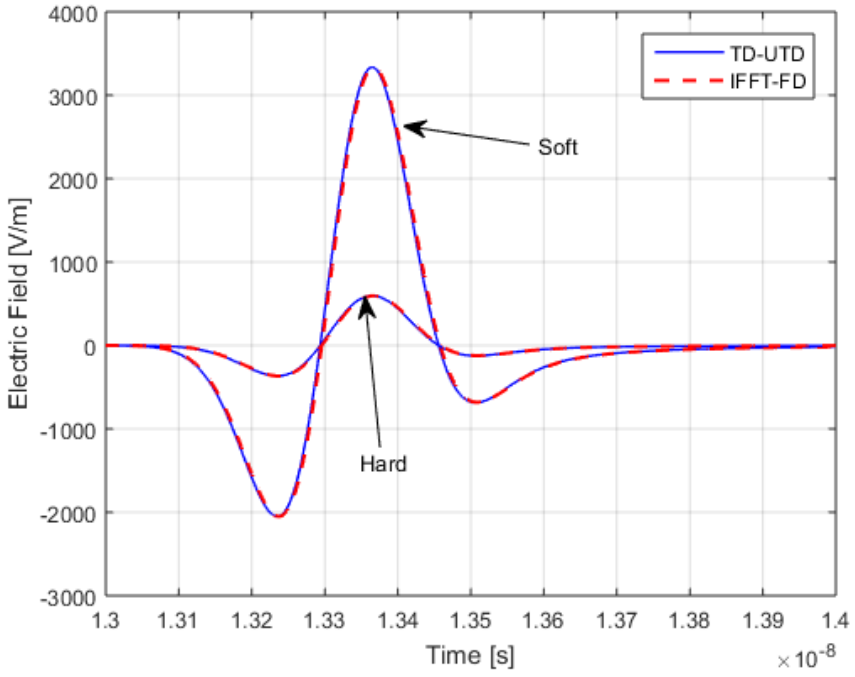

Fig. 6.10 TD received field for the scenario shown in Fig. 6.1. $\phi' = 105°$, $\phi = 345°$, $r_2 = 1\text{m}$, $\varphi = 10°$, relative permittivity $\varepsilon_r = 10$, conductivity $\sigma = 0.001\,\text{S/m}$. Gaussian 2nd-order input pulse and single diffraction.

Figs. 6.11 (a) and (b) show the received signal for the scenario shown in Fig. 6.2 in response to first- and fourth-order Gaussian input pulses which again confirms the overall performance of the TD-UTD solution. There are good matching between TD-UTD and IFFT-FD results in both the polarization. It is also observed that the diffraction coefficient is frequency-dependent which distorts the input pulses. These input pulses are of very short duration (in ns). Therefore, it is very well suitable for UWB communication in 5G that supports wide bandwidth and high data rates.

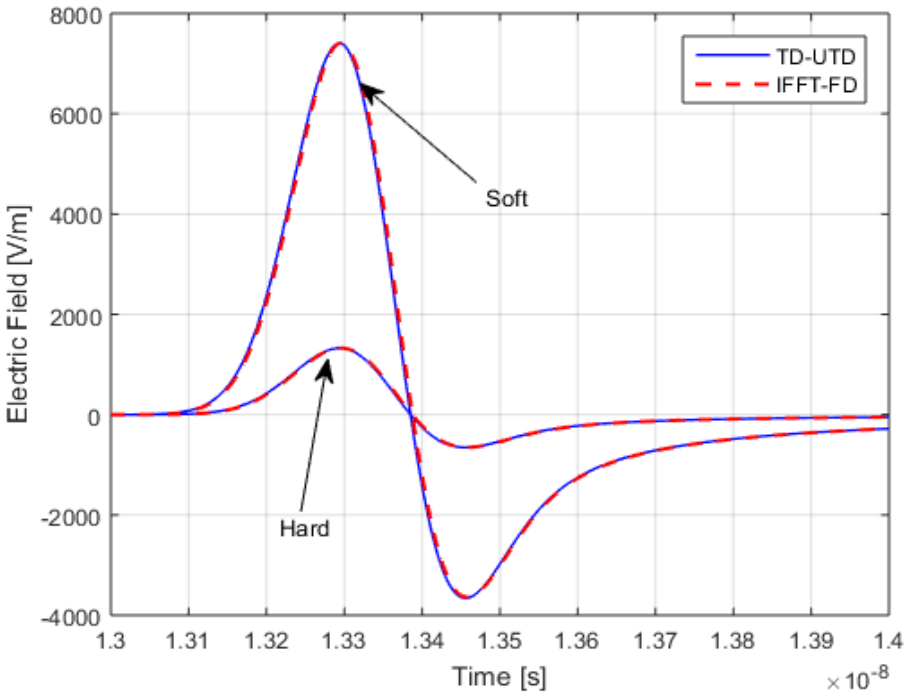

(a)

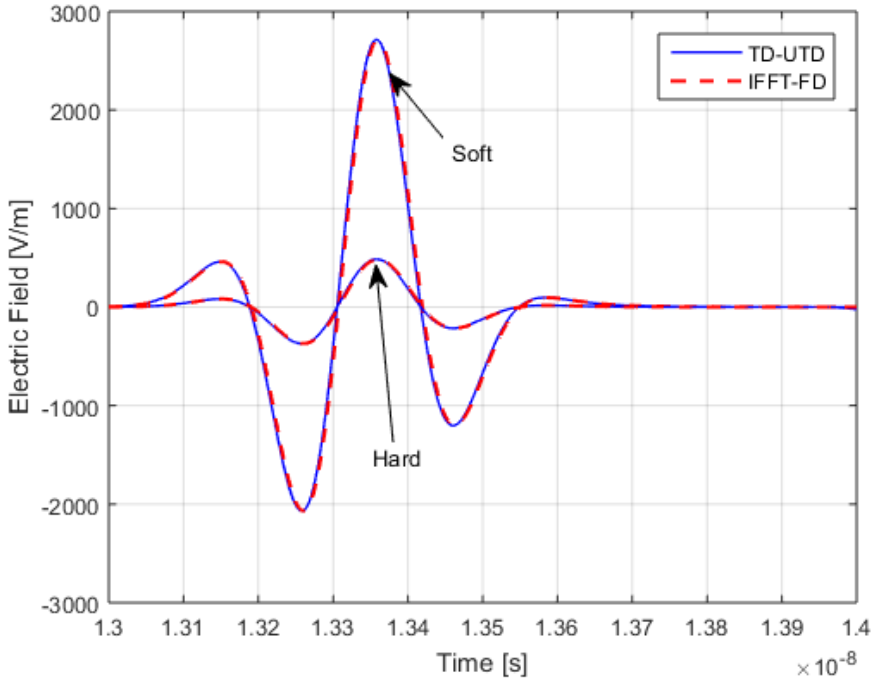

(b)

Fig. 6.11 TD received field due to single diffraction by the scenario shown in Fig. 6.2. $\phi' = 105°$, $\phi = 345°$, $r_2 = 1\,\text{m}$, $\varphi = 10°$, $\varepsilon_r = 10$, $\sigma = 0.001\,\text{S/m}$. (a) Response for first-order gaussian pulse. (b) Response for fourth-order Gaussian pulse.

Furthermore, the wave propagation of signals has different behaviour for different dielectric wedge materials. The following wedge materials shown in Table 6.2 are considered in the simulation to see the TD-UTD behaviour.

Table 6.2 Different wedge materials [103].

Wedge materials	Relative permittivity ε_r	Conductivity σ (S/m)
Concrete	10	0.001
Glass	6.7	0.001
Brick	4.4	0.018
Wood	2	0.01

Fig. 6.12 shows the diffracted signals in response to the Gaussian 2nd -order input pulse for the scenario stated in Fig. 6.2 considering soft polarization. Here, also attenuation and pulse distortion is observed in the received signals due to the same reasons stated earlier. Moreover, it is seen that the strength of diffracted signals decreases for further lossy wedge materials.

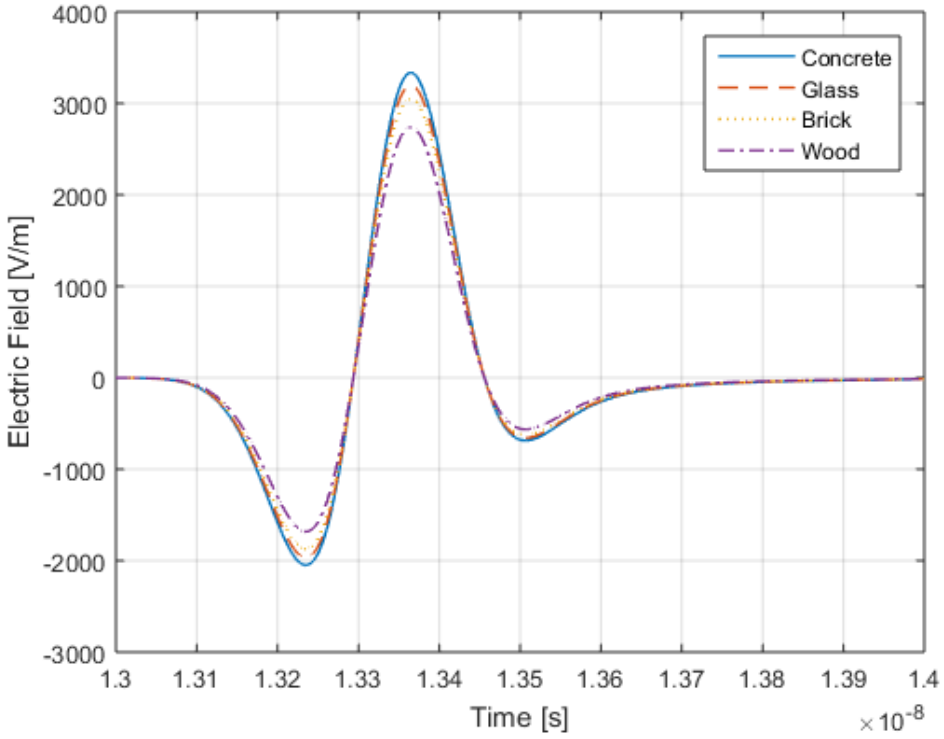

Fig. 6.12 TD received fields for the scenario shown in Fig. 6.1 in which wedge is made with different building materials. $\phi' = 105°$, $\phi = 345°$, $r_2 = 1\text{m}$, $\varphi = 10°$. Single diffraction and 2nd-order Gaussian input pulse.

Figs. 6.13 and 6.14 show the doubly diffracted field at the receiver for 2nd -order Gaussian input pulse by two wedges of the same structure Fig. 6.3 (a) and a high lossy building Fig. 6.3 (b) under soft polarization. There are good matching among TD-UTD and IFFT-FD results. Therefore, it confirms the exactness of the TD-UTD solution. It is also seen that the doubly diffracted fields are extremely attenuated and distorted to the input pulse applied due to the high-frequency dependence of the response. This attenuation and pulse distortion is more for the case of building scenarios than the two wedge structure. This is due to the case of grazing incidence where only slope diffracted fields are available at the receiver.

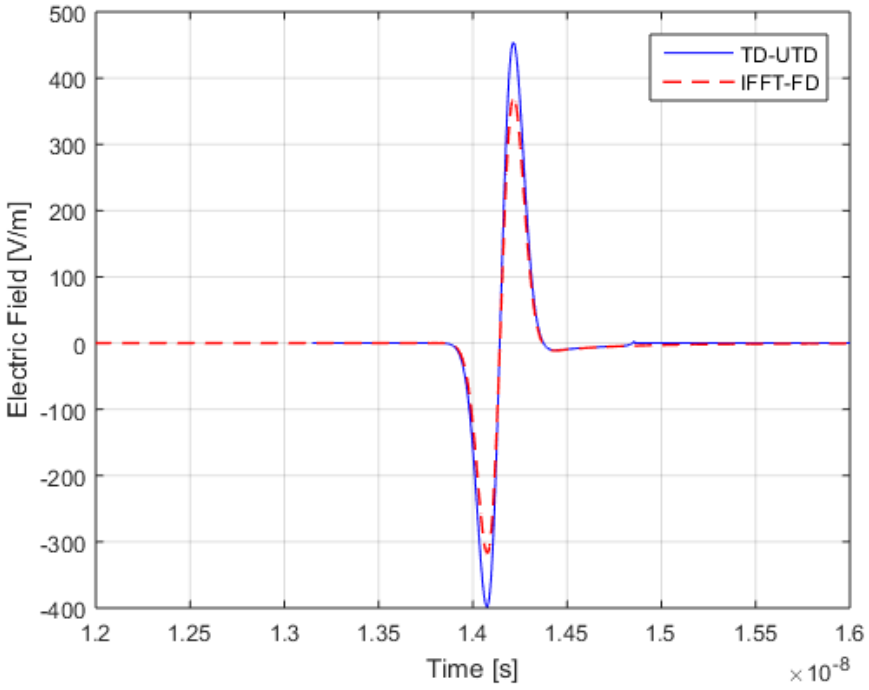

Fig. 6.13 TD received field for the scenario shown in Fig. 6.2 (a). $\phi_1' = 55°$, $\phi_1 = 290°$, $r_2 = 0.9\,\text{m}$, $r_3 = 1\,\text{m}$, $\varphi = 10°$, $\varepsilon_r = 10$, $\sigma = 0.001\,\text{S/m}$. Double diffraction.

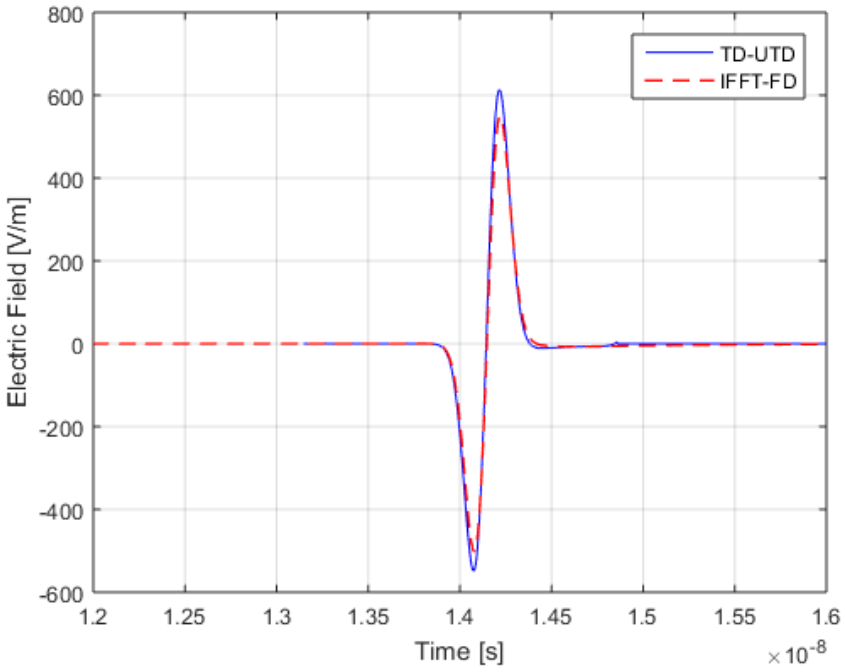

Fig. 6.14 TD received field for the scenario shown in Fig. 6.3 (b). $\phi_1' = 55°$, $\phi_1 = 290°$, $r_2 = 0.9\,\text{m}$, $r_3 = 1\,\text{m}$, $\varphi = 90°$, $\varepsilon_r = 10$, $\sigma = 0.001\,\text{S/m}$. Double diffraction (gazing incidence case) .

It is seen that the received signal is not similar to the input pulse in shape and is distorted. Fig. 6.15 demonstrates the impulse response for the scenario shown in Figs. 6.2 and 6.3 considering soft polarization. We know that the different frequency components of the TD-UTD coefficient have different attenuation. Due to this, the shape of the received signal is not similar to the impulse signal and hence, it is distorted. Furthermore, it is also observed that the doubly diffracted fields are more distorted due to the only consideration of slope diffraction.

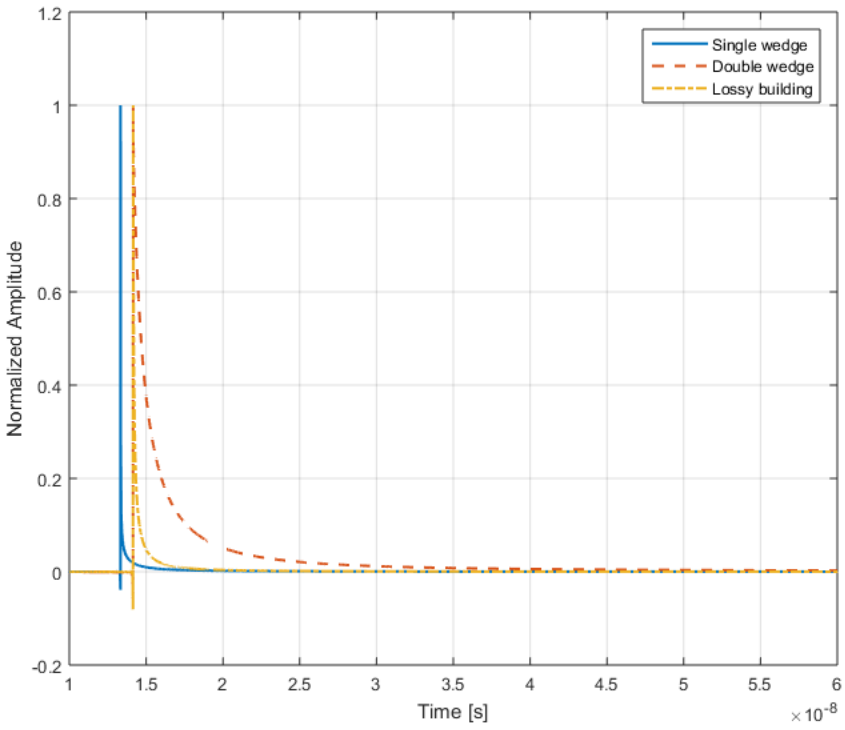

Fig. 6.15 The channel impulse response for the scenario shown in Figs. 6.2, 6.3 (a) and (b).

Table 6.3 and Fig. 6.16 project the details of the time taken in simulation by the TD-UTD and IFFT-FD techniques. It is seen that the IFFT-FD solution consumes more time than the TD-UTD technique due to the following reasons.1) The TD-UTD technique is based on the effective convolution method. 2) The IFFT-FD method computes a large range of frequency due to the short duration of the input Gaussian pulse.

Table 6.3 Details of the time taken in simulation by the TD-UTD and IFFT-FD techniques.

Dielectric Wedge Scenario	Time (TD-UTD) in (Sec.)	Time (IFFT-FD) in (Sec.)	Time (IFFT-FD)/ Time (TD-UTD)
Single Wedge	0.26	12.69	47.09
Building	0.99	22.76	22.95
Two wedge structure	0.85	20.67	24.18

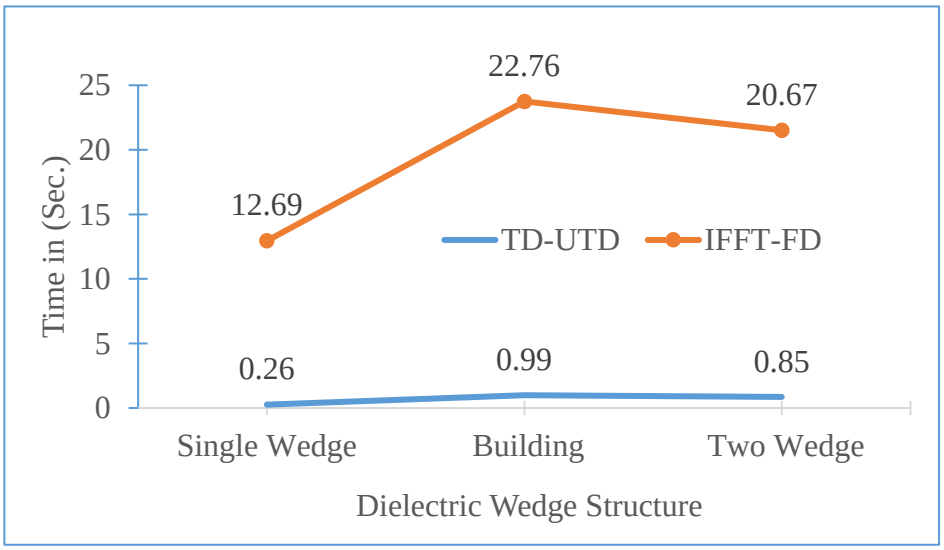

Fig. 6.16 Time taken by the direct TD-UTD method and the IFFT-FD method.

6.6 Conclusion

Novel diffraction coefficients in FD and TD have been presented in this chapter. The FD-UTD coefficient was shown to be accurate in all the regions for a thin lossy wedge. It permits the computation of the transmitted ray through the dielectric wedge by including two more terms in the four-terms FD-UTD coefficient. This novel six-terms FD-UTD coefficient has been verified with the available FDTD technique. Next, the doubly diffracted field due to the slope diffraction coefficient behind the double wedge structure and a high lossy building is also presented. Furthermore, a novel TD-UTD coefficient has been presented based on the IFFT of the proposed FD solutions. The different input pulses and wedge materials have been used to test the overall performance of the proposed TD techniques. The TD-UTD results have been verified with IFFT-FD results, and very good agreements have been reported. The impulse response is also presented to explain the pulse distortion for the different scenarios. Finally, it is seen that the TD-UTD technique is shown to be computationally more efficient than the IFFT-FD technique.

Chapter 7

Conclusion and Future Scope

This chapter deals with the conclusion of the complete work that has been done in the thesis and the future scope of the proposed concept. This thesis is mainly focused on TD modeling of the wireless channel for UWB applications.

7.1 Conclusion

The main conclusions of this thesis are abridged as follows:

Chapter 1 starts with the significance of UWB communications in 5G innovation, the need for channel modeling for Ultra-wideband applications, and the high-frequency phenomenon of electromagnetic waves. From that point onward, the study positions and research objectives are clarified.

In Chapter 2, a new TD diffraction coefficient is proposed. It is based on the direct convolution method by taking inverse Laplace transform of FD diffraction coefficients that apply to the situation when the source illuminates possibly one or the two sides of the non-perfectly conducting wedge with arbitrary internal angles.

In Chapter 3, a TD double diffraction is presented that applies to the case when the source illuminates either one or both sides of the non-perfectly conducting wedge with arbitrary internal angles.

In Chapter 4, TD multiple-order diffraction coefficients are introduced. Just, the first-order TD-UTD coefficient is applied for calculating the higher-order diffraction without utilizing any higher-order diffraction terms such as slope diffraction coefficients.

In chapter 5, novel six-terms UTD diffraction coefficients in TD has been introduced to consider transmission and diffraction phenomena from a thin dielectric wedge

Novel diffraction coefficients in FD and TD have been introduced in chapter 6. The FD-UTD coefficient was demonstrated to be exact in every one of the regions for a thin lossy wedge. It allows the calculation of the transmitted ray through the dielectric wedge by including two additional terms in the four-terms FD-UTD coefficient. Besides, a novel TD-UTD coefficient has been introduced dependent on the IFFT of the proposed FD solutions.

In the above parts, The TD-UTD results have been checked with IFFT-FD results, and excellent matchings have been accounted for. At long last, it is seen that the TD-UTD procedures are demonstrated to be computationally more productive than the IFFT-FD method.

7.2 Future Scope

In this thesis, a time-domain model has been presented for rectangular shaped wedge structure maximum up to two wedges but there are also other structures even more than two need to be investigated in future work.

- The self-consistent method in the time-domain for UWB applications may be applied for considering multiple order-diffracted fields between more than two wedges with all possible orders of diffraction.

- The six-terms UTD formulation of diffraction and transmission phenomenon in time-domain may be extended for curved shaped wedge structure for UWB applications.

- Field measurements at the receiver can be carried out for various scenarios and compared to simulated results to determine the accuracy of the proposed TD solutions.

References

1. M. Shafi, A. F. Molisch, P. J. Smith, T. Haustein, P. Zhu, P. D. Silva, F. Tufvesson, A. Benjebbour, and G. Wund, " 5G: A tutorial overview of standards, trials, challenges, deployment, and practice," *IEEE Journal on Selected Areas in Communications,* vol. 35, no. 6, pp. 1201-1221, Jun 2017.
2. M. Z. Chowdhury, MD. Shahjalal, S. Ahmed, and Y. M. Jang, " 6G wireless communication systems: applications, requirements, technologies, challenges, and research directions," *IEEE Communication Society,* vol. 1, pp. 957-975, Aug 2020.
3. H. Viswanathan, and P. E. Mogensen, "Communications in the 6G era," *IEEE Access,* vol. 8, pp. 57063- 57074, Mar 2020.
4. R. Puerta, S. Rommel, D. J. Ramirez, and I. T. Monroy, " Ultra-wideband technology: Prospective solution for 5G ultra-small cell networks," *International Journal of Communication Systems,* vol. 33, no. 16, Oct 2020.
5. T. S. Rappaport, G. R. MacCartney, S. Sun, H. Yan, and S. Deng, "Small-scale, local area, and transitional millimeter-wave propagation for 5G communications," *IEEE Trans. Antennas Propag.*, vol. 65, no. 12, pp. 6474 - 6490, Aug. 2017.
6. A. Tajvidy, "Diffraction loss model at 0.3–6 GHz for 5G cellular system in microcell urban areas," Electromagnetics, vol. 39, no. 3, pp. 168 - 185, Dec. 2018.
7. Hsi-Tseng Chou, "An UTD-Analysis of Electromagnetic Scattering From Periodic Array Structures With a Straight Truncation Boundary," *Antennas and Propagation IEEE Transactions on,* vol. 64, no. 7, pp. 3108-3119, 2016.
8. E. T. Michailidis and A. G. Kanatas, *Radio Wave Propagation and Channel Modeling for Earth–Space Systems*. 1st ed., CRC Press, 2016, pp. 299.

9. P. Lyu, X. Xu, S. Yan and Z. Ren, “60 GHz Indoor Propagation With Time-Domain Geometric-Optics”, *IEEE Transactions on Magnetics*, vol. 52 (3), pp. 1-4, 2016.
10. V. U. Zavorotny and A. G. Voronovich, “ Validity of the Kirchhoff-Geometric Optics Approach for Modeling of Ocean Bistatic Radar Scattering,” in *IEEE International Geoscience and Remote Sensing Symposium (IGARSS 2019)*, Jul. 2019, pp. 668-671.
11. Peter D. Holm, “On Geometric Optics Over a Spherical Earth With an Exponential Refraction Index,” *IEEE Transactions on Antennas and Propagation*, vol. 66(12), pp. 6580 – 6587, Dec. 2018.
12. P. L. E. Uslenghi, “Exact Geometrical Optics Scattering by a 45 degree Metal Wedge Illuminated by Multiple Plane Waves,” in *URSI EM Theory Symposium (EMTS 2019)*, San Diego, CA, May 27– 31, 2019, pp. 1-3.
13. T. Wang, C. M. Tong, X. M. Li, B. Chen and T. Song, “A two-scale model modified by improved geometrical optics”, in *IEEE International Conference on Signal Processing, Communications and Computing (ICSPCC)*, Xiamen, China, Oct. 22-25, 2017, pp. 1-3.
14. I. O. Sukharevsky, “Beyond Geometrical Optics: Higher Order Diffraction at Thin Curved Dielectric Layers”, *IEEE Transactions on Antennas and Propagation*, vol. 66 (3), pp. 1404 – 1412, Mar. 2018.
15. K. W. Kim and S. J. Oh, “Geometric Optics-Based Propagation Prediction Model in Urban Street Canyon Environments,” *IEEE Antennas and Wireless Propagation Letters*, vol. 15, pp. 1128 – 1131, Oct. 2016.
16. L. B. Stotts, *Free Space Optical Systems Engineering: Design and Analysis*. Wiley Telecom, 2017, pp. 95 – 121.
17. C. Kim and Y. B. Park, “Prediction of Electromagnetic Wave Propagation in Space Environments Based on Geometrical Optics,” *Journal of Electromagnetic Engineering and Science*, vol. 17 (3), pp. 165-167, Jul. 2017.

18. E M. Cheng, et. al., “Geometrical optics based path loss model for furnished Indoor environment,” *ACES Journal*, vol. 31 (9), pp. 1125-1134, Sept. 2016.
19. T. K. Geok, et al., “A Comprehensive Review of Efficient Ray-Tracing Techniques for Wireless Communication,” *International Journal on Communications Antenna and Propagation*, vol. 8 (2), pp.123-136, Apr. 2018.
20. A. Ishimaru, “Geometric Theory of Diffraction and Low-frequency Techniques,” *Electromagnetic Wave Propagation, Radiation, and Scattering: From Fundamentals to Applications*, 2nd Ed, Wiley-IEEE Press, 2017, pp. 443 – 471.
21. S. W. Ellingson,“An Introduction to the GTD Edge Diffraction via Equivalent Currents,” *IEEE Antennas and Propagation Magazine*, vol. 59 (4), pp. 94 – 99, Aug. 2017.
22. A. L. Bot, “Geometrical theory of diffraction for sound radiation and structural response,” *Wave Motion*, vol. 87, pp. 179-192, Apr. 2019.
23. N. P. B. Kammersgaard *et al.*, “Ear-to-Ear Propagation Model Based on Geometrical Theory of Diffraction,” *IEEE Transactions on Antennas and Propagation*, vol. 67(2), pp. 1153 – 1160, Feb. 2019.
24. N. P. B. Kammersgaard *et al*., “Geometrical Theory of Diffraction Formulation for On-Body Propagation,” *IEEE Transactions on Antennas and Propagation*, vol. 67 (2), pp. 1143 - 1152, Feb. 2019.
25. H. Yan *et al.*, “Monostatic GTD Model for Double Scattering due to Specular Reflections or Edge Diffractions,” *in IEEE International Conference on Computational Electromagnetics (ICCEM)*, Chengdu, China, Mar. 26-28, 2018, pp. 1-3.
26. R. Paknys, “Uniform Theory of Diffraction,” in *Applied Frequency-Domain Electromagnetic*, 1st Ed., Wiley-IEEE Press, 2016, pp. 268 – 316.

27. O. Ozgun, “New Software Tool (GO+UTD) for Visualization of Wave Propagation,” *IEEE Antennas and Propagation Magazine*, vol. 58 (3), pp. 91 – 103, Jun. 2016.
28. H. T. Chou, “An UTD-Analysis of Electromagnetic Scattering From Periodic Array Structures With a Straight Truncation Boundary”, *IEEE Transactions on Antennas and Propagation*, vol. 64 (7), pp. 3108 – 3119, Jul. 2016.
29. L. Azpilicueta *et al*., “Characterisation of radio wave propagation in complex indoor environments with and accurate Ray Launching and UTD method,” in *10th European Conference on Antennas and Propagation (EuCAP)*, Apr. 10-15, 2016, pp. 1-4.
30. P. Sharma, P. Dhuliya and D. Pant, “Comprehensive analysis of spherical wave propagation in a hilly terrain using uniform theory of diffraction,” in *3rd International Conference on Computing for Sustainable Global Development (INDIACom)*, Mar. 16-18, 2016, pp. 602-606.
31. S. Kim and A. Zajic, “UTD-based modeling of diffraction loss by dielectric circular cylinders at D-band,” *IEEE International Symposium on Antennas and Propagation (APSURSI)*, Fajardo, PR, USA, 26 Jun.-1 Jul., 2016, pp. 1365-1366.
32. M. Alban and G. Carluccio, “Frequency and time domain UTD vertex diffraction: A heuristic solution and a step toward the exact one,” *URSI International Symposium on Electromagnetic Theory (EMTS)*, Espoo, Finland, Aug. 14-18, 2016, pp. 1-3.
33. A. E. Aydin and M. B. Tabakcioglu, “Determination of optimum base station location by using UTD model,” *26th Signal Processing and Communications Applications Conference (SIU)*, Izmir, May 2-5, 2018, pp. 1-4.
34. M. Rashedi and A. Torabi, “A uniform geometrical theory of diffraction formulation for the diffraction by a perfect electric conductor and impedance finite width strip,” *International Applied Computational Electromagnetics Society Symposium - Italy (ACES)*, Mar. 26-30, 2017, pp. 1-2.

35. O. Ozlem, “Modeling of Diffraction Effects in Urban Radio wave Propagation,” *Applied Computational Electromagnetics Society Journal*, vol. 32 (7), pp. 593-599, Jul. 2017.
36. E. Arık and M. B. Tabakcıoğlu, “Full Coverage Prediction with UTD and GO model,” *J. Inno. Sci. Eng.*, vol. 2(1): pp. 34-39, Jun. 2018.
37. Y. Z. Umul, “Diffraction of waves by a wedge residing between two different media,” *Optik*, vol. 162, pp. 8-18, Jun. 2018.
38. L. Azpilicueta et al., “An accurate UTD extension to a ray-launching algorithm for the analysis of complex indoor radio environments,” *Journal of Electromagnetic Waves and Applications*, vol. 30 (1), pp. 43-60, 2016.
39. I. Gershenzon, Y. Brick, and A. Boag, “Shadow Radiation Iterative Physical Optics Method for High-Frequency Scattering,” *IEEE Transactions on Antennas and Propagation*, vol. 66 (2), pp. 871 – 883, Feb. 2018.
40. A. Aktepe, H. A. Serim, and H. A. Ülkü “Evaluation of Time Domain Physical Optics Integral on Curved Surfaces,” *2nd URSI AT-RASC*, Gran Canaria, 28 May – 1 June, 2018, pp. 1-3.
41. O. Garten et al., “Considering Nonsurface Scattering in Physical Optics Approximations,” *IEEE Transactions on Antennas and Propagation*, vol. 69 (8), pp. 4798 – 4807, Aug. 2021.
42. J. V. Rodríguez et al., “UTD-PO Formulation for the Analysis of Multiple-Plateau Diffraction When Considering Illumination From a Low Source,” *IEEE Transactions on Antennas and Propagation*, vol. 69 (7), pp. 4241 – 4245, July 2021.
43. J. V. Rodríguez et al., “Plane-Wave UTD-PO Formulations for Multiple-Diffraction by Trees and Buildings at Millimeter-Wave Frequencies,” *IEEE Antennas and Wireless Propagation Letters*, vol. 19 (10), pp. 1793 – 1797, Oct. 2020.

44. M. J. Mencagli, et. al., “A Physical Optics Approach to the Analysis of Metascreens,” *IEEE Access*, vol. 8, pp. 162634 – 162641, 2020.
45. A. Aktepe, and H. A. Ülkü, “Exact Evaluation of Time-Domain Physical Optics Integral on Quadratic Triangular Surfaces,” *IEEE Transactions on Antennas and Propagation*, vol. 68 (11), pp. 7447 – 7456, Nov. 2020.
46. T. T. Fan et al., “Time-Domain Line-Integral Representations of Physical-Optics Scattered Fields,” *IEEE Transactions on Antennas and Propagation*, vol. 65 (1), pp. 309 – 318, Jan. 2017.
47. N. Zhang, Y. M. Wu, and Y. Q. Jin, “Multilevel Second-Order Physical Optics Method for Calculating the High-Frequency Scattered Fields,” *IEEE Antennas and Wireless Propagation Letters*, vol. 19 (4), pp. 651 – 655, Apr. 2020.
48. O. A. Iupikov, et al., “Indoor Received Power Prediction Based on Physical Optics (PO): Simulations and Experimental Validation in Industrial Environment,” *13th European Conference on Antennas and Propagation (EuCAP)*, Krakow, Poland, 31 Mar.-5 Apr., 2019, pp. 1-5.
49. Q. Zeng, et al., “On propagation prediction based on physical optics,” *Progress in Electromagnetic Research Symposium (PIERS)*, Shanghai, China, Aug. 8-11, 2016, pp. 1.
50. J. C. Su, et al., “A High Frequency Electromagnetic Scattering Algorithm Based on Physical Optics Method,” *IEEE International Symposium on Antennas and Propagation and North American Radio Science Meeting*, Montreal, QC, Canada, Jul. 5-10, 2020, pp. 1-2.
51. R. Paknys, “Physical Theory of Diffraction,” in *Applied Frequency-Domain Electromagnetics*. 1st Ed, Wiley-IEEE Press, 2016, pp. 317 – 334.

52. M. Behdani et al., “Electromagnetic scattering from a pec target over a random rough sea surface using hybrid KA-PO-PTD method,” *IEEE International Symposium on Antennas and Propagation & USNC/URSI National Radio Science Meeting*, San Diego, CA, USA, Jul. 9-14, 2017, pp. 2045-2046.
53. M. A. Shah et al., “Bistatic Radar Cross Section Prediction Using Iterative Physical Optics with Physical Theory of Diffraction for Plate Geometries,” *IEEE International Symposium on Antennas and Propagation and North American Radio Science Meeting, Montreal*, QC, Canada, Jul. 5-10, 2020.
54. G. Apaydin, L. Sevgi, and P. Y. Ufimtsev, “Extension of PTD for Finite Objects With Rounded Edges: Diffraction at a Soft Trilateral Cylinder,” *IEEE Antennas and Wireless Propagation Letters*, vol. 16, pp. 2590-2593, Aug. 2017.
55. G. Guo, and Lixin Guo, “Hybrid Time-Domain PTD and Physical Optics Contour Integral Representations for the Near-Field Backscattering Problem,” *IEEE Transactions on Antennas and Propagation*, vol. 67 (4), pp. 2655 – 2665, Apr. 2019.
56. G. Apaydin et al., “Diffraction at a Rectangular Plate: First-Order PTD Approximation,” *IEEE Transactions on Antennas and Propagation*, vol. 64 (5), pp. 1891 – 1899, May 2016.
57. M. Darmon et al., “A system model for ultrasonic NDT based on the Physical Theory of Diffraction (PTD),” *Ultrasonics*, vol. 64, pp. 115-127, Jan. 2016.
58. D. Guijier, “Research on the Radio Frequency Simulation Method for Wide-band Radar Complex Target based on Physical Optics and Physical Diffraction Theory,” *IEEE International Conference on Signal, Information and Data Processing (ICSIDP)*, Chongqing, China, Dec. 1-13, 2019, pp. 1-5.
59. J. Li, M. Zhang, and P. Wei, “Combination of GO/PO and PTD Method for EM Scattering and SAR Image Simulation from Complex Targets,” *IEEE International*

Symposium on Antennas and Propagation & USNC/URSI National Radio Science Meeting, Boston, MA, USA, Jul. 8-13, 2018, pp. 2467-2468.

60. M. Sarnık, and U. Yalçın, "Modified Theory of Physical Optics and solution for scattering fields from a perfectly conducting parabolic reflector," *IEEE International Conference on Mathematical Methods in Electromagnetic Theory (MMET)*, Lviv, Ukraine, Jul. 5-7, 2016, pp. 349-352.
61. M. Sarnik, and U. Yalçin, "Uniform diffracted fields from non-conducting cylindrical surface by modified theory of physical optics," in *5th Telecommunication Forum (TELFOR)*, Belgrade, Serbia, Nov. 21-22, 2017, pp. 1-3.
62. Y. Z. Umul, "Three dimensional modified theory of physical optics," *Optik*, vol. 127 (2), pp. 819-824, Jan. 2016.
63. Y. Z. Umul, "Modified theory of physical optics and the correction terms of the physical theory of diffraction," *Optik*, vol. 171, pp. 421-430, Oct. 2018.
64. Y. Z. Umul, "Diffraction of cylindrical waves by a perfectly conducting half-screen: A modified theory of physical optics solution," *Microwave and Optical Technology Letters*, vol. 58 (8), pp. 1996-2001, Aug. 2016.
65. M. Sarnıka, and U. Yalçın, "Uniform scattered fields from a perfectly conducting parabolic reflector with modified theory of physical optics," *Optik*, vol. 135, pp. 320-326, Apr. 2017.
66. Y. Z. Umul, "Wave diffraction by a soft/hard strip: Modified theory of physical optics solution," *Optik*, vol. 156, pp. 857-865, Mar. 2018.
67. Y. Z. Umul, "The factorization process in the modified theory of physical optics," *Optik*, vol. 205, pp. 164-249, Mar. 2020.
68. Y. Z. Umul, "Modified theory of physical optics approach to impedance surfaces for skew incidence," *Optik*, vol. 205, Mar. 2020.

69. H. D. Basdemir, “Review on the Modified Theory of Physical Optics,” *IEEE 17th International Conference on Mathematical Methods in Electromagnetic Theory (MMET)*, Kyiv, Ukraine, Jul. 2-5, 2018, pp. 51-55.
70. M. Sarnika, and U. Yalçin, “Diffraction from Various Surfaces with Modified Theory of Physical Optics,” *Sensors & Transducers*, vol. 233 (5), pp. 58-63 May 2019.
71. M. Frongillo, G. Gennarelli, and G. Riccio, “FD-UAPO solutions for the diffraction by a composite wedge,” *Progress in Electromagnetic Research Symposium (PIERS)*, Shanghai, China, Aug. 8-11, 2016, pp. 1-4.
72. G. Gennarelli, and G. Riccio, “UAPO Solution for the Plane Wave Diffraction by a 90° Coated Wedge,” *2nd URSI AT-RASC*, Gran Canaria, 28 May – 1 Jun., 2018, pp. 1-4.
73. G. Gennarelli, and G. Riccio, “The UAPO Solution for the Plane Wave Diffraction by a DPS/DNG Material Coated Wedge,” *Photonics & Electromagnetics Research Symposium - Spring (PIERS-Spring)*, Rome, Italy, Jun. 17-20, 2019, pp. 1477-1480.
74. G. Gennarelli, and G. Riccio, “Diffraction by a Planar Junction between DPS and DNG Material Sheets: the UAPO Solution for Plane Waves at Skew Incidence,” *URSI GASS 2020*, Rome, Italy, 29 Aug. - 5 Sep. 2020, pp. 1-4.
75. G. Gennarelli, and G. Riccio, “Diffraction by an arbitrary-angled coated wedge: An alternative uniform asymptotic solution,” *Baltic URSI Symposium (URSI)*, Poznan, Poland, May 15-17, 2018, pp. 111-114.
76. M. Frongillo G. Riccio and G. Gennarelli, “TD-UAPO solutions for the diffraction by co-planar adjacent blocks,” *2017 International Applied Computational Electromagnetics Society Symposium - Italy (ACES)*, Firenze, Italy, Mar. 26-30, 2017, pp. 1-2.

77. M. Frongillo G. Riccio and G. Gennarelli, “TD-UAPO diffraction by a wedge composed of PEC and lossless dielectric,” *International Conference on Electromagnetics in Advanced Applications (ICEAA)*, Verona, Sep. 11-15, 2017, pp. 502-505.
78. G. Gennarelli, and G. Riccio, “The UAPO Diffraction Contribution in the IPO Method for RCS Evaluations,” *Photonics & Electromagnetics Research Symposium - Spring (PIERS-Spring)*, Rome, Italy, Jun. 17-20, 2019, pp. 3273-3277.
79. G. Gennarelli, and G. Riccio, “A Uniform Asymptotic Solution for the Diffraction by an Arbitrary-Angled Wedge Coated by Lossy DNG Metamaterials: the Case of Normal Incidence,” *13th European Conference on Antennas and Propagation (EuCAP)*, Krakow, Poland, 31 Mar.-5 Apr., 2019, pp. 1-4.
80. G. Gennarelli, and G. Riccio, “On the Accuracy of the Uniform Asymptotic Physical Optics Solution for the Diffraction by a PEC–DNG Metamaterial Junction,” *IEEE Antennas and Wireless Propagation Letters*, vol. 19 (4), pp. 581 – 585, Apr. 2020.
81. G. Gennarelli, and G. Riccio, “Plane Wave Diffraction by a 90° Wedge Coated by Metamaterial Slabs: A Uniform Asymptotic Solution in the Case of Normal Incidence,” in *12th International Congress on Artificial Materials for Novel Wave Phenomena (Metamaterials)*, Espoo, Finland, 27 Aug.-1 Sept. 2018, pp. 334-336.
82. E. L. Mokole and T. K. Sarkar, “Introduction to ultrawideband theory / technology / systems,” in *Int. Conf. on Electromagnetics in Advanced Applications*, Cairns, Australia, 2016, pp. 768–771.
83. V. A. Fono, L. Talbi and K. Hettak, “Electromagnetic wave propagation modeling in a complex environment using uniform geometrical theory of diffraction,” in *9th European Conference on Antennas and Propagation (EuCAP)*, 2015, pp. 1-5.

84. H. M. El-Sallabi, and P. Vainikainen, “Improvements to diffraction coefficient for non-perfectly conducting wedges,” *IEEE Trans. on Antennas and Propagation*, vol. 53, no. 9, pp. 3105-3109, Sep. 2005.

85. R. C. Qiu and C. Zhou, “Pulse distortion caused by cylinder diffraction and its impact on UWB communications,” *IEEE Trans. Veh. Technol*., vol. 56, no. 4, pp. 2385–2391, Jul. 2007.

86. F. Capolino and M. Albani, “Time domain double diffraction at a pair of coplanar skew edges,” *IEEE Trans. Antennas Propag*., vol. 53, no. 4, pp. 1455–1469, Apr. 2005.

87. P. Górniak and W. Banduriski, “Direct time domain analysis of an UWB pulse distortion by convex objects with the slope diffraction included,” *IEEE Trans. Antennas Propag.*, vol. 56, no. 9, pp. 3036–3044, Sep. 2008.

88. P. R. Rousseau and P. H. Pathak, “A time domain formulation of the uniform geometrical theory of diffraction for scattering from a smooth convex surface,” *IEEE Trans. Antennas Propag.*, vol. 55, no. 6, pp. 1522– 1534, Jun. 2007.

89. A. Karousos and C. Tzaras, “Time-domain diffraction for a double wedge obstruction,” in *Proc. IEEE Antennas Propag. Soc. Int. Symp*., Honolulu, HI, USA, Jun. 2007, pp. 4581–4584.

90. A. Karousos, G. Koutitas, and C. Tzaras, “Transmission and reflection coefficients in time-domain for a dielectric slab for UWB signals,” in *Proc. IEEE VTC-Fall*, Singapore, 2008, pp. 455–458.

91. A. Karousos and C. Tzaras, “Multiple time-domain diffraction for UWB signals,” *IEEE Trans. on Antennas and Propagation*, vol. 56, no. 5, pp. 1420-1427, May 2008.

92. P. Liu, J. Wang, and Y. Long, “Time-domain double diffraction for UWB signals,” in *PIERS Proceedings*, Beijing, pp. 848-852, 2009.

93. T. Han and Y. Long, “Time-domain UTD-PO analysis of a UWB pulse distortion by multiple-building diffraction,” *IEEE Antennas Wireless Propag. Lett.,* vol. 9, pp. 795–798, Aug. 2010.

94. P. Liu, J. Guo, J. Liu, J. Wang, and Y. Long, “Multiple time-domain diffraction of plane waves by an array of perfectly conducting wedges for UWB signals,” in *Proc. IEEE ICMMT*, 2010, pp. 1173–1176.

95. P. Liu, J. Tan, and Y. Long, “Time domain UTD-PO solution for the multiple diffraction of spherical waves for UWB signals,” *IEEE Trans. Antennas Propag*., vol. 59, no. 4, pp. 1420–1424, Apr. 2011.

96. P. Tewari, S. Soni and S. Goswami, "A comparison between transmitted and diffracted field in a microcellular scenario for UWB signals," in *Proc. IEEE Asia-Pac. Conf. Antennas Propag.*, Aug. 2012, pp. 221-222.

97. S Li, Y Liu, X Zhang et al., “Study on the multipath propagation model of UWB signal in the indoor environment based on TD-UTD,” in *IEEE Asia-Pacific Microwave Conference (APMC)*, 2015, pp. 1-3.

98. S. Li, Y. Liu, Q. Shi and X. Zhang, “Simulation and analysis of indoor propagation characteristics for UWB based on TD-UTD,” in *Asia-Pacific Microwave Conference*, 2015.

99. P. Tewari, S. Soni, B. Bansal, “Time-domain solution for transmitted field through low-loss dielectric obstacles in a microcellular and indoor scenario for UWB signals”, *IEEE Trans. Veh. Technol.*, vol. 64, no. 2, pp. 541–552, Feb. 2015.

100. C.A. Balanis, *Advanced Engineering Electromagnetics*. Wiley, 2nd Ed., 2012, pp. 824-827.

101. W. Yang, Z. Qinyu, Z. Naitong, Z. Xinwei, “Time Domain Analysis of UWB Pulsed Field Diffraction,” in *International Conference on Microwave and Millimeter Wave Technology*, 2017 .

102. Z. Chen, Y. Liu, S. Li and Z. Sheng, “Simulation and analysis of UWB propagation characteristics in indoor complex environments based on TD-UTD,” in *Sixth Asia-Pacific Conference on Antennas and Propagation (APCAP)*, 2017, pp. 1-3.

103. B. Bansal, S. Soni, V. Mishra, A. Gupta, and A. Agrawal, “A Novel heuristic time-domain diffraction model for UWB diffraction by lossy wedges and buildings”, *Physical Communication*, vol. 34, pp. 80–89, Mar. 2019.

104. J. F. Rouviere, N. Douchin, and P. F. Combes, “Diffraction by lossy dielectric wedges using both heuristic UTD formulations and FDTD”, *IEEE Trans. on Antennas and Propagation*, vol. 47, no. 11, pp. 1702-1708, Nov. 1999.

105. R. J. Luebbers, “A heuristic UTD slope diffraction coefficient for rough lossy wedges,” *IEEE Trans. Antennas Propag*., vol. 37, no. 2, pp.1678-1682, Feb. 1989.

106. P. D. Holm, “A new heuristic UTD diffraction coefficient for non-perfectly conducting wedges,” *IEEE Trans. Antennas Propagat*., vol. 48, pp. 1211–1219, Aug. 2000.

107. H. M. El-Sallabi, I. T. Rekanos, and P. Vainikainen, “A new heuristic diffraction coefficient for dielectric wedges at normal incidence,” *IEEE Antennas Wireless Propag. Lett.,* vol. 1, pp. 165–168, 2002.

108. D. N. Schettino, F. J. S. Moreira, K. L. Borges, and C. G. Rego, “Novel heuristic UTD coefficients for the characterization of radio channels,” *IEEE Trans. on Magnetics*, vol. 43, no. 4, pp. 1301-1304, April 2007.

109. W. Yang, Z. Qinyu, Z. Naitong, and C. Peipei, “Transmission characteristics of ultra-wide band impulse signals,” *In Proceedings of the IEEE International Conference on*

Wireless Communications, Networking and Mobile Computing, Shanghai, Sep. 2007, pp. 550-553.

110. E. L. Mokole, and T. K. Sarkar, "Introduction to ultrawideband theory /technology /systems," in *International Conference on Electromagnetics in Advanced Applications (ICEAA)*, Cairns, QLD, Australia, Sept. 19-23, 2016, pp. 768-771.

111. M. Bhatt, "A New Solution Based on UTD-PO Method for Multiple-Diffraction by a Series of Buildings with Irregular Height and Spacing," *International Journal of Wireless Information Networks*, vol. 28, pp. 217–229, Mar. 2021.

112. S. A. Vavilov, and M. S. Lytaev, "Modeling Equation for Multiple Knife-Edge Diffraction," *IEEE Transactions on Antennas and Propagation*, vol. 68 (5), pp. 3869 – 3877, May 2020.

113. E. Weisstein, "Calculus and Analysis: Integral Transforms: Convolution," *Wolfram Web Resources*, Oct. 27, 2021. [Online]. Available: https://mathworld.wolfram.com/Convolution.html. [Accessed: Nov. 5, 2021].

114. V. Serov, "Fourier Series, Fourier Transform and Their Applications to Mathematical Physics," in Applied Mathematical Sciences, vol. 197, pp. 85, 2017.

115. V. Kumar, B. Bansal, S. Soni, N. S. Raghava, "A new time domain diffraction coefficient for non-perfectly conducting wedges," in *Asia-Pacific Microwave Conference*, New Delhi, pp. 1-3, 2016.

116. R. C. Qiu, and Q. Liu, "Physics-based pulse distortion for ultra-wideband signals," *IEEE Trans. Veh. Tech.*, vol. 54 (5), Sep. 2005.

117. P. Tewari, S. Soni, and B. Bansal, "Time-domain solution for transmitted field through low-loss dielectric obstacles in a microcellular and indoor scenario for UWB signals," *IEEE Trans. Veh. Technol.*, vol. 64, pp. 541–52, May 2014.

118. B. Bansal, S. Soni, R. K. Jaiswal, and V. Kumar, “Time-domain solution for corner diffraction of UWB signals by flat plate structures with the higher-order diffraction included,” *IETE Journal of Research,* vol. 64, no. 5, pp. 728-735, Sep. 2017.

119. T. Han and Y. Long, “Time-domain UTD-PO analysis of a UWB pulse distortion by multiple-building diffraction*,” IEEE Antennas Wireless Propag. Lett*., vol. 9, pp. 795–798, Aug. 2010.

120. B. Bansal, “A New UTD Based Time-Domain Solution for UWB Diffraction in 3-D Environments,” *Wireless Personal Network,* vol. 59, pp. 2365–2382, Feb. 2021.

121. Y. L. C. de Jong, M. H. J. L. Koelen, and M. H. A. J. Herben, “A building-transmission model for improved propagation prediction in urban microcells,” *IEEE Trans. Veh. Technol.*, vol. 53, no. 2, pp. 490–502, Mar. 2004.

122. S. Soni and A. Bhattacharya, “An analytical characterization of transmission through a building for deterministic propagation modeling,” *Microw. Opt. Technol. Lett.*, vol. 53, no. 8, pp. 1875–1879, Aug. 2011.

123. Z. Chen, Y. Liu, S. Li, and Z. Sheng, "Simulation and analysis of UWB propagation characteristics in indoor complex environments based on TD-UTD," *Sixth Asia-Pacific Conference on Antennas and Propagation (APCAP)*, pp. 1-3, 2017. DOI: 10.1109/APCAP.2017.8420970

124. G. Narimani, P.A. Martin, D.P. Taylor, “Analysis of ultra-wideband pulse distortion due to lossy dielectric walls and indoor channel models”, *IEEE Trans. Antennas Propag.*, vol. 64, no. 10, pp. 4423–4433, 2016.

125. K. R. Jakobsen, “An alternative diffraction coefficient for the wedge,” *IEEE Trans. Antennas Propagat.*, vol. AP-32, pp. 175-177, Feb. 1984.

List of Research Papers in Journals and Conferences

International Journals:

1. **Vinod Kumar,** Sanjay Soni, and N. S. Raghava, "A new time-domain heuristic diffraction coefficient for characterization of diffracted and transmitted field with UWB applications," *Physical Communication (Elsevier Journal)*, vol. 48, pp. 1-9, Oct. 2021.

   Indexing: SCIE; IF: 1.594; DOI: https://doi.org/10.1016/j.phycom.2021.101398

2. Bajrang Bansal, Sanjay Soni, Rahul Kumar Jaiswal, **Vinod Kumar**, "Time-domain solution for corner diffraction of UWB signals by flat plate structures with the higher-order diffraction included**, "** *IETE Journal of Research*, vol. 64, no. 5, pp. 728-735, Sep. 2017.

   Indexing: SCIE; IF: 1.125; DOI: 10.1080/03772063.2017.1369364

3. **Vinod Kumar,** N. S. Raghava, Sanjay Soni, "Time-domain Multiple-order Diffraction for Two Wedges of Arbitrary Angles," *International Journal of Innovative Technology and Exploring Engineering (IJITEE)*, ISSN: 2278-3075, vol. 8 (9), pp. 2241-2244, Jul. 2019**.**

   Indexing: Scopus

4. **Vinod Kumar,** N. S. Raghava, Sanjay Soni, " Time-domain double diffraction for Non-perfectly conducting Wedges," *International Journal of Recent Technology and Engineering (IJRTE),* ISSN: 2277-3878, vol. 8 (3), pp. 6450-6453, Sept. 2019.

   Indexing: Scopus

International Conferences:

5. **Vinod Kumar,** Bajrang Bansal, Sanjay Soni, N. S. Raghava, "A New Time-Domain Diffraction Coefficient for Non-Perfectly Conducting Wedges," in *Asia-Pacific Microwave Conference (APMC)*, Dec. 05-09, 2016, pp. 1-3. (ISSN: 2165-4743). Organized By: IEEE MTT SOCIETY, Asia Pacific Microwave Conference Office: FITT, IIT DELHI, NEW DELHI – 110 016.
6. **Vinod Kumar,** Sanjay Soni, N. S. Raghava, "Time-domain Formulation of Diffraction by a Dielectric Wedge" in *Proceedings of IIRAJ International Conference (ICCI-SEM-2K17)*, GIFT, Bhubaneswar, India, Feb. 18-19, 2017, pp. 275-276. ISBN: 978-93-86352-38-5.
7. **Vinod Kumar,** Sanjay Soni, and N. S. Raghava, "A novel TD-UTD coefficients for evaluation of diffraction and transmission from dielectric wedges," In *International Conference on VLSI & Microwave and Wireless Technologies (ICVMWT 2021)*, March 2021, Jointly organised by Madan Mohan Malaviya University of Technology Gorakhpur, J.K. Institute of Applied Physics and Technology, University of Allahabad and Manipal University Jaipur **(Presented)**

Author Biography

Vinod Kumar was born in Sant Kabir Nagar (Uttar Pradesh), India on 2nd Feb 1982. He received his Diploma in Electronics Engineering from Govt. Polytechnic Ghaziabad, Uttar Pradesh, India in 2002. After this, He received his B. Tech. in Electronics & Communication Engineering from Uttar Pradesh Technical University, Lucknow, Uttar Pradesh, India in 2008 and M. Tech. in Networked Control Systems from Jaypee University of Information Technology, Solan, Himachal Pradesh, India in 2012. He joined the PhD program in the Department of Electronics and Communication Engineering from Delhi Technological University, New Delhi, India in July 2014. He has worked as an Associate Lecturer in the Electronics and Communication Engineering Department at Jaypee University of Information Technology, Hamirpur, Himachal Pradesh, India from July 2008 to June 2014. Currently, he is working as an Assistant Professor in the Electronics and Communication Engineering Department at DR. B. R. Ambedkar Institute of Technology, Port Blair, Andaman and Nicobar Islands, India. He has authored or co-authored many research papers in International Journals/Conferences proceedings of repute. His research interests include wireless communications and wireless channel modelling for UWB applications.